Stony Brook University

Records of $\delta^{13}C$, $\delta^{18}O$ and Concentration of Atmospheric CO In The Past

A Dissertation Presented

by

Zhihui Wang

to

The Graduate School

in Partial Fulfillment of the

Requirements

for the Degree of

Doctor of Philosophy

in

Marine and Atmospheric Science

Stony Brook University

December 2009

Stony Brook University

The Graduate School

Zhihui Wang

We, the dissertation committee for the above candidate for the **Doctor of Philosophy** degree, hereby recommend acceptance of this dissertation.

Dr. John E. Mak, Advisor

Associate Professor, School of Marine and Atmospheric Sciences, SUNY at Stony Brook

Dr. Minghua Zhang, Chairperson

Professor, School of Marine and Atmospheric Sciences, SUNY at Stony Brook

Dr. Daniel Knopf, Third Member

Assistant Professor, School of Marine and Atmospheric Sciences, SUNY at Stony Brook

Dr. Carl A. Brenninkmeijer., Fourth Member

Max Planck Institute for Chemistry, Mainz, Germany/Adjunct Professor of SoMAS/ITPA

Dr. Jérôme Chappellaz, Outside Member

Laboratoire de Glaciologie et Géophysique de l'Environnement, Grenoble, France

This dissertation is accepted by the Graduate School.

Lawrence Martin

Dean of the Graduate School

Abstract of the Dissertation

Records of $\delta^{13}C$, $\delta^{18}O$ and Concentration of Atmospheric CO In The Past

by

Zhihui Wang

Doctor of Philosophy

in

Marine and Atmospheric Science

Stony Brook University

2009

Atmospheric carbon monoxide (CO) plays a significant role in atmospheric chemistry, as CO is a major sink for atmospheric hydroxyl radicals (OH) and thus strongly influences the oxidizing capacity of the atmosphere. In this thesis, new high precision measurements of atmospheric CO concentration and isotope composition during the past 700 years have been accomplished by analyzing the air in polar snow and ice.

The first part of this study focuses on the trends of atmospheric CO over the past several decades. Firn air samples from the North Greenland Ice Core Project, Berkner

Island, and North Greenland Eemian Ice Drilling (NEEM) have been analyzed to reconstruct atmospheric CO concentration and isotopic compositions during the past half century in both hemispheres. Firn diffusion models have been applied for NEEM firn air data to reconstruct past atmospheric trend in CO, indicating that the maximum of CO concentration and $\delta^{18}O$ in high latitude Northern Hemisphere occurred in 1970s-1980s, reflecting the largest contribution of CO emissions from fossil fuel combustion in this time.

The second part of this study focuses on atmospheric CO records over the past 700 years. New decade-scale records of CO concentration as well as isotopic ratios have been produced from 40 Antarctic ice core samples (D47 and South Pole). CO concentration in the 13th century was ~50 ppbv, which is comparable with today's CO level in high-latitude Southern Hemisphere. CO level then gradually dropped to 38 ppbv during the following 300 years, followed by a gradual increase to 55 ppbv in 1900. $\delta^{13}C$ and $\delta^{18}O$ decreased by about 3‰ and 5‰ respectively from 1380 to 1700, then increased by about 3‰ and 5‰ respectively by 1900. Mass balance model implies biomass burning emissions were high in the 13th century, but reduced by ~50% over the next 300 years and then almost doubled by 1900. We conclude biomass burning strongly modulated the CO budget during preindustrial time and considerably decreased since the early 20th century. This decrease was nearly compensated by the concomitant CH_4 increase, bringing back CO mixing ratio close to its maximum level observed over the last 700 years.

Table of Contents

List of Figures..... ix

List of Tables xx

Abbreviations xxii

Acknowledgements xxv

Chapter 1. Introduction.....1

1.1 Carbon Monoxide in The Atmosphere..... 1

1.2 Isotope Signatures of Atmospheric CO..... 5

1.3 Seasonal and Interannual Variations and of Atmospheric CO 12

1.3.1 Seasonal variations 12

1.3.2 Interannual variations 16

1.4 Atmospheric Gases in Snow and Ice 19

1.4.1 Gases in Firn..... 20

1.4.2 Gases in Ice..... 21

1.4.3 Isotopes of Gases in Ice..... 23

1.5 Physical Characteristics of Polar Snow and Ice..... 25

1.5.1 Structure of Firn Layer 25

1.5.2 Impacts on Firn Air Measurements 29

1.6 Concluding Remarks..... 31

Chapter 2. Measurement of Firn and Ice Core Air Samples.....33

2.1 Instrumentation 34
2.1.1 Introduction of CF-IRMS 34
2.1.2 Instrumentation 36
2.2 Diagnostic Experiments 39
2.2.1 Bypass Blank 40
2.2.2 Schütze Blank 41
2.2.3 Ice Blank 42
2.3 Flow Rate Analysis 43
2.4 Reproducibility Analysis 45
2.5 Accuracy Analysis 46
2.6 Calibration Gas 48
2.7 Field Sample Measurement 51
2.8 Ice Cores Samples 52
2.8.1 D47 Ice Core Extraction and Gas Analysis 53
2.8.2 South Pole Ice Core Extraction and Gas Analysis 55
2.9 U Trap Test 59
2.10 Tedlar Bag Test 61
2.11 Concluding Remarks 62
Chapter 3. Records of Atmospheric CO in Firn 64
3.1 Introduction 64

3.2 Berkner Island and NGRIP Firn 66
3.2.1 Physical characteristic 66
3.2.2 Experiment 68
3.2.3 Results and Discussions 68
3.3 NEEM Firn Air 73
3.3.1 Methodology 73
3.3.2 Results 77
3.3.3 LGGE Firn Diffusion Model 80
3.3.4 Discussions 84
3.4 Concluding Remarks 91
Chapter 4. Records of Atmospheric CO in Antarctic Ice Cores 93
4.1 Introduction 95
4.2 Drilling site and ice core characteristics 96
4.3 Dating of D47 and South Pole ice cores 98
4.3.1 D47 ice core 98
4.3.2 South Pole ice core 100
4.4 Corrections for Ice Core Isotopes 102
4.5 Results and Discussions 105
4.5.1 CO concentration 105
4.5.2 CO Isotopes 111

4.5.3 Mass Balance Model 114

4.5.4 Residual results 123

4.5.5 Discussions 128

4.5.5.1 Residual data 128

4.5.5.2 CO partitioning 130

4.6 Implications to Atmospheric Chemistry 139

4.7 Outlooks 141

4.8 Concluding Remarks 142

Chapter 5. CO Records in the Pakitsoq Ice of Greenland 144

5.1 Introduction 144

5.2 Methodology 146

5.3 Results and Discussions 148

5.4 Concluding Remarks 153

References 155

Appendix A: South Pole Ice Core Measurements 190

Appendix B: D47 Ice Core Measurements 191

List of Figures

Figure 1.1 Isotopic signatures of atmospheric CO in terms of major sources based on data in table 1.2. References are the same as those in table 1.2. 7

Figure 1.2 Seasonal cycles of (a) [CO], (b) $\delta^{13}C$, and (c) $\delta^{18}O$ from Scott Base, New Zealand at 77º51'S 166º46'E in 1994-2004 [*Brailsford*, personal communication]. 15

Figure 1.3 Seasonal cycles of (a) [CO], (b) $\delta^{13}C$, and (c) $\delta^{18}O$ from Alert, Canada, at 82º27'N 62º31'W in 1996-1997 [*Brenninkmeijer*, personal communication]..... 16

Figure 1.4 Long-term trend of atmospheric CO concentration at three stations: top left (Iceland, 63ºN 1992-2009), top right (American Samoa, 14ºS 1988-2009), bottom left (Mauna Loa, 19.54ºN 1989-2009), and bottom right (South Pole, 89ºS 1992-2009) based on NOAA/ESRL Global Monitoring Division Carbon Cycle Sampling Network (http://www.esrl.noaa.gov/gmd/ccgg/iadv/). Data shown in grey are preliminary. 18

Figure 1.5 Schematic diagram showing the three different zones of firn layer. The depth at which the pore close-off occurs is typically in the range: 50-100m below the surface, depending on the site characteristics (temperature and accumulation rate)[*Barnola et al.*, 1991; *Raynaud et al.*, 1993]..... 27

Figure 1.6 Different zones and modes of air movement in the firn layer with increasing depth at the firn at DE08-2 (Law Dome ice core, 16 km east of Law Dome summit). Solid line is density and triangles are porosity [*Meure*, 2004]. 28

Figure 1.7 Schematic diagram of the air movement in firn layer, which is accounted for in the firn diffusion model: (left) firn, (middle) air, and (right) trace gas [*Rommelaere et al.*, 1997]. 28

Figure 2.1 A schematic diagram for the cryogenic extraction system attached with gas chromatography - isotope ratio mass spectrometry (GC-IRMS) which was used to measure mixing ratio, $\delta^{13}C$ and $\delta^{18}O$ of CO in ambient air, firn air and ice core air samples..... 37

Figure 2.2 The isotopic ratios of Iceland air sample (395ICE) measured based on different flow rate and the same sample size (100 mL at STP). Details on field sample processing are presented in section 2.7..... 44

Figure 2.3 CO concentration, $\delta^{13}C$, and $\delta^{18}O$ of the eight field air samples. All sample runs are shown as open diamonds, averages of each sample are shown as close squares, and error bars are 1σ standard deviations. (a) [CO]: with average error of 2.6 ppbv; (b) $\delta^{13}C$: with average error of 0.2‰; (c) $\delta^{18}O$: with average error of 0.3‰..... 45

Figure 2.4 The comparison between the measurements by the conventional off-line method and our new on-line analysis method. All sample runs are shown as open diamonds, averages of shifts for each sample are shown as close squares, and error bars are 1σ standard deviations. (a) shifts of [CO], ranging from +3.9 to -4.7 ppbv; (b) shitfs of $\delta^{13}C$, ranging from +0.06 to -0.41‰; (c) shifts of $\delta^{18}O$, ranging from +0.31 to -0.95‰. 47

Figure 2.5 Measurements of (a) $\delta^{13}C$ and (b) $\delta^{18}O$ for calibration gas as a function of voltage for mass-44 ranging from 400mv to 6 V. Mean value of $\delta^{13}C(CO)$: -45.40‰ (with standard deviation 0.33‰); mean value of $\delta^{18}O(CO_2)$: 0.42‰ (with standard deviation 0.32‰). Sample size is linear with voltage of mass-44 and 700 pmol CO gives 1V for the signal of voltage mass-44. We show $\delta^{18}O(CO_2)$ in (b) instead of $\delta^{18}O(CO)$ because the calibration run values of $\delta^{18}O$ themselves are used to determine the $\delta^{18}O$ of I_2O_5 [*C. A. M. Brenninkmeijer*, 1993]. 50

Figure 2.6 Schematic diagram for wet extraction system in LGGE [*Chappellaz et al.*, 1997]. Ice container is submerged in liquid nitrogen-alcohol cold bath (-20˚C) when evacuating and in hot water bath (70˚C) when melting. 54

Figure 2.7 On-line analysis system for ice core samples: wet extraction system including ice container, zero air flask, pirani gauge, pressure gauge, turbomolecular pump, and 4-loop water trap attached to the cryogenic extraction line to remove water coming out from the ice container [*Z H Wang and Mak*, 2009]..... 57

Figure 2.8 A mass spectrogram of a South Pole ice core sample. The mass spectrogram shows the measured ion intensities of m/z 44, 45 and 46 (lower) and the m/z ratios of 45/44 and 46/44 (upper). The first three peaks and the last three are the reference CO_2 gas injections. The peak at 241.20 s is the sample CO_2 peak. 58

Figure 2.9 Pressure drop function for HaySep D adsorption performance. In 30 min, the pressure drops to 0.9% of the initial pressure. Pressure drop lines of molecular sieve 13X

and 5A indicate the similar adsorption performance. 60

Figure 2.10 [CO], $\delta^{13}C$, $\delta^{18}O$ of the CO eluted from the HaySep D, molecular sieve 13X and molecular sieve 5A U traps. Also shown are those for the standard gas used in the tests. Isotopic fractionations occur for both $\delta^{13}C$ and $\delta^{18}O$. 61

Figure 3.1 Location of Berkner Island and other deep ice-core drilling sites in Antarctica [*Mulvaney et al.*, 2007]. 67

Figure 3.2 Map of Greenland, showing the locations of the deep ice core drilling sites including NGRIP (75.1°N, 42.3°W) [*Andersen et al.*, 2004]. 67

Figure 3.3 Concentration of carbon monoxide in firn air samples. Opem circles are CO concentrations for Berkner Island firn air from previous study [*Assonov et al.*, 2007]. Black squares are CO concentrations for Berkner Island firn air samples in this study. Green diamonds are CO concentrations for NGRIP firn air samples in this study. The red triangle is the CMDL/NOAA CO observation in Antarctic in Jan, 2003 and the blue cross is the CMDL/NOAA CO observation in Iceland in Jun, 2001. 71

Figure 3.4 Preliminary measurements of $\delta^{13}C$ of CO in firn air samples. The black squares are results of Berkner samples in this study. The green diamonds are $\delta^{13}C$ records of Berkner island firn air from other study [*Assonov et al.*, 2007]. Red triangles are $\delta^{13}C$ records for NGRIP firn air and blue cross is the observation in Scott Base in June, 2003 by NIWA, New Zealand [*Brenninkmeijer*, personal communication]. 72

Figure 3.5 The vertical profile of $\delta^{18}O$ for NGRIP firn air samples. Black squares are

$\delta^{18}O$ from NGRIP firn air samples and the red cross is observation of $\delta^{18}O$ in June, 2004, Iceland by [*J Mak*, personal communication]. 73

Figure 3.6 Location of NEEM and firn-air sampling sites [*Schwander et al.*, 2008]. 74

Figure 3.7 Measurements of (a) $\delta^{13}C$ and (b) $\delta^{18}O$ for calibration gas. Mean value of $\delta^{13}C(CO)$: -45.42‰ (with standard deviation 0.25‰); mean value of $\delta^{18}O(CO_2)$: 0.41‰ (with standard deviation 0.32‰). Solid lines are show the mean values and dashed lines indicate mean value plus and subtract 1σ standard deviation. $\delta^{13}C(CO)$ of calibration gas indicates good performance of the extraction system. $\delta^{18}O(CO)$ of calibration gas is used to calculate the $\delta^{18}O$ of Schütze reagent and derive the $\delta^{18}O$ of CO in air samples (see details in chapter 2). 76

Figure 3.8 Observations for the mixing ratio and isotopic ratios of CO in NEEM firn air. Top panel: [CO] in this study (red diamonds), [CO] by NOAA based on US borehole (cross) and [CO] by University of Bern based on EU borehole (triangle); middle panel: $\delta^{13}C(CO)$ in this study (cross); bottom: $\delta^{18}O(CO)$ in this study. Error bars are ±1σ standard deviatons. 78

Figure 3.9 Depth profiles of observed mixing ratios (symbols) for CO_2, CH_4, N_2O, SF_6, CH_3Cl_3 and CCl_4 in NEEM firn air, along with LGGE firn diffusion model simulations (curves). For symbols: Black: NOAA observations; Blue: CSIRO observations; Pink: University of Heidelberg observations. Crosses: EU borehole; triangles: US borehole. Curves: forward model simulations from LGGE firn diffusion model, green: diffusivity

tuned with CH_4; blue: diffusivity tuned with CO_2; purple: diffusivity tuned with CH_3Cl_3. 79

Figure 3.10 Flow chart for diffusivity calculation and depth-profile in firn diffusion model [*Martinerie*, personal communication]. 81

Figure 3.11 Flow chart for atmospheric trend calculations in firn diffusion model [*Martinerie*, personal communication]. 82

Figure 3.12 LGGE firn diffusion model simulation performed on NEEM firn air. (a)-(c): Reconstruction of atmospheric trend for [CO] and isotopic ratios since 1950 based on diffusivities derived from the direct model and our measurements on the NEEM firn air samples. (a): CO mixing ratio; (b): $\delta^{13}C$ of CO; (c): $\delta^{18}O$ of CO. Green lines: diffusivity tuned with CH_4; blue lines: diffusivity tuned with CO_2; purple lines: diffusivity tuned with CH_3Cl_3. Also shown (grey dashed lines) are: (a) NOAA atmospheric data (GAW database) at Barrow (71.32ºN 156.61ºW) in 1988-2008; (b) and (c): observations at Alert (82º27'N 62º31'W) in 1996-1998 by [*Brenninkmeijer*, personal communication] and observations at Iceland (63º15'N 20º09'W) in 2003-2004 [*J Mak*, personal communication]. (e)-(f): Calculated depth profiles of [CO] and isotopic ratios for NEEM firn air samples based on direct diffusion model with firn diffusivity and the calculated atmospheric trend in (a)-(c), compared with our observations. Colors of the lines stand for the same as in (a)-(c). 83

Figure 3.13 High-resolution, continuous measurements of Pb concentration in an ice core

from Summit, Greenland from 1750 to 1998 [*McConnell et al.*, 2002]. 88

Figure 3.14 LGGE firn diffusion model performed on NEEM fir nair. (a): Evolution of the atmospheric CH_4 concentration since 1950. (b) Calculated depth profile and observations of [CH_4] in NEEM firn air. Colors of the lines stand for the same as in Fig 3.12..... 89

Figure 3.15 The linear correlation between $\delta^{18}O$ and 1/[CO] for NEEM firn air (known as a keeling plot). $R^2 = 0.77$ is obtained, indicating a strong correlation. Data has already been corrected by gravitational fractionation based on NEEM $\delta^{15}N$ data [*Landais and Capron*, personal communication]..... 90

Figure 4.1 Location of D47 (67˚23'S 154˚03'E 1550 m.a.s.l.) and South Pole (89˚57'S 17˚36'W 2800 m a.s.l.) ice core drilling site, together with other core sites including Law Dome (66°44' S, 112°50' E, 1390 m a.s.l.) ice core [*Ferretti et al.*, 2005] which will be discussed in section 4.5. Map is edited based on that from NICL Science Management Office website: nicl-smo.unh.edu/icecoresites/antarctica.html..... 97

Figure 4.2 Linear regression curve used for D47 ice core dating, data from [*Barnola et al.*, 1995; *Haan et al.*, 1996]. 99

Figure 4.3 Linear regression curve for South Pole ice core dating, data from [*Friedli et al.*, 1984; *Neftel et al.*, 1985; *Schwander and Stauffer*, 1984]. 101

Figure 4.4 Firn air isotopic measurements of $\delta^{15}N$ (black circles), $\delta^{40}Ar$ (open circles), and $\delta^{18}O$ (crosses) performed on Berkner Island [*Landais et al.*, 2006]. Shading strip

stands for the non-diffusive zone and the dashed line is 0‰. 104

Figure 4.5 The D47 ice core (triangles) and South Pole ice core (diamonds) records from 1360 to 1900. (a) CO mixing ratio; (b) $\delta^{13}C$ of CO; (c) $\delta^{18}O$ of CO. Error bars show the analytical uncertainties ($\pm 1\sigma$) of [CO], $\delta^{13}C$ and $\delta^{18}O$ as 4.8 ppbv, 0.3‰ and 0.7‰, respectively. Shading area shows the little ice age (1500-1800). Also shown are observations of annually averaged atmospheric CO (crosses) in Scott Base (77° 51′S, 166° 46′E) in 2000-2003 [*L K Emmons et al.*, in preparation]. The ice core analytical method is discussed in previous study [*Z H Wang and Mak*, 2009] and chapter 2 of this thesis. The original ice core data are shown in appendix A and B..... 108

Figure 4.6 The 1000-year Law Dome ice core records for CH_4, CO_2, N_2O and CO [*Meure*, 2004; *Meure et al.*, 2006], also shown is CO_2 records in Dronning Maud Land (DML), South Pole (SP) and D47 ice cores [*Barnola et al.*, 1995; *U. Siegenthaler et al.*, 2005]. Shading area stands for the Little Ice Age (LIA)..... 110

Figure 4.7 D47 ice core records (the same data as those in Fig 4.5), shown as new method (red squares, on-line analysis system, section 2.8.2) and old method (green squares) prepare with wet extraction in LGGE and analyze in Stony Brook University, section 2.8.1). Dashed line indicates the depth below which thermal drilling started and kerosene was used..... 113

Figure 4.8 The 700-year Law Dome records for $[CH_4]$ and $\delta^{13}CH_4$, based on air measurements from ice cores (DSS, DE08, and DE08-2), firn, and archives (Cape Grim,

Australia and Baring Head, New Zealand) [*Etheridge et al.*, 1998; *Ferretti et al.*, 2005]. 119

Figure 4.9. Records of $\delta^{13}C$ (circles) and $\delta^{18}O$ (squares) and [CO] (triangles) for residual sources of CO based on different scenarios of mass balance model simulation. Scenario 1: model with ocean and biogenic source; scenario 2: model with biogenic source but without ocean source; scenario 3: model without ocean or biogenic source; scenario 4: model with ocean but without biogenic source. Discrepancies among different scenarios indicate sensitivities of ocean and biogenic source to the model simulations. Uncertainties of residual [CO], residual $\delta^{13}Cr$, and residual $\delta^{18}O$ are 4.8 ppbv, 0.46‰, and 1.05‰, respectively. See the details on the uncertainty determination in text. 127

Figure 4.10 Modeled CO source partitioning based on ice core data and mass balance model. Also shown are [CO] derived from the three major sources at Scott Base in modern atmosphere (annually average in 1997-2004) at Scott Base [*K.H. Park et al.*, in preparation]. Scenarios are the same as Fig 4.9. The uncertainties ($\pm 1\sigma$) of $[CO]_{CH4}$,$[CO]_{Biomass\ Burning}$, and $[CO]_{NMHC}$ are 0.07 ppbv, 4.8 ppbv, and 3.7 ppbv, respectively. See details on uncertainties in text. [CO] from CH_4 oxidation was relatively stable between 1360 and 1900, however large variations are observed for [CO] from biomass burning even with large uncertainties. Due to large uncertainties, no clear trend can be found on CO from NMHC oxidation. 131

Figure 4.11. (a) Sedimentary charcoal record in tropics (solid line) (30˚N-20S) and

uncertainties (dashed lines) for tropical region (30˚N- 20˚S) from 1200 to 2000 indicates biomass burning in tropics dropped from 1200 and increased from 1750 to 1900 [*Marlon et al.*, 2008]; also shown is deduced biomass burning CO in the present study (open diamonds). (b) The relation between $\delta^{13}CO$ (open squares) and NH temperature anomaly reconstructions [relative to 1961-1990 mean] (green line [*Mann and Jones*, 2003] and blue line [*Moberg et al.*, 2005], blue dashed lines are largest errors at 95% confidence interval) as well as SH temperature anomaly reconstruction [relative to 1961-1990 mean] (red line) [*Mann and Jones*, 2003]. The multicentenial changes that the Moberg record better incorporates by use of low-resolution proxies. 134

Figure 5.1 Diluted CO concentrations (left scale) of the Pakitsoq ice samples in this study (green circles) and given by NIWA (red squares). Also shown (right scale) are the original CO concentrations in this study (purple triangles) and those from NIWA (blue diamonds) and concentrations of CH_4 (black dashes and bars) [*Petrenko et al.*, 2006]. [CO] error ($\pm 1\sigma$) in this study is 1.6 ppbv based on calibration runs. Errors ($\pm 1\sigma$) for original [CO] are calculated to be 13-15 ppbv based on errors for subsamples and dilution factors in Table 5.1. Gas age and age errors are derived from $\delta^{15}N$ and $\delta^{18}O_{atm}$ and GISP2 timescale [*Petrenko et al.*, 2006; *Schaefer et al.*, 2006]. Kyr BP is thousand years before present, with present defined as 1950 AD. 149

Figure 5.2 Isotopic ratios of CO in Pakitsoq ice samples. Green circles denote $\delta^{13}C$ (left scale) and red squares are for $\delta^{18}O$ (right scale). Error bars for $\delta^{13}C$ and $\delta^{18}O$ are 1σ

standard deviations: 0.1‰ and 0.43‰ respectively. The two circles stand for the two contaminated samples (contaminated PB and contaminated OD in Table 5.1). Kyr BP is thousand years before present, with present defined as 1950 AD. 150

List of Tables

Table 1.1 Estimates of the global atmospheric CO budget (in Tg(CO)/yr) from different sources..... 3

Table 1.2 The isotopic source signatures for atmospheric CO 6

Table 2.1 Schütze blank of the cryogenic system determined with zero air with flow rate of 50 mL/min[#] 41

Table 2.2 Ice blanks tested with calibration gas and artificial bubble free ice from LGGE, France..... 43

Table 2.3 Comparison of $\delta^{13}C$ and $\delta^{18}O$ results of field CO samples obtained by off-line dual inlet microvolume analysis and on-line extraction CF-IRMS 52

Table 3.1 Field site information of CRYOSTAT: CRYOspheric Studies of Atmospheric Trends in stratospherically and radiatively important gases (After [*BADC*, 2007])..... 66

Table 4.1 Present-day physical characteristics for D47 ice core and South Pole ice core.97

Table 4.2 Calculated mean gas age for D47 ice core samples based on the linear regression in Fig 4.2..... 100

Table 4.3 Calculated mean gas age for South Pole ice core samples based on the linear regression in Fig 4.3..... 102

Table 4.4 MOZART-4 simulations on CO at Scott Base in Jan 1, 1997-Dec 31, 2004 [*K.H. Park et al.*, in preparation] 114

Table 4.5 MOZAR simulation on $\delta^{13}C$ isotopic ratio at Scott Base [*L K Emmons et al.*, in preparation] 122

Table 5.1 Pakitsoq ice samples preparation and dilution information 147

Abbreviations

BP	before present (years before AD 1950)
CH_4	methane
CFC	Chlorofluorocarbon
CMDL	Climate Monitoring and Diagnostics Laboratory (NOAA, USA)
CO	carbon monoxide
CO_2	carbon dioxide
COD	Close-off Depth
D47	D47 ice core, 67˚23'S 154˚03'E 1550 m.a.s.l.
δD	deuterium isotopic ratio
DOM	Dissolved organic matter
DE08	Law Dome ice core, 16 km east of Law Dome summit
DE08-2	A second DE08 ice core, 300m from DE08
DSS	Dome Summit South (Law Dome ice core)
GC	Gas Chromatograph
GISP2	Greenland Ice Sheet Project 2
IPCC	Intergovernmental Panel on Climate Change
IRMS	Isotope ratio mass spectrometry
KIE	Kinetic Isotope Effect

LGGE	Laboratoire de Glaciologie et Géophysique de l'Environnement(France)
LIA	Little Ice Age
LID	Lock-in Depth
LPIH	Late preindustrial Holocene (circa 0 to 1700 A.D.)
m a.s.l.	meters above sea level
MOZART	Model of Ozone and Related Tracers
NMHC	Non-methane hydrocarbon
MWP	Medieval Warm Period
NGRIP	North Greenland Ice Core Project
NH	Northern Hemisphere
NICL	National Ice Core Laboratory (Colorado, USA)
NOAA	National Oceanic and Atmospheric Administration (USA)
N_2O	nitrous oxide
O_3	ozone
OH	hydroxyl radical
ppb	parts per billion
ppm	parts per million
SH	Southern Hemisphere
SP	South Pole ice core, bore hole 5, 89˚57'S 17˚36'W 2800 m.a.s.l.
STP	Standard temperature and pressure (273.15K and 101.325 kpa)

VOC	Volatile organic compounds

Acknowledgements

I would like to thank the School of Marine and Atmospheric Sciences (SoMAS)/Institute of Terrestrial and Planetary Atmospheres (ITPA) and Stony Brook University for giving me the opportunity to study such an interesting and challenging field of research. My advisor, Prof. John E. Mak, provided me research assistantship and paid my tuition with his research grant. The SoMAS and Stony Brook University were responsible for providing the necessary technical support. I need to thank my three supervisors Professor John E. Mak, Dr. Jérôme Chappellaz and Dr. Carl Brenninkmeijer, for generously sharing their knowledge and skills with me. I have learnt a lot from them during the last few years. Thanks also to Dr. Patricia Martinerie for her help for firn diffusion modeling for NEEM firn air samples, for which I am very grateful. I particularly thank Prof. Daniel Knopf for providing good advices on experiments and valuable comments on data interpretations. I also thank Prof. David Black for his comments on ice core data interpretations.

Thank you to Laboratoire de Glaciologie et Géophysique de l'Environnement (LGGE) and National Ice Core Laboratory (NICL) for kindly supporting this project by providing D47 and South Pole ice cores. I greatly thank Dr. Jérôme Chappellaz for

providing D47 ice core samples and the necessary facilities. I greatly thank Mark Twickler for his help for ice allocation. Thank you to Mr Geoffrey Hargreaves and Mr Eric Cravens for their help in transporting ice cores from NICL in Colorado to Stony Brook. I also thank Prof. Ed Brook from Oregon State University for providing bubble free ice and Maurine Montagnat of LGGE for providing monocrystalline and polycrystalline bubble free ice. I thank Andy Matthews from Mt. Sinai High School for providing walk in freezer to prepare some South Pole ice core samples.

I gratefully thank the Iceland Meteorology Office and in particular Johanna, Oscar and Elvar for Iceland air sample collection and logistical support. I also thank the National Oceanic and Atmospheric Administration / Climate Monitoring and Diagnostics Laboratory (NOAA/CMDL) network for air sample collection and logistical support at Mauna Loa Observatory. This work was supported by the National Science Foundation grant OCE0713406. I thank this NSF funding for paying all of my lab equipments.

Many people on the faculty and staff of the SoMAS assisted and encouraged me in various ways during my course of studies. I am especially grateful to Profs. Nicole Riemer and Minghua Zhang for all that they have taught me. Thank you to Kolby Jardine, Key Hong Park, Jianhua Hao, Tracey Evans, Bingbing Wang, Peter Alpert, and Joseph Ruggieri. Thank you to John for reading this thesis without prejudice and providing timely constructive criticism.

Lots of thanks to my wife, Dongli, for her continuing support during my research, and for editing of this thesis. And of course, lots of thanks to my pretty cutie, Vanessa, for her sweet hugs and kisses during the tough time of my study.

Chapter 1. Introduction

1.1 Carbon Monoxide in The Atmosphere

Carbon monoxide (CO) plays a key role in atmospheric chemistry because of its close link with hydroxyl radical (OH) and methane (CH_4) [*Crutzen and Zimmermann*, 1991; *Logan et al.*, 1981; *A.M. Thompson*, 1992]. The reaction between CO and OH radical is the major sink for OH in both hemispheres [*Houghton et al.*, 2001]; thus CO plays an important role in the oxidizing capacity of the atmosphere [*Khalil and Rasmussen*, 1994]. Because of the role of OH in the oxidation of most reduced trace gases, changes in CO can thus considerably affect mixing ratios of a host of atmospheric gases, including the greenhouse gas methane (CH_4), non methane hydrocarbons (NMHCs) and even ozone (O_3), thus indirectly affecting global climate [*A.M. Thompson*, 1992]. Though CO is not a significant greenhouse gas itself, it has been shown that the emission of five CO molecules is equivalent to the emission of one CH_4 molecule as regards to greenhouse warming [*Prather*, 1996]. Moreover, the estimated cumulative radiative forcing due to the direct anthropogenic emission of CO may be larger than the cumulative forcing due to anthropogenically emitted N_2O for current emission levels [*Daniel and Solomon*, 1998]. More recent studies indicate anthropogenic CO emissions contribute a ~0.20 W m^{-2} radiative forcing of climate change [*IPCC*, 2007], mainly through chemical effects on the

concentrations of tropospheric O_3 and CH_4.

CO has a complex of mixture of sources [*Seiler*, 1974] and has relatively short lifetime [*Weinstock*, 1969], resulting in large temporal and spatial variations and adding difficulties in determining global CO budget [*Brenninkmeijer and Rockmann*, 1997].

Atmospheric CO has been investigated based on in situ observations at various atmospheric monitoring stations over the last two decades [*Khalil and Rasmussen*, 1984; 1990; 1994; *Novelli et al.*, 1992; *Novelli et al.*, 1998a; *Novelli et al.*, 1994a]. The first direct determination of CO concentration was reported for 1950-1951 at the Jungfrau Scientific Station in the Swiss Alpines, which is deduced from infrared total column amount measurements [*Rinsland and Levine*, 1985]. More comprehensive field measurement of atmospheric CO started in the early 1970s [*Heidt et al.*, 1980; *Seiler*, 1974; *Seiler and Junge*, 1970] and systematic global monitoring of atmospheric CO by National Oceanic and Atmospheric Administration Climate Monitoring & Diagnostics Laboratory (NOAA/CMDL) started in the late 1980s [*Novelli et al.*, 1992; *Novelli et al.*, 1994b]. Since the 1990s more and more attention has been paid to CO due to its significant role in atmospheric chemistry and even its indirect role in global climate [*Brunke et al.*, 1990; *Khalil and Rasmussen*, 1994; *Novelli et al.*, 1998a; *Novelli et al.*, 1998b]. Observations of atmospheric CO from satellites have also become available. The Measurements of Pollution in the Troposphere (MOPITT) instrument has been making observations of CO from the NASA Earth Observing System (EOS) Terra satellite since

March 2000 [*Deeter et al.*, 2003; *L K Emmons et al.*, 2004]. Numerical models have also been applied to refine CO budget calculations based on observed CO distribution, using all available information about atmospheric chemistry and physics [*Bergamaschi et al.*, 2000a; *Bergamaschi et al.*, 2000b; *L K Emmons et al.*, in preparation; *Hauglustaine et al.*, 1998; *Manning et al.*, 1997; *K.H. Park et al.*, in preparation].

Table 1.1 Estimates of the global atmospheric CO budget (in Tg(CO)/yr) from different sources

	Reference	Bergamachi et al., 2000[1]	IPCC-SAR (1996)[2]
Sources	Fossil fuel	641±23	300-550
	Biomass burning	768[#]	300-700
	CH_4 oxidation	795±24	400-1000
	NMHC oxidation	607[§]	200-600[¶]
	Vegetation		60-160
	Oceans	49±4	
Sinks	OH reaction	2570	1500-2700
	Surface deposition	288	250-640

Notes: 1: [*Bergamaschi et al.*, 2000a; *Bergamaschi et al.*, 2000b]; 2: [*IPCC-SAR*, 1996]; #: include forest burning 598±53 Tg(CO)/yr, savanna burning 140±36 Tg(CO)/yr, and biomass burning > 30ºN 30±9 Tg(CO)/yr. §: include oxidation of isoprene 268±41 Tg(CO)/yr, oxidation of terpenes 136±12 Tg(CO)/yr, and oxidation of industrial NMHC 203±26 Tg(CO)/yr. ¶: only consider oxidation of isoprene.

Estimates of the global atmospheric CO budget are listed in Table 1.1, along with their uncertainties. First of all, one has to be aware that limitations in modeling itself as well as the observational data make estimates of CO budget challenging. Large uncertainties as well as discrepancies between model results and observations are observed [*Bergamaschi et al.*, 2000a]. By introducing isotope information into the inverse model, the source strengths can be better constrained [*Bergamaschi et al.*, 2000b]. More reliable CO budget estimates will be available soon based on the most complete

observational data and MOZART (Model for OZone and Related chemical Tracers) simulations [*K.H. Park et al.*, in preparation].

On the global scale, major sources of atmospheric CO include fossil fuel combustion, biomass burning, as well as the oxidation of methane and NMHC's [*Bergamaschi et al.*, 2000a; *Bergamaschi et al.*, 2000b; *Houghton et al.*, 2001; *Logan et al.*, 1981; *J Mak and Kra*, 1999; *J Mak et al.*, 2003]. Minor sources of atmospheric CO include direct emission from vegetation, microorganisms [*Guenther et al.*, 2000] and oceanic emissions [*Seiler*, 1974; *Seiler and Junge*, 1970], which account for only ~10% of the total source emissions [*K.H. Park et al.*, in preparation]. Fractional contributions of different sources have temporal and spatial variability (section 3.2.5 and section 4.5). For example, CH_4 oxidation is the dominant in austral summer (accounts for ~50%) at Scott Base (77º51'S 166º46'E), whereas biomass burning and NMHC oxidation also contributes significantly in austral winter at the same place [*L K Emmons et al.*, in preparation; *K.H. Park et al.*, in preparation]. Fossil fuel combustion dominates CO emission in Iceland (63º15'N 20º09'W) and Alert (82º27'N 62º31'W) in northern winter except for an unusual wildfire year (1997-1998: [*Novelli et al.*, 2003]), but oxidation of CH_4 and NMHC also shows their significant contribution in other seasons [*L K Emmons et al.*, in preparation; *K.H. Park et al.*, in preparation].

The major sink of atmospheric CO is reaction with OH [*Hauglustaine et al.*, 1998; *Logan et al.*, 1981; *Weinstock and Niki*, 1972]. Surface deposition is considered as a

minor sink of CO [*IPCC-SAR*, 1996; *Sanhueza et al.*, 1998]. Roughly 75% of the hydroxyl radical is removed from the atmosphere by CO [*Crutzen and Zimmermann*, 1991]. The sink of tropospheric CO by OH reaction was previous estimated to be 1500-2700 Tg CO yr^{-1} by [*IPCC-SAR*, 1996] and was more recently estimated to be 2570 Tg CO yr^{-1} by inverse model [*Bergamaschi et al.*, 2000b]. The global soil sink for atmospheric CO is estimated to be 115-230 Tg CO yr^{-1} by [*Sanhueza et al.*, 1998] and 288 Tg CO yr^{-1} by [*Bergamaschi et al.*, 2000b].

1.2 Isotope Signatures of Atmospheric CO

Isotopic signature is reported as a ratio relative to a standard:

$$\delta(per\ mil, ‰) = \left[\frac{R_{sample}}{R_{ref}} - 1 \right] \times 1000$$

where R_{sample} and R_{ref} are the ratios of the minor isotope to the major isotope (e.g. $^{13}C/^{12}C$ and $^{18}O/^{16}O$) in the sample and the reference material. $^{13}C/^{12}C$ ratio is expressed relative to Vienna Pee Dee belemnite (VPDB) [*Craig*, 1957; *Gonfiantini*, 1978] and $^{18}O/^{16}O$ ratio is expressed relative to Vienna Standard Mean Ocean Water (VSMOW) [*Coplen*, 1994; *Gonfiantini*, 1978].

The individual atmospheric sources usually show distinct isotopic signatures and slightly different rate constants for different isotopomers occur during chemical reactions such as photochemical removal and surface deposition [*Kaye*, 1987]. Certain sources

producing atmospheric CO with distinct ratios of $^{13}C/^{12}C$ and $^{18}O/^{16}O$ have been observed and discussed [*Bergamaschi et al.*, 2000b; *C.A.M. Brenninkmeijer*, 1993; *Stevens and Wagner*, 1989; *Stevens et al.*, 1972]. The different isotopic signatures provide independent variables that can help to resolve the contributions of the certain sources and thus to better estimate the global CO budget [*Bergamaschi et al.*, 2000b; *C. A. M. Brenninkmeijer*, 1993; *L K Emmons et al.*, in preparation; *K.H. Park et al.*, in preparation; *Rockmann et al.*, 2002]. The isotope source signatures for major sources of atmospheric CO are presented in Table 1.2 and Fig 1.1.

Table 1.2 The isotopic source signatures for atmospheric CO

Sources	$\delta^{13}C$ (‰ VPDB)	$\delta^{18}O$ (‰ VSMOW)
Fossil fuel	-27.5‰[1]	23‰-26‰[3]
Biomass burning	-12[a] to-25[b]	18‰[1]
CH_4 oxidation	-51‰[2]	0‰[5]
NMHC oxidation	-32.2‰[3]	0‰[5]
Biogenic	-12[4] to -25[4]	0[6]
Ocean	-25[c], -40[d]	15[d]

1: [*Stevens et al.*, 1972]; 2: based on $\delta^{13}CH_4$ of -47‰ [*Lowe et al.*, 1991; *Lowe et al.*, 1997; *J. E. Mak et al.*, 2000; *Quay et al.*, 1999] and 3.9‰±0.4‰ (2σ 296K) isotope fractionation in [*Saueressig et al.*, 2001]; 3: [*Stevens and Wagner*, 1989]; 4: assume δ^{13} of biogenic emission the same as that in plants [*L K Emmons et al.*, in preparation]; 5: [*Brenninkmeijer and Rockmann*, 1997]; 6: assume the same as oxidation source [*K.H. Park et al.*, in preparation]; a: for C4 plants [*Manning et al.*, 1997]; b: for C3 plants [*Manning et al.*, 1997]; c: [*Goericke and Fry*, 1994]; d: [*Nakagawa et al.*, 2004]. See more details in text.

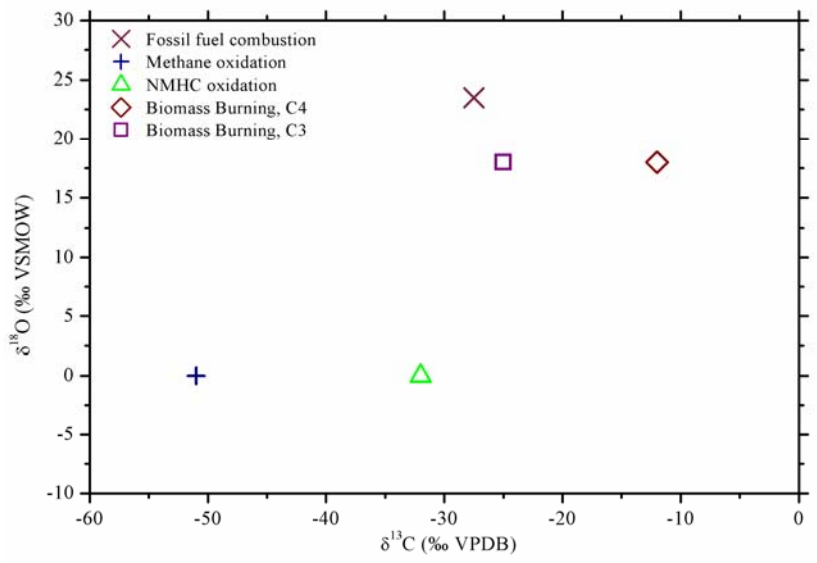

Figure 1.1 Isotopic signatures of atmospheric CO in terms of major sources based on data in table 1.2. References are the same as those in table 1.2.

$\delta^{13}C$ of CO from fossil fuel combustion is fairly well characterized as -27.5‰, which close to the isotopic compositions of fuels used [*Stevens and Wagner*, 1989; *Stevens et al.*, 1972]. However, recent direct measurements on the exhaust from individual automobile running normally indicate $\delta^{13}C$ of CO as -23.8±0.8‰ for gasoline vehicles and -19.5±0.7‰ for diesel vehicles [*Tsunogai et al.*, 2003]. CO from fossil fuels has the highest $\delta^{18}O$ of 23‰-26‰ [*Brenninkmeijer and Rockmann*, 1997; *Stevens and Wagner*, 1989], which is very close to the $\delta^{18}O$ of atmospheric oxygen (23.5‰) [*Bergamaschi et al.*, 2000b] and much higher than that of atmospheric CO (section 1.3). Measurements from urban air show very low variability for $\delta^{18}O$ [*Brenninkmeijer and Rockmann*, 1997; *Stevens and Wagner*, 1989], however a large range of $\delta^{18}O$ (11-29‰) was observed from the ambient air stream in three different locations in California (La Jolla, Pasadena, and White Mountain) [*Huff and Thiemens*, 1998]. Possibilities for this large variability

include the different mixture of gasoline automobiles and diesel automobiles and varying conditions of idling and running, both of which produce CO with different $\delta^{18}O$ [*Tsunogai et al.*, 2003]. The direct measurements on the exhaust from individual automobile running normally indicate $\delta^{18}O$ of CO as 25.3±1.0‰ for gasoline vehicles and 15.1±1.0‰ for diesel vehicles [*Tsunogai et al.*, 2003].

$\delta^{13}C$ of CO from CH_4 oxidation is estimated to be -51‰ based on an average $\delta^{13}CH_4$ of ~-47‰ in the SH [*Lowe et al.*, 1991; *Lowe et al.*, 1997; *J. E. Mak et al.*, 2000; *Quay et al.*, 1999] and 3.9±0.4‰ (2σ 296K) isotope fractionation constant [*Saueressig et al.*, 2001] and the assumption that after the formation of CH_3 radicals no further fractionation takes place [*Brenninkmeijer*, 1999]. This kinetic isotope effect (KIE) in [*Saueressig et al.*, 2001] is different from the earlier value of 5.4±0.9‰ (2σ 273-353K) [*Cantrell et al.*, 1990]. We use the KIE of [*Saueressig et al.*, 2001] because of considerably higher precision and experimental reproducibility than earlier study [*Cantrell et al.*, 1990]. $\delta^{13}C$ of CO from NMHC oxidation was estimated to be -32‰ based on measurements of selected NMHC in air samples from rural region in Northern Illinois [*Stevens and Wagner*, 1989]. In global scale, vegetation contributes about 90% of the NMHC emissions, with isoprene dominating the contribution [*Guenther et al.*, 1995]. Model simulation indicated oxidation of isoprene provides 331 Tg CO yr^{-1} (~15% of the total CO emission), showing this is the second largest contribution to CO chemical production [*G G Pfister et al.*, 2008]. In more recent studies, $\delta^{13}C$ of isoprene was estimated to be -27.7±2.0‰ [*Rudolph*

et al., 2003] and a KIE was estimated to be 6.94‰ for isoprene + OH [*Rudolph et al.*, 2000], therefore $\delta^{13}C$ of CO from isoprene was derived to be -34.6‰. No direct measurements are available for $\delta^{18}O$ from the oxidation of CH_4 and NMHC [*Bergamaschi et al.*, 2000b; *Brenninkmeijer and Rockmann*, 1997]. $\delta^{18}O$ of CO from oxidation of CH_4 and NMHC was estimated to be near 0‰ by using southern hemisphere CO budget and based on atmospheric observations [*Brenninkmeijer and Rockmann*, 1997]. $\delta^{18}O$ of CO from NMHC oxidation was previously estimated to be 14.9‰ by [*Stevens and Wagner*, 1989] based on the CO- $\delta^{18}O$ correlation in the rural air sample measurements, some of which have relatively high $\delta^{18}O$ values. However, large uncertainties appeared in their indirect derivations and their measurements might be complicated by the oxygen exchange between water vapor and lots of intermediates in the CH_4 and NMHC oxidation chains [*Stevens*, 1993]. Therefore, 0‰ is used in this study.

It has been suggested that the isotopic compositions of CO from actual biomass burning is close to the isotopic compositions of the biomass burned [*Stevens and Engelkemeir*, 1988]. C4 plants have a $\delta^{13}C$ of approximately -15‰, and C3 plants -23.5‰ [*Ehleringer*, 1993; *Farquhar*, 1993]. Consequently the ecosystem burnt, such as savanna (mainly C4) or forest (mainly C3), has a distinct impact on the $\delta^{13}C$ of the CO emitted. Biomass burning is suggested to have a $\delta^{13}C$ signature of around -12‰ for C4 plants and around -25‰ for C3 plants by [*Manning et al.*, 1997]. $\delta^{18}O$ of CO from

biomass burning was reported as 18±1‰ in [*Stevens and Wagner*] and it was estimated to be 10±1‰ based on the measurements of Siberian plumes [*Bergamaschi et al.*, 1998]. Laboratory chamber experiments on biomass burning indicate a very large range for both $\delta^{13}C$ (-33.8‰ to -10.2‰) and $\delta^{18}O$ (3.0‰ to 26.0‰) as for different plants (C3 or C4) and different burning stage (flaming or smoldering) [*Kato et al.*, 1999].

Biogenic emissions of CO refer to the formation and emission of CO on or in the live and dead plant matter, most likely resulted from direct photodegradation or photooxidation of cellular material [*Tarr et al.*, 1995]. The factors controlling these emissions are not well known [*Guenther et al.*, 2000]and there have been limited studies on the isotopic signatures. $\delta^{13}C$ is estimated to be -12‰ for C4 plants and -25‰ for C3 plants [*L K Emmons et al.*, in preparation], whereas $\delta^{18}O$ is assumed to be 0‰, the same as that in oxidation sources [*K.H. Park et al.*, in preparation]. Emmons et al. suggested a $\delta^{13}C$ of oceanic CO to be -25‰ [*L K Emmons et al.*, in preparation] based on the measurements of $\delta^{13}C$ in marine particulate organic carbon (POM) [*Goericke and Fry*, 1994], however the fractionation during the oxidation of POM is negligible. The mean $\delta^{13}C$ and $\delta^{18}O$ for CO emitted from the oceans were estimated to be -40% VPDB and +15% VSMOW, respectively based on the measurements of produced CO in seawater from coastal and open ocean in the Pacific, considering both the isotopic ratios in dissolved organic matters and fractionation during the photochemical production [*Nakagawa et al.*, 2004]. It has to be noted that ocean emission is a small contributor for

CO [*Bergamaschi et al.*, 2000b; *K.H. Park et al.*, in preparation].

In summary, there still exist large uncertainties in $\delta^{13}C$ and $\delta^{18}O$ source signatures, which sometimes will obscure their application in solving scientific problems. But generally speaking, $\delta^{13}C$ is very sensitive to the fraction of methane oxidation due to depletion in ^{13}C, thus $\delta^{13}C$ is a very good tracer for CH_4 oxidation. $\delta^{18}O$ is a good tracer for combustion processes including biomass burning and fossil fuel combustion since CO from them is enriched in ^{18}O.

Isotopic fractionation occurs when CO reacts with OH due to the kinetic isotope effect (KIE), which is a result of the lower zero point energy of the quantum vibrational state for an isotope of greater mass. The kinetic fractionation of ^{13}C is strongly pressure dependent and has an average strength of 4 to 5‰ in the lower troposphere, as measured by [*Rockmann et al.*, 1998; *Smit et al.*, 1982; *Stevens et al.*, 1980]. An inverse isotope effect of about −10‰ occurring for ^{18}O was measured [*Rockmann et al.*, 1998; *Stevens et al.*, 1980] and this KIE shows only a weak pressure dependence [*Rockmann et al.*, 1998; *Stevens and Wagner*, 1989]. This observed inverse kinetic isotope effect of ^{18}O is most likely due to the effect of isotopic substitution on the relative rate of unimolecular dissociation of the HOCO intermediate to reform reagents versus dissociation to products [*Feilberg et al.*, 2002]. This laboratory value was confirmed by [*Brenninkmeijer and Rockmann*, 1997]. They used southern hemisphere aircraft data to calculate the fractionation and derived a value of about -8‰, which is in reasonable agreement.

Consequently both ^{12}CO and $C^{18}O$ will preferentially react with OH, leaving behind CO enriched in ^{13}C and depleted in ^{18}O. One has to bear in mind that below 400 mbar the isotope effect for ^{13}C reverts into an inverse effect, where ^{13}CO reacts faster with OH than ^{12}CO [*Brenninkmeijer*, 1999].

1.3 Seasonal and Interannual Variations and of Atmospheric CO

1.3.1 Seasonal variations

Seasonal variations of atmospheric CO have been reported both on concentration and isotopic ratios [*J Mak et al.*, 2003; *Manning et al.*, 1997; *Novelli et al.*, 1992; *Rockmann et al.*, 2002]. The seasonal cycle for OH generally follows the actinic flux, with maximum in summer and minimum in winter, leading a seasonal cycle for the main CO sink. Stevens et al. have discussed the seasonal variations in the isotopic composition of CO driven by characteristic isotopic signatures of different sources [*Stevens et al.*, 1972].

Based on weekly monitoring CO mixing ratio in eight locations from mid-1988 to December of 1990, Novelli et al. observed that CO mixing ratios as well as the difference in CO levels between northern and southern latitudes varied seasonally and they argued that CO levels were affected by both local and regional scale processes [*Novelli et al.*, 1992].

A large seasonal cycle has been observed in the $^{13}C/^{12}C$ ratio of CO in clean air in the

extratropical southern hemisphere [*Manning et al.*, 1997]. With a 2-D inverse model, Manning et al. relate atmospheric CO concentrations and $^{13}C/^{12}C$ isotopic ratios to the magnitude and distribution of CO sources and explain the average seasonal cycles observed [*Manning et al.*, 1997]. Observed average seasonal cycles can be explained by taking into account seasonal variation in the net $\delta^{13}C$ from surface sources due to the different seasonal patterns of forest and savanna burning as well as the progressive enrichment of ^{13}C in CO with age in the atmosphere [*Manning et al.*, 1997].

Based on measurements of 130 samples collected from the middle troposphere and the boundary layer, Mak and Brenninkmeijer (1998) observed seasonally dependent spatial trends for both CO concentrations and isotopic ratios in different regions, reflecting both the changing relative strengths of CO sources and the strength of CO loss by CO + OH.

The long lifetime of CH_4 indicates that there is little variation in the seasonal or interannual source strength of CH_4-derived CO [*J Mak et al.*, 2003; *J.E. Mak and C.A.M. Brenninkmeijer*, 1998; *Manning et al.*, 1997]. Fossil fuel combustion, the dominant source in the mid-latitude Northern Hemisphere [*J Mak and Kra*, 1999; *Novelli et al.*, 1998b], has been reported to show a seasonal trend [*Randerson et al.*, 1997] and thus lead a seasonal variation of fossil fuel-derived CO [*Gros et al.*, 2001; *Kato et al.*, 2000; *Petron et al.*, 2004; *G Pfister et al.*, 2004; *Rockmann and Brenninkmeijer*, 1997]. Fossil fuel combustion sources are concentrated in 30º-55ºN latitude band [*Khalil and Rasmussen*,

1990], thus they have smaller contribution to the seasonality of tropical and SH CO compared to the mid- to high-latitude NH. Biomass burning varies both spatially and temporally, and is strongest during the dry season, or (generally speaking) January-March for the NH and July-September for the SH [*Crutzen and Andreae*, 1990]. By using a 3-D inverse model [*Bergamaschi et al.*, 2000b] with field measurements of CO concentration and isotopic ratios in Barbados, West Indies (13ºN, 59ºW), Mak and Brenninkmeijer concluded that NMHC oxidation also has seasonal cycles and it appears to be strongest in the summer and weakest in the winter [*J Mak et al.*, 2003].

Fig 1.2 shows the seasonal cycle of CO in the high-latitude Southern Hemisphere during 1994-2004 [*Brenninkmeijer*, personal communication]. [CO] ranged from 35 to 70 ppbv, with seasonal minimum in austral summer (January-February) and seasonal maximum in austral winter (August). The seasonal maximum of $\delta^{13}C$ occurred in November-December, ranging from -25‰ to -27‰, whereas seasonal minimum of $\delta^{13}C$ occurred in March-April, ranging from -31‰ to -32‰. The seasonal maximum of $\delta^{18}O$ occurred in August-September, ranging from -1‰ to 2‰, whereas seasonal minimum of $\delta^{18}O$ occurred in November-December, ranging from -6‰ to -10‰. The annual average of CO concentration (51.9 ppbv) and isotopic ratios ($\delta^{13}C$ = -29.4‰ and $\delta^{18}O$ = -3.6 ‰) at Scott Base in 2000-2003 will be used as CO data in modern atmosphere and compared with preindustrial values (section 4.6).

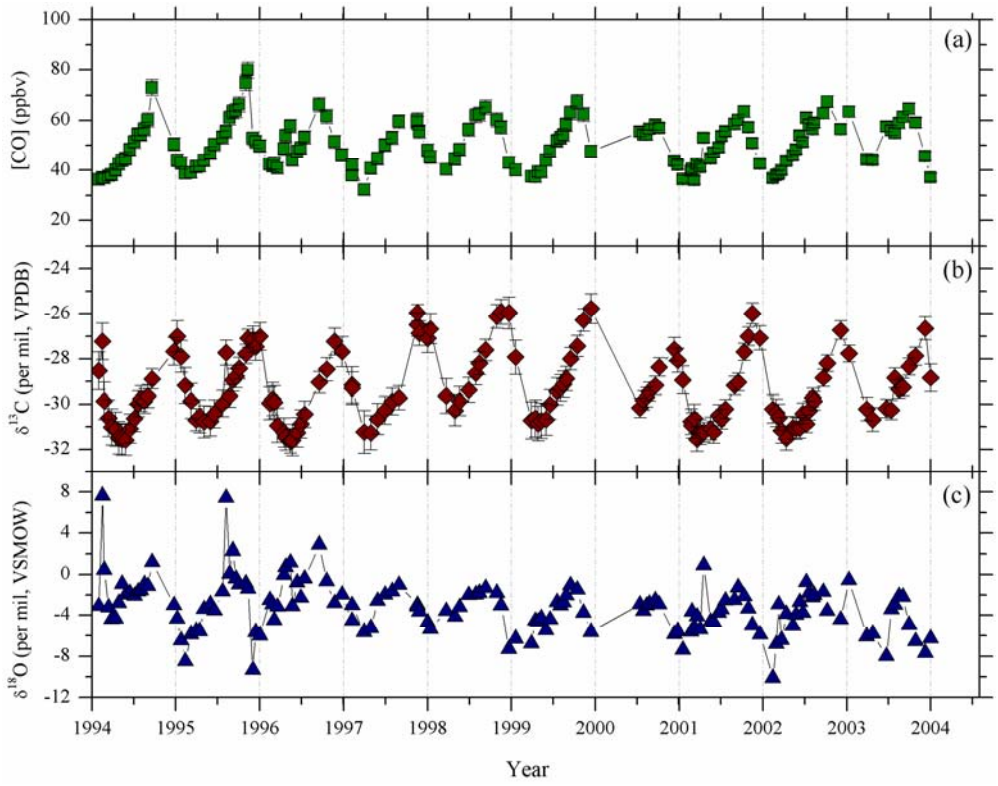

Figure 1.2 Seasonal cycles of (a) [CO], (b) $\delta^{13}C$, and (c) $\delta^{18}O$ from Scott Base, New Zealand at 77º51'S 166º46'E in 1994-2004 [*Brailsford*, personal communication].

Fig 1.3 shows the seasonal cycles of CO in high-latitude of Northern Hemisphere in 1996-1998 [*Brenninkmeijer*, personal communication]. Although there was a gap in sample collection for one and a half months in 1997, we can still observe a seasonal variation of [CO] (~60 ppbv), along with seasonal variation of $\delta^{13}C$ (~4‰) and $\delta^{18}O$ (~14‰). The seasonal maximum of [CO] occurred in March and seasonal minimum occurred in August-September. The seasonal maximum of $\delta^{13}C$ occurred in June and the seasonal minimum occurred in October. $\delta^{18}O$ follows the same temporal structure as [CO], with a minimum in August and a maximum in March. Model simulation helps to better understand the reasons of these seasonal variations [*Bergamaschi et al.*, 2000a;

Bergamaschi et al., 2000b; *L K Emmons et al.*, in preparation; *K.H. Park et al.*, in preparation].

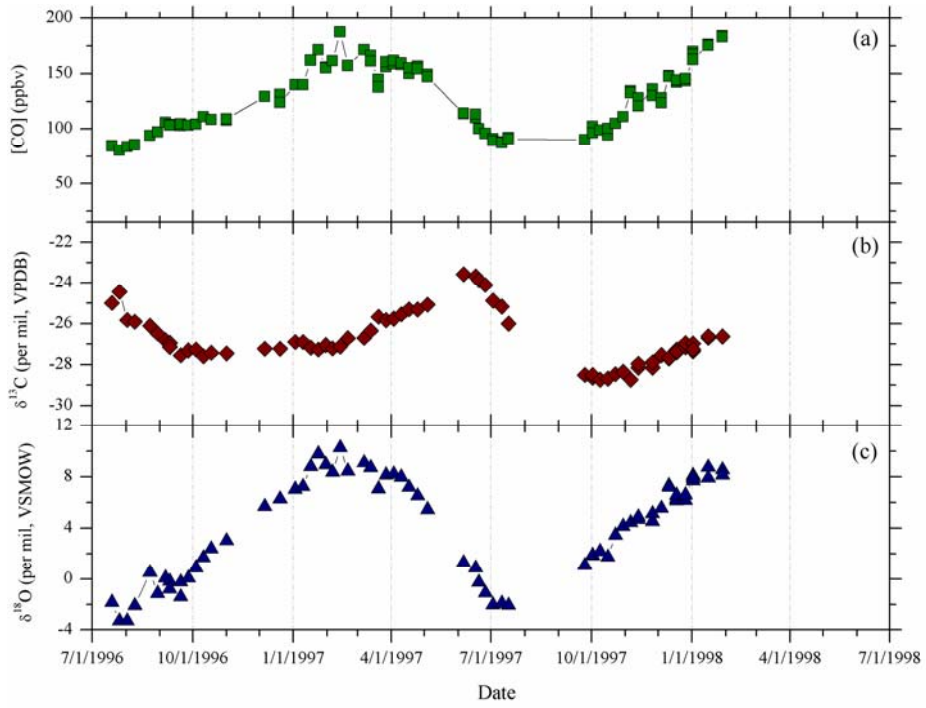

Figure 1.3 Seasonal cycles of (a) [CO], (b) $\delta^{13}C$, and (c) $\delta^{18}O$ from Alert, Canada, at 82º27'N 62º31'W in 1996-1997 [*Brenninkmeijer*, personal communication].

1.3.2 Interannual variations

An increasing trend of atmospheric CO was first recognized in 1979-1982 [*Khalil and Rasmussen*, 1984], however a decrease in global CO was observed in early 1990s [*Khalil and Rasmussen*, 1994; *Novelli et al.*, 1994a].

Observations of CO in different locations between 71 degrees N and 41 degrees S show that atmospheric levels decreased globally between 1990-1993 [*Novelli et al.*, 1994a]. In the Northern Hemisphere, CO decreased at an average rate of 7.3±0.9 ppbv/yr

(6.1%/yr) from June 1990 to June 1993, whereas in the Southern Hemisphere, CO decreased 4.2±0.5 ppbv/yr (7.0%/yr) [*Novelli et al.*, 1994a]. This change was opposite a long-term trend of a 1 to 2 percent per year increase inferred from measurements made in the Northern Hemisphere during the past 30 years [*Novelli et al.*, 1994a]. Subsequent study indicate the globally averaged CO mixing ratio during the period 1990 through 1995 decreased at a rate of approximately 2 ppb/yr [*Novelli et al.*, 1998a].

A more recent study supports previous reports of a decline in tropospheric CO [*Novelli et al.*, 2003]. However, in this study the decrease of CO is found mainly confined to the Northern Hemisphere, where dramatic reductions in fossil fuel emissions occurred in the 1990s [*Boden et al.*, 2009]. In contrast, no significant trend is determined in the Southern Hemisphere between 1991 and 2001 [*Novelli et al.*, 2003]. It is also noticed that globally averaged CO exhibits large interannual variability, primarily reflecting interannual variation in emissions from biomass burning [*Novelli et al.*, 2003]. The exceptionally widespread wildfires in 1997-1998 provided a strong pulse of CO to the atmosphere [*Novelli et al.*, 2003].

The 10-year records of atmospheric CO in Fig 1.2 indicate atmospheric CO concentration was relatively constant high-latitude Southern Hemisphere in 1996-2004. Significant interannual variations in $\delta^{13}C$ and $\delta^{18}O$ are mostly observed during the seasonal minimum and during the seasonal maximum. Both seasonal minimum and seasonal maximum of $\delta^{13}C$ increased at least 1‰ in 1998-2000, whereas seasonal

maximum of $\delta^{18}O$ decrease in 1997-2001 and seasonal minimum of $\delta^{18}O$ increase during the same period.

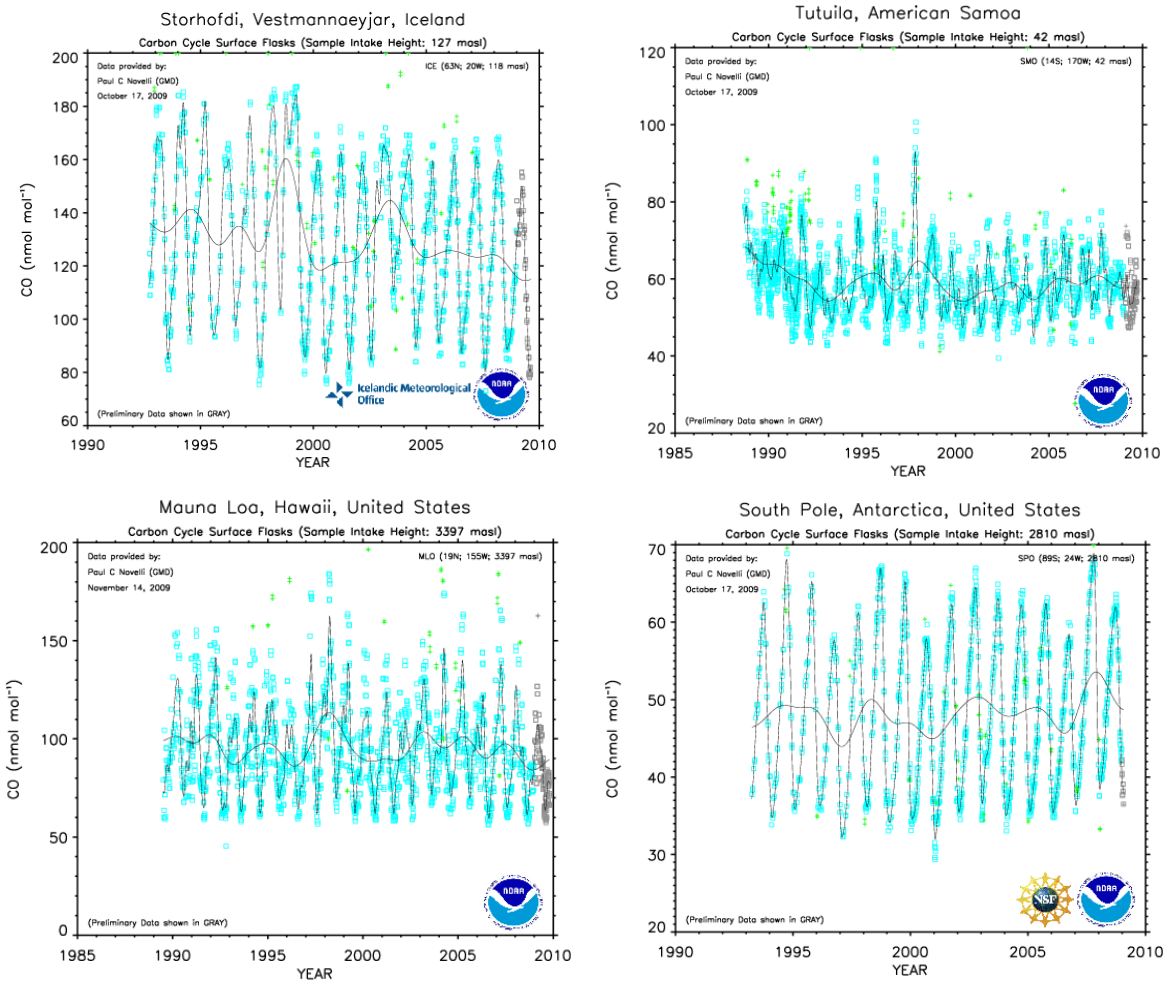

Figure 1.4 Long-term trend of atmospheric CO concentration at three stations: top left (Iceland, 63ºN 1992-2009), top right (American Samoa, 14ºS 1988-2009), bottom left (Mauna Loa, 19.54ºN 1989-2009), and bottom right (South Pole, 89ºS 1992-2009) based on NOAA/ESRL Global Monitoring Division Carbon Cycle Sampling Network (http://www.esrl.noaa.gov/gmd/ccgg/iadv/). Data shown in grey are preliminary.

Fig 1.4 shows atmospheric CO trends in mid-latitude NH (Iceland), tropics (American Samoa and Mauna Loa), and high-latitude SH (South Pole). A slight decrease of CO level starting from early 1990s was found in Iceland and South Pole CO data

indicate a relatively constant CO level over Antarctica during the past two decades. In American Samoa, CO concentration dropped around 20 ppbv in 1988-1993 and kept constant since then.

1.4 Atmospheric Gases in Snow and Ice

Our knowledge of the human's impacts on the contents of the atmosphere comes from direct measurements and studies of the composition of air trapped in ice cores for earlier times [*Battle et al.*, 1996]. Air bubbles trapped in glacial ice provides a means of reconstructing variations in the concentrations and isotope compositions of atmospheric gases over time scales ranging from anthropogenic (last 200 yr) to glacial/interglacial (hundreds of thousands of years) [*Bender et al.*, 1997]. To reconstruct the past trend of atmospheric gases, both firn air and air bubbles trapped in ice core are needed. Air extracted from polar firn provides us information of atmosphere composition during the past several decades with a relatively higher resolution [*Battle et al.*, 1996; *Butler et al.*, 1999; *Francey et al.*, 1999a], whereas air bubbles occluded in ice help us reconstruct past atmospheric histories of some gases such as CH_4 and CO_2 and back to 800,000 years [*Loulergue et al.*, 2008; *Luthi et al.*, 2008; *U. Siegenthaler et al.*, 2005; *Spahni et al.*, 2005] N_2O back to 650,000 years[*Spahni et al.*, 2005].

1.4.1 Gases in Firn

Air extracted from polar firn has been widely measured in a number of studies to reconstruct past atmospheric histories of trace gas mixing ratios [*Butler et al.*, 1999; *Martinerie et al.*, 2009; *Reeves et al.*, 2005a], isotopic ratios [*Assonov et al.*, 2007; *Bernard et al.*, 2006; *Braunlich et al.*, 2001; *Francey et al.*, 1999a; *Rockmann et al.*, 2003a; *Sowers et al.*, 2005b] and elemental ratios [*Battle et al.*, 1996; *Bender et al.*, 1994]. The record of atmospheric halocarbons during the twentieth century from polar firn air demonstrates that natural sources of the CFCs, halons, and SF_6 are minimal or non-existent [*Butler et al.*, 1999; *Martinerie et al.*, 2009; *Reeves et al.*, 2005a]. Historical trends of halon gases in polar firn air from Dome C, Devon Island, and NGRIP also show the concentrations of four halons (H-1301, H-1211, H-2402, and H-1201) to be zero at the base of the firn thus indicating their entirely anthropogenic origin [*Reeves et al.*, 2005b]. $\delta^{13}C$ of atmospheric CH_4 over the last 2 centuries has been reconstructed by analyzing South Pole firn air and a 1.8±0.2‰ increase between 1820 and 2001 has been observed [*Sowers et al.*, 2005b]. One explanation for this enrichment involves a 16 Tg/yr increase in CH_4 emissions associated with biomass burning over the past 2 centuries [*Sowers et al.*, 2005b]. Atmospheric CO trapped in firn air from Berkner Island has been measured to reconstruct the history of CO concentration as well as isotope compositions in the high-latitude SH [*Assonov et al.*, 2007]. Their results suggest that CO has increased by around 38%, from 38±7 to 52.5±1.5 ppbv over a period of roughly 100 years and CO

was isotopically heavier in the past, in agreement with a lower contribution of methane [*Assonov et al.*, 2007].

1.4.2 Gases in Ice

Ice core records provide valuable information on the climate change in the past [*Alley*, 2000]. The ice record of greenhouse gases shows how these gases varied during the past [*Barnola et al.*, 1987; *Chappellaz et al.*, 1997; *Petit et al.*, 1999; *Urs Siegenthaler et al.*, 2005; *Sowers et al.*, 2003; *Spahni et al.*, 2005] and reflects how anthropogenic forcings influence the climate change [*Etheridge et al.*, 1998; *Ferretti et al.*, 2005; *Meure*, 2004; *Meure et al.*, 2006; *Raynaud et al.*, 1993].

The changes in the levels of greenhouse gases observed in ice core overall paralleled, at least at high southern latitudes, changes in temperature, suggesting that greenhouse gases play a significant role as an amplifier of the initial orbital forcing of Earth's climate and also helps to evaluate the feedbacks on the biogeochemical cycles in a climate system in which the components are changing at different rates [*Raynaud*, 1993]. The relationship between the climate change and atmospheric history over the past 420,000 years has been discussed based on Vostok ice core, showing atmospheric concentrations of CO_2 and CH_4 correlate well with Antarctic air-temperature throughout the record [*Petit et al.*, 1999]. Reconstructions of atmospheric N_2O over the past 650,000 year based on Dome C ice core indicate preindustrial maximum N_2O concentration (278±7 ppbv) is

slightly higher than early Holocene values [*Spahni et al.*, 2005]. Reconstructions of atmospheric CO_2 and CH_4 covering the past 800,000 years based on Dome C ice core indicated CH_4 concentration over Antarctica ranged between ~350 and ~800 ppbv and CO2 concentration ranged between 172 and 300 ppmv [*Loulergue et al.*, 2008; *Luthi et al.*, 2008; *U. Siegenthaler et al.*, 2005; *Spahni et al.*, 2005].

High resolution records of trace gases in ice core focus on the past two millennia. High resolution records of greenhouse gases including CO_2, CH_4 and N_2O on Law Dome ice core indicate major increases in CO_2, CH_4, and N_2O concentrations over the past 2000 years followed a period of relative stability beforehand [*Meure et al.*, 2006]. High resolution records of carbonyl sulfide (COS) over the past two millennia from South Pole ice core show that the late 20th century COS levels of 500 ppt are greatly increased over preindustrial levels and represent the highest atmospheric levels over the past 2000 years [*Aydin et al.*, 2008]. A 2000 year atmospheric history of methyl chloride (CH_3Cl) from a South Pole ice core shows a climate-controlled variability and that CH_3Cl levels were elevated from 900-1300 AD by about 50 ppt relative to the previous 1000 years, coincident with the Medieval Warm Period (MWP) and CH_3Cl levels decreased to a minimum during the Little Ice Age (LIA: 1650 - 1800 AD) [*Williams et al.*, 2007].

Compared to greenhouse gases in ice, little is known about CO in core because of experimental challenges such as limitation of sample size [*Z H Wang and Mak*, 2009] and contamination due to in situ production [*Haan et al.*, 2001; *Meure*, 2004]. The pioneering

study on atmospheric CO history in ice core started in 1973 [*Robbins et al.*, 1973], however the CO levels are either too scattered or too high to be interpreted. The more recent CO measurements in polar ice was reported in [*Haan and Raynaud*, 1998; *Haan et al.*, 1996]. CO measurements on Eurocore and D47 ice indicate CO mixing ratio in NH started to increase from 1850, whereas CO levels over Antarctica remained fairly constant between 1860 and 1916 [*Haan et al.*, 1996]. History of atmospheric CO during the last two millennia in Vostok indicates CO levels were relatively constant between 237 BC and 1375 AD and that, by contrast, high variability for CO concentration (100-180 ppbv) in Eurocore over the last 1,000 years indicates CO in Greenland ice could have been altered by in-situ oxidation of organic matters either before or after its trapping in the ice [*Haan and Raynaud*, 1998]. Since Antarctic ice contains much less impurities [*Meure*, 2004] and shows no particular variability in CO concentration [*Haan and Raynaud*, 1998; *Haan et al.*, 1996], we focus on Antarctic ice cores in this study (chapter 4).

1.4.3 Isotopes of Gases in Ice

Ice cores are local paleothermometers, indicating past temperature where they are [*Alley*, 2000]. The stable isotopic composition (δD and $\delta^{18}O$) of ice hase been use to infer paleothermometers based on the linear relationship between the mean annual isotope content of precipitation and the mean annual temperature at the precipitation site [*Jouzel*

et al., 1997]. δD and $\delta^{18}O$ in ice has been used as temperature proxies in different cores in both both hemispheres. δD in the ice of EPICA Dome provides a climate record for the past 740,000 years and shows less pronounced warmth in interglacial periods in Antarctica, but a higher proportion of each cycle was spent in the warm mode between 740,000 and 430,000 years ago compared with the period over the past 430,000 years [*Augustin et al.*, 2004]. The oxygen isotopes in the NGRIP ice imply that climate was stable during the last interglacial period, with temperatures 5ºC warmer than today [*Andersen et al.*, 2004].

Isotopic ratios of trace gases in air bubbles trapped in ice assist in determining the various sources and sinks in the past and their historic relative magnitudes [*Ferretti et al.*, 2005; *Francey et al.*, 1999b; *Schaefer and Whiticar*, 2008; *Schaefer et al.*, 2006; *Sowers et al.*, 2002; *Sowers et al.*, 2005b]. Harmon Craig pioneered the study on isotope composition of CH_4 in polar ice cores by measurements of several large (~25 kg) samples, and found an increase of 2‰ of $\delta^{13}CH_4$ over the industrial period, indicating anthropogenic biomass burning is the principle cause of this enrichment [*Craig*, 1953; *Craig et al.*, 1988b]. More recent high resolution reconstruction of the CH_4 concentration and $\delta^{13}CH_4$ in Law Dome ice core over the last 2,000 years provides a more comprehensive insight into the unexpected variability of the CH_4 budget during the late preindustrial Holocene (LPIH) [*Ferretti et al.*, 2005]. Their data suggest that both human activities and natural climate change influenced preindustrial biomass burning emissions,

which causes the 2‰ shift of $\delta^{13}CH_4$ over the last 2,000 years [*Ferretti et al.*, 2005]. Records of the isotopic composition of atmospheric N_2O from Antarctica ice core and GISP II ice core help to determine the changes in the various sources and sinks of atmospheric N_2O over the last 250 years, which is important for a better understanding of the biogeochemical cycles involving atmospheric N_2O [*Bernard et al.*, 2006; *Sowers et al.*, 2002]. The observed depletion of 1.9‰ for $\delta^{15}N$ and 2.9‰ for $\delta^{18}O$ since 1785 in [*Sowers et al.*, 2002] supports the previous prediction of 30% increase in total N_2O emissions during this time, which are primarily related to agricultural activities. A comparable decrease of 2.8‰ for $\delta^{15}N$ and 1.8‰ for $\delta^{18}O$ since 1700 observed in [*Bernard et al.*, 2006] also supports the increasing importance of agriculture for the present atmospheric N_2O budget.

1.5 Physical Characteristics of Polar Snow and Ice

1.5.1 Structure of Firn Layer

Firn is the porous layer of compacted snow, usually with a thickness between 40 m to 100 m [*Trudinger et al.*, 2002]. The snow and firn layers usually consist of three vertical zones according to gas transport [*Sowers et al.*, 1992]: convective zone, diffusive zone, and non-diffusive zone (Fig 1.5-1.6). The air in the upper convective zone is well mixed with surface atmosphere by wind convection [*Colbeck*, 1989]. Based on $\delta^{15}N$ and $\delta^{18}O$

firn measurements, the thickness of this zone was estimated to be zero at DE08 [*Trudinger et al.*, 1997], less than 1 m at South Pole [*Battle et al.*, 1996] and 13 m at Vostok [*Bender et al.*, 1994]. Below, gas diffuses in the open pore space until the open porosity of the firn becomes too low, at a depth defined from modeling as the lock-in depth (LID), where air no longer mixes with surface atmosphere [*Landais et al.*, 2006]. Air begins to be trapped in bubbles a few meters below the LID, at the bottom of a non-diffusive zone and the close-off depth (COD), where the complete bubble close-off physically isolates air from the atmosphere [*Landais et al.*, 2006]. The COD can be estimated from firnification models [*Martinerie et al.*, 1994] and LID can be determined from the air isotopic composition ($\delta^{15}N$ and $\delta^{40}Ar$) [*Schwander et al.*, 1993; *Sowers et al.*, 1992]. Due to different temperature and accumulation rate, the COD is estimated to be 98 m at Dome C [*Landais et al.*, 2006], whereas this becomes 116 m at the South Pole [*Battle et al.*, 1996].

Non-diffusive zone is thus the layer between the LID and the COD, with a thickness of 2 m at Vostok [*Bender et al.*, 1994], 7 m at South Pole [*Battle et al.*, 1996], and 13 m at Berkner Island [*Landais et al.*, 2006]. According to the thickness of the convective zone and non-diffusive zone of different cores, the diffusive zone is thus the main component of the firn [*Landais et al.*, 2006].

The schematic diagram showing the three vertical zones of firn layer along with density change and gradual compression process of snow is presented in Fig 1.5.

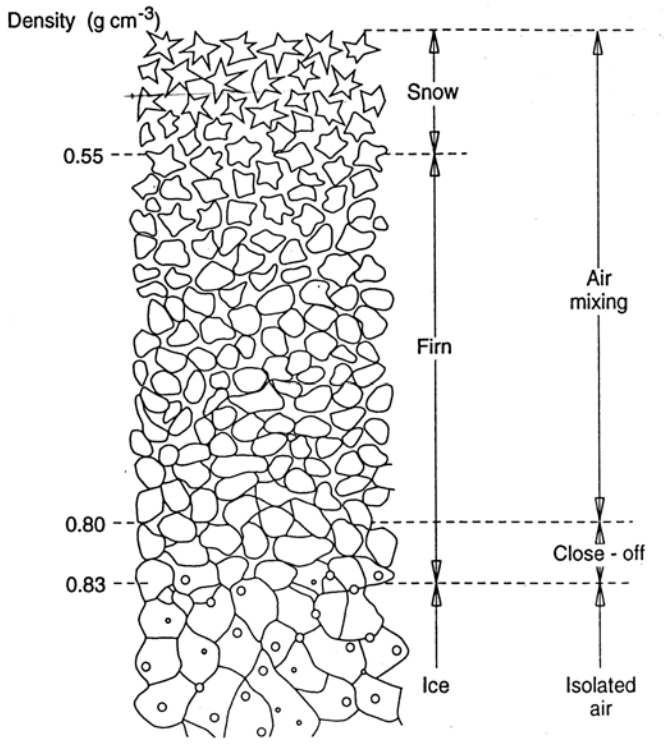

Figure 1.5 Schematic diagram showing the three different zones of firn layer. The depth at which the pore close-off occurs is typically in the range: 50-100m below the surface, depending on the site characteristics (temperature and accumulation rate)[*Barnola et al.*, 1991; *Raynaud et al.*, 1993].

Figure 1.6 describes the vertical profile of density and porosity of firn in Law Dome ice core (66°44'S, 112°50'E, 1390 m a.s.l.) [*Meure*, 2004]. The density at the surface is around 0.3-0.35 g cm^{-3}, followed by rapid rises to about 0.6 g cm^{-3} by a depth of 20 m due to settling and packing. Below, recrystallization and other processes cause a slower increase in density, which continues until individual grainsare fused together into an impermeable mass of glacial ice [*Herron and Langway*, 1980]. Most bubbles close off between 70-80 m, at average density of 0.805 g cm^{-3} in Law Dome ice core [*Meure*, 2004]. The closed porosity increases rapidly as the density reaches the point where

bubbles form and decreased at a greater depths due to compression [*Meure*, 2004].

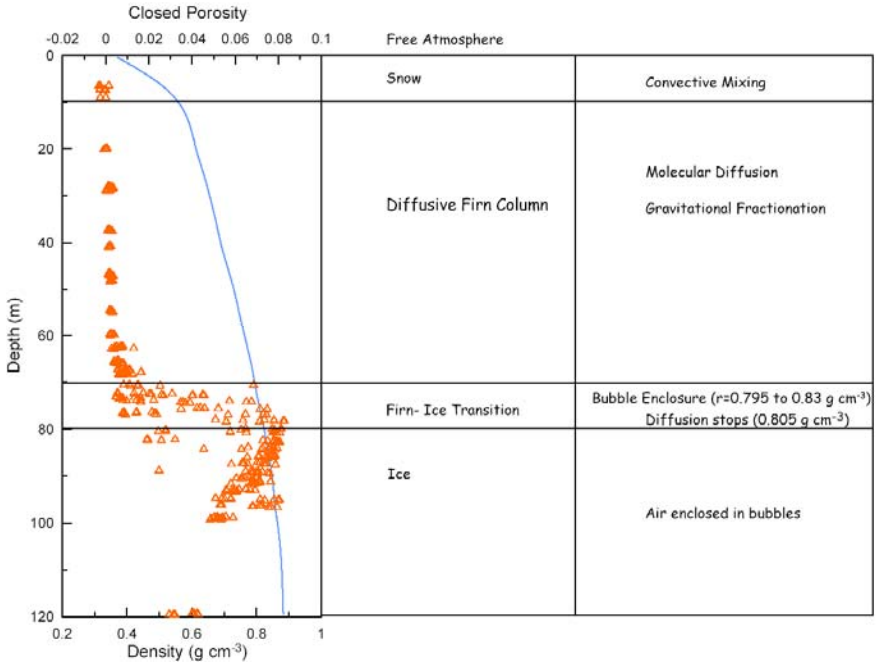

Figure 1.6 Different zones and modes of air movement in the firn layer with increasing depth at the firn at DE08-2 (Law Dome ice core, 16 km east of Law Dome summit). Solid line is density and triangles are porosity [*Meure*, 2004].

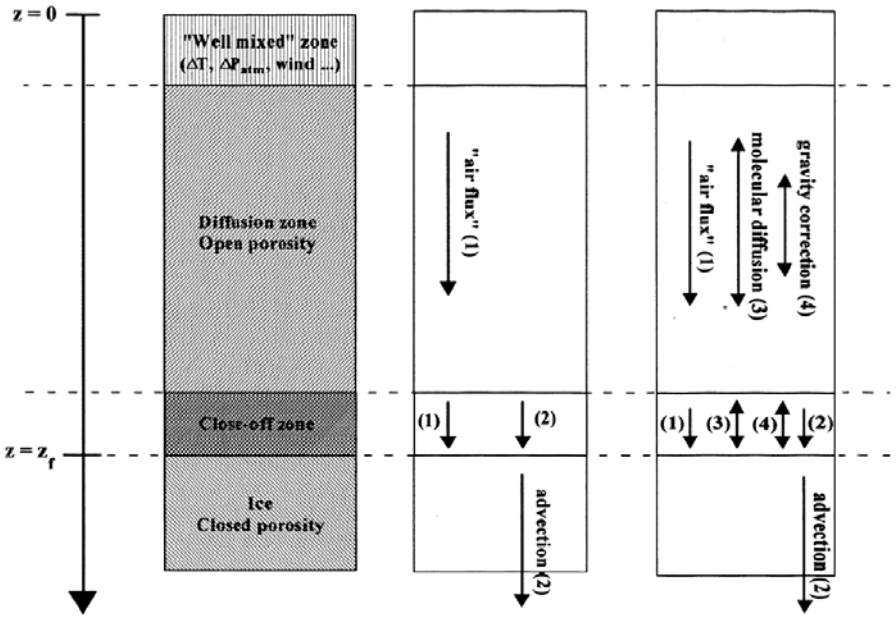

Figure 1.7 Schematic diagram of the air movement in firn layer, which is accounted for in

the firn diffusion model: (left) firn, (middle) air, and (right) trace gas [*Rommelaere et al.*, 1997].

Fig 1.7 is the schematic view of the physical processes in firn layer that are accounted for in the firn diffusion model [*Rommelaere et al.*, 1997]. Arrow (1) denotes air mixing by pressure and temperature gradient down to a few meters from the surface. Arrow (3) denotes molecular diffusion in the open pore space. The diffusion is affected by gravitation, thus the entrainment toward the deeper firn depends on the molar mass (arrow 4). A downward air flux (arrow 1) in the open porosity zone due to bubble closure removing air from open pores; this removed air (arrow 2) has to be replaced by air coming from the upper parts of the firn, thus creating this downward flux [*Rommelaere et al.*, 1997].

1.5.2 Impacts on Firn Air Measurements

The diffusion of gas determines the vertical distribution of gas concentration [*Battle et al.*, 1996; *Bender et al.*, 1997], and the factors including gravitational and thermal fractionation influence the isotopic ratios of trace gases [*Craig et al.*, 1988a; *Severinghaus et al.*, 2001; *Sowers et al.*, 1989].

The diffusivity of certain elements or compounds decreases with increasing mass and increasing atomic or molecular diameter, resulting in certain compound and each isotope of a compound diffuses at a certain rate [*Bender et al.*, 1997]. Light isotopes diffuse faster than heavy isotopes, thus the concentration of certain gas in firn air will be more

depleted in heavy isotopes than was the atmosphere at the time it had the same concentration as a firn air sample [*Bender et al.*, 1997]. Battle et al. suggest the impact of differential diffusivity to be taken into account when interpreting data on the concentration and isotopic composition of gases in firn air and ice cores [*Battle et al.*, 1996]. This impact is taken into account in NEEM firn data, but not in our ice core data because the significant variations of concentrations occur a much longer time scales than firn processes [*Martinerie*, personal communication]. This impact is considered to be negligible in our ice core data due to the small variations of [CO] in decadal scale (chapter 4).

Additional factors affecting the composition of air in the firn include gravitational fractionation [*Craig et al.*, 1988b; *Sowers et al.*, 1989] and thermal fractionation [*Severinghaus et al.*, 2001]. The relative enrichment with depth for different species is directly proportional to the mass difference [*Craig et al.*, 1988a] and is around 0.005‰/amu per meter at typical firn air temperature [*Bender et al.*, 1997]. Severinghaus et al. first recognized that the thermal fractionation influences the isotopic composition of firn air and found heavier gases or isotopes enriched in colder regions [*Severinghaus et al.*, 2001]. However, due to the relative stable temperature in the past 1000 years, thermal diffusion is considered to be negligible in our ice core measurements (chapter 4). Gravitational fractionation for firn can be quantified with the difference of $\delta^{15}N$ of N_2 between close-off depth and surface. The value of difference of $\delta^{15}N$ of N_2 between

close-off depth and surface is 0.5‰ at South Pole and 0.25‰ at Berkner Island, respectively [*Landais et al.*, 2006]. The quantification of gravitationalfractionation will be taken into account in our South Pole and D47 ice core observations in section 4.4.

1.6 Concluding Remarks

The purpose of this chapter is to outline the objectives to study atmospheric CO in ice core and basic physical characteristics of polar snow and ice. As an important sink for OH radical in the atmospheric, CO was considered to play an important role in controlling the oxidizing capacity of the atmosphere. CO was also identified as a significant indirect greenhouse gas due to its close link with atmospheric CH_4 and O_3. Isotopic compositions ($\delta^{13}C$ and $\delta^{18}O$) of atmospheric CO help to determine the various sources and their relative magnitudes based on that certain sources have inherent isotopic signatures**.** Therefore, study on isotopic compositions of atmospheric CO of the air trapped in ice helps better understand the CO budget in paleoatmosphere and the CH_4-OH-CO paleochemistry.

Firn layer consists of three regimes based on air transport: convective zone, diffusive zone and non-diffusive (or close-off zone). Physical processes in the firn layer, including diffusion, gravitational fractionation, and thermal fractionation influence the composition as well as isotopic ratios of the enclosed air. Molecular diffusion and thermal

fractionation is considered to be negligible in our ice core data. However, it is important to consider the gravitational fractionation in our ice core data.

Chapter 2. Measurement of Firn and Ice Core Air Samples

The recent comprehensive study on ice core CO concentration analysis was reported in [*Haan and Raynaud*, 1998; *Haan et al.*, 1996]. Their method consists of melting and refreezing the ice in order to extract air, which is then separated by gas chromatography (GC) and analyzed using a mercuric oxide reduction detector (RGD). A sample of about 50 g ice is used, giving enough sample size for the detection.

The experimental focus of this thesis is to derive detailed records of preindustrial atmospheric CO concentrations and isotopic ratios from Antarctic ice cores with high analytical precision. Such measurements allow real atmospheric variations to be reconstructed and their causes to be investigated. Unfortunately, based on the ~50 ppbv preindustrial CO mixing ratio in Antarctic ice core reported in [*Haan and Raynaud*, 1998; *Haan et al.*, 1996], the amount of CO trapped in 1 kg ice is only around 5 nL (STP). Because of this limitation of sample size and the arising experimental challenges [*Z H Wang and Mak*, 2009], none has been reported in ice core CO isotopes analysis yet.

In this study, air samples are extracted from ice core followed using the wet extraction technique in [*Haan et al.*, 1996], where the bubbles are opened by melting the ice samples under vacuum. An on-line cryogenic vacuum extraction followed by continuous-flow isotope ratio mass spectrometry (CF-IRMS) has been built up for

measuring stable isotope ratios ($\delta^{13}C$ and $\delta^{18}O$) of atmospheric carbon monoxide (CO) from ice core and firn air samples. Several diagnostic tests relevant to the performance of the measurement of the isotope compositions of the air samples are considered in detail in this chapter.

2.1 Instrumentation

2.1.1 Introduction of CF-IRMS

Off-line extraction followed by conventional dual-inlet IRMS method has been used for measuring stable isotopes of CO in the ambient atmosphere [*C. A. M. Brenninkmeijer*, 1993; *J Mak and Kra*, 1999; *J. E. Mak and C. A. M. Brenninkmeijer*, 1998]. This CO analysis with IRMS is based on electron impact ionization and followed by acceleration and subsequent monitoring of the relative abundances of masses 44, 45, and 46 [*J. E. Mak and Brenninkmeijer*, 1994]. This dual inlet method provides reliable repetition of measurements by supplying continuous streams of the reference and sample gases, which are sequentially switched by changeover valves. Sample size requirements are mostly determined by the minimum operating pressure needed to generate a reasonable current at the collector end, which are on the order of 0.1 μmol [*Merritt and Hayes*, 1994]. For the Finnigan Delta Plus used in this study, the minimum sample size is around 3-5 μL (STP) of CO_2 to provide reliable precisions for both $\delta^{13}C$ (±1σ uncertainty 0.4‰) and $\delta^{18}O$ (±1σ

uncertainty 0.5‰) [*J. E. Mak and Brenninkmeijer*, 1994; *J E Mak and W B Yang*, 1998].

Continuous-flow isotope ratio mass spectrometry (CF-IRMS), which is based on the introduction of a sample in a helium stream via capillary leak directly into the ion source [*J E Mak and W B Yang*, 1998], can reduce the sample size to subnanomoles [*Merritt and Hayes*, 1994; *Merritt et al.*, 1995]. The earliest application of CF-IRMS was presented in [*Sano et al.*, 1976], who coupled a GC to an organic MS by means of a combustion furnace to identify ^{13}C-labeled peaks as indicative of metabolic activity. Matthews and Hayes et al. reported a GC-combustion-MS system based on a single collector organic MS soon after [*Matthews and Hayes*, 1978]. Since 1990s, experiments by [*Merritt and Hayes*, 1994; *Merritt et al.*, 1994] suggest CF-IRMS can be successfully applied to the analysis of atmospheric trace gases. CF-IRMS systems have been widely developed for measuring isotopic ratio of atmospheric CH_4 [*Merritt et al.*, 1995; *Rice et al.*, 2001], CO_2 and N_2 [*Ricci et al.*, 1994], N_2O [*Rockmann et al.*, 2003b], H_2 [*Rhee et al.*, 2004] and volatile organic compounds (VOC) in ambient air [*Rudolph et al.*, 1997].

Mak and Yang have developed a method to analyze both ^{13}C and ^{18}O in atmospheric CO using CF-IRMS [*J E Mak and W B Yang*, 1998]. As mentioned, the primary advantage of using CF-IRMS for CO isotope analysis is that sample size requirements are much less, by 2 or more orders of magnitude, and analysis times are reduced [*J E Mak and W B Yang*, 1998]. In the present study, we use a new cryogenic vacuum extraction system, which is principally based on the approach originally outlined in previous studies

[*C.A.M. Brenninkmeijer*, 1993; *Stevens and Krout*, 1972], to extract and oxidize CO on-line, combined with similar technique to separate CO_2 in GC and load into a Finnigan Delta Plus IRMS [*J E Mak and W B Yang*, 1998]. This new system is thus applied to analyze isotope ratios of CO for small air samples (~250-650 pmol CO), specifically for CO in air bubbles trapped in Antarctic ice cores.

A recent study by Tsunogai et al. 2002 has shown the advantage of isotope analysis for atmospheric CO using CF-IRMS by simultaneously monitoring the CO^+ ion currents at masses 28, 29, and 30 [*U. Tsunogai et al.*, 2002]. However, both preparing CO standard gas with known isotope ratios and extracting CO from air present challenges. Furthermore, high precision mass spectrometry is usually based on CO_2 [*Brenninkmeijer*, 1999]. Thus in the present study we still use the technique of oxidizing CO to CO_2 [*C.A.M. Brenninkmeijer*, 1993; *Stevens and Krout*, 1972].

2.1.2 Instrumentation

As mentioned, details of the cryogenic extraction system have been discussed in [*C. A. M. Brenninkmeijer*, 1993; *Stevens and Krout*, 1972], thus a brief summary including modifications made in this study is give here.

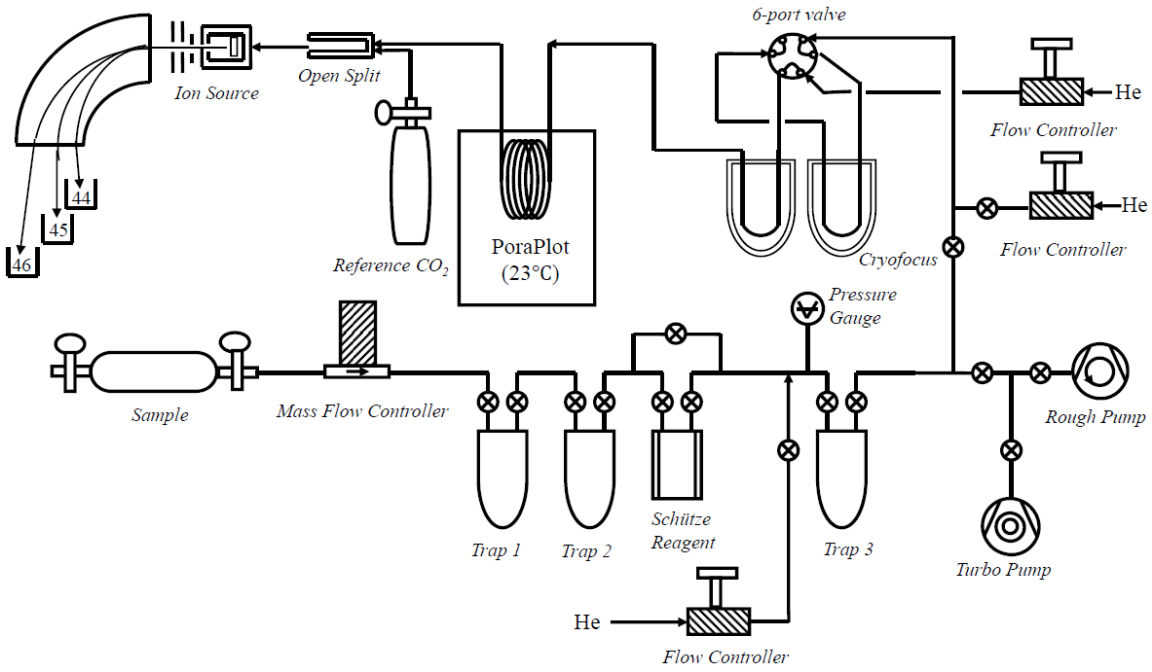

Figure 2.1 A schematic diagram for the cryogenic extraction system attached with gas chromatography - isotope ratio mass spectrometry (GC-IRMS) which was used to measure mixing ratio, $\delta^{13}C$ and $\delta^{18}O$ of CO in ambient air, firn air and ice core air samples.

The schematic diagram of the on-line analysis system in the present study is presented in Fig 2.1. Air sample canister is attached to the inlet of the cryogenic vacuum system (bottom part of the panel). After passing through the cryogenic cleanup traps (1/4" OD four-loop, borosilicate glass), atmospheric CO_2, H_2O, N_2O and other condensable species present in air samples are removed due to condensation at liquid nitrogen temperature. The purified CO is then selectively and quantitatively oxidized to CO_2 by acidified I_2O_5 on a silica gel support (Schütze reagent [*Schütze*, 1949], prepared according to [*Smiley*, 1949]), retaining the original ^{18}O signature of CO [*Stevens and Krout*, 1972]. A bypass is installed for the Schütze reactor tube as well, allowing

evaluation of the complete stripping of CO_2 (section 2.2.1) and continuous back-flushing the system with ultra high pure (UHP) helium between sample conversions [*C. A. M. Brenninkmeijer*, 1993]. The degradation of Schütze is indicated by its color change, from yellow to brown, making the replacement necessary [*J E Mak and W Yang*, 1998].

The CO-derived CO_2 collected in trap 3 (1/4" OD four-loop, borosilicate glass) is then eluted with cryogenically purified ultrapure helium with flow rate of 40 mL/min for 5 minutes and cryogenically focused in a microvolume trap of the modified Finnigan Preconcentration unit through a Valco six-port valve (Fig. 2.1). The cryofocus trap is then heated to room temperature and the CO_2 is loaded into the GC column (25m×0.25mm Poraplot Q capillary) with helium flow of 1mL/min from the back inlet of GC (Fig 2.1). The resolved CO_2 then passes through an open split into the Finnigan Delta plus isotope ratio mass spectrometer at a flow rate of about 0.4 mL/min and ~2/3 of the sample is lost through the open split.

The volume of the first two cleanup traps are both ~10 mL and that for the collection trap is ~13 mL. The volume of the Schütze reagent is 2 mL. Ultra-torr 1/4" fittings (Swagelok) are used for the pluming of 1/4" glass parts. The mesh size of glass beans used is 8-12 and glass beans used in each trap is ~0.5 mL. The pure reference CO_2 (OzTech Trading Corporation) used to calibrate the mass spectrometer during a sample injection has a $\delta^{13}C$ of -40.73‰ (VPDB) and a $\delta^{18}O$ of 10.39‰ (VSMOW).

The detailed calculation of $\delta^{13}C$ and $\delta^{18}O$ is based on the two observable ion-current

ratios (45/44 and 46/44) as discussed in a previous study [*Santrock et al.*, 1985], which is carried out by the Finnigan software ISODAT 2.0. Basic ideal is ^{17}O-correction algorithm: i) abundance of the ^{17}O-bearing molecules with mass 45 is calculated from an assumed relationship between the ^{17}O and ^{18}O isotopic abundances; ii) $^{13}C/^{12}C$ isotope ratios is calculated by correcting the raw isotope ratio 45/44 for the participation of ^{17}O-bearing molecules, and iii) the ^{18}O abundance is determined by correcting the raw isotopic ratio 46/44 for the participation of ^{17}O-bearing molecules and based on the calculated $^{13}C/^{12}C$ isotope ratios [*Assonov and Brenninkmeijer*, 2003; *Santrock et al.*, 1985].

$\delta^{13}C$ of the original CO is determined by the $\delta^{13}C$ of derived CO_2, whereas $\delta^{18}O$ is determined based on calibration gas (section 2.6) [*C.A.M. Brenninkmeijer*, 1993]. The mixing ratio of CO for an air sample is determined by the ratio of peak areas between a sample and a calibration gas.

2.2 Diagnostic Experiments

Diagnostic experiments have been conducted on the cryogenic extraction system, and results indicate this new technique produces reliable isotope ratios for 100 mL air samples with CO mixing ratio as low as 60 ppbv (~270 pmol CO). The diagnostic tests include analytical blank tests, precision tests and accuracy tests. Analytical blank is lower than 40 pmol CO for 100 mL air sample (table 2.1). Analytical precision of 2 ppb ($\pm 1\sigma$)

for CO mixing ratio, 0.2‰ (±1σ) for $\delta^{13}C$ and 0.6‰ (±1σ) for $\delta^{18}O$ can be obtained for sample size of 268 pmol CO (100 mL sample at STP with CO mixing ratio of 60 ppbv). Meanwhile, both $\delta^{13}C$ and $\delta^{18}O$ from CF-IRMS were compared with those from dual inlet IRMS to examine the accuracy of this new technique (table 2.3). Diagnostic analysis carried on artificial bubble free ice provides the ice blank and characterization of total system blank (Schütze blank plus ice blank).

2.2.1 Bypass Blank

A major issue that has to be clarified is the complete stripping of the original CO_2 content of the air prior to the oxidation by Schütze reagent [*C. A. M. Brenninkmeijer*, 1993]. To determine the breakthrough of CO_2 through trap 1 and trap 2, different samples of the cylinder air (section 2.7) and room air are processed through the bypass from July 2006 to February 2007, with flow rates ranging from 25 mL min^{-1} to 100 mL min^{-1}, collection time ranging from 5 min to 30 min, downline pressure ranging from 50 mbar to 140 mbar. The [CO] from bypass blank was observed to be 3.8 ppbv, averaged from 40 runs. Large discrepancies of the isotopic ratios were observed among the replicates, due to tiny peak peak height smaller than 30 mv. This is not a concern since the bypass blank will be combined with the blank derived from Schütze reagent, giving the Schütze blank.

2.2.2 Schütze Blank

As mentioned in section 2.1.2, the Schütze reagent effectively, selectively and quantitatively converts CO to CO_2 at room temperature, preserving the original carbon isotopic ratio of the CO [*Stevens and Krout*, 1972].

Table 2.1 Schütze blank of the cryogenic system determined with zero air with flow rate of 50 mL/min[#]

Date	Sample Volume (mL)	Collection time (min)	CO blank (pmol)	$\delta^{13}C$ (‰, VPDB)	$\delta^{18}O$ (‰, VSMOW)
7/30/2008	100	2	38	-14.8	33.7
7/30/2008	100	2	38	-15.4	33.0
7/30/2008	250	5	49	-15.6	33.0
7/30/2008	500	10	68	-15.2	34.2
7/30/2008	750	15	89	-15.3	33.9
7/30/2008	1500	30	145	-15.0	33.8
5/14/2009	100	2	39	-15.2	33.1
5/20/2009	100	2	39	-15.0	33.1
5/21/2009	100	2	38	-15.3	33.6
5/22/2009	100	2	37	-15.4	33.0
6/10/2009	100	2	40	-14.9	33.6
6/13/2009	100	2	34	-15.2	33.9
6/14/2009	100	2	32	-15.6	33.8
6/15/2009	100	2	39	-14.7	33.4

Note: [#]: flow rate analysis is discussed in section 2.3.

The possible contaminants released from Schütze reagent have been discussed in [*C. A. M. Brenninkmeijer*, 1993]: water, trace amount of I_2, and SO_2. The impact due to these contaminants is reduced by cooling trap 3 with dry ice-alcohol bath when transferring CO_2 to the cryofocus. To quantify the Schütze blank signal, a flow of zero air devoid of any CO is processed through Schütze reagent. Zero air is generated by passing ambient air through a platinum catalyst heated to 200ºC followed by a molecular sieve trap to

remove large fraction of CO_2, H_2O, N_2O and NMHC [*J.E. Mak*, 1992]. Characterization of Schütze blank is crucial for the correction of sample signals. Air sample signal will be corrected by subtracting from this Schütze blank. Schütze blanks estimated from July 2008 to June 2009 were list in Table 2.1. The averaged [CO] blank is dependent on collection time and it is ~68 pmol for 10 min collection, which is around 11 ppbv. The isotopic ratios are also consistent during the period of the study. The blank is dependent on the collection time.

2.2.3 Ice Blank

For ice core analysis, the system blank includes the Schütze blank and ice blank. System blank is estimated to be around 60 pmol for 10 minutes collection time. Ice blank is determined by tests base on artificial bubble free ice from LGGE (Laboratoire de Glaciologie et Géophysique de l'Environnement), France (table 2.2). Both monocrystalline and polycrystalline bubble free ice core samples were tested, and no significant difference was found for their blanks. Ice blank is independent on the mass of ice. A large ice blank of 140 pmol CO was observed, which decreased significantly after the ice was flushed with zero air for a few times to a level of 20 pmol CO. Thus we suspect this large blank arises from CO adsorption on the ice surface. The bubble free ice was also tested with or without light exposure to rule out the possibility of photochemical production. The isotope composition ($\delta^{13}C$=-15‰) of the ice blank and the similar blank

between light and dark environment (table 2.2) indicates the ice blank is from air diffusion/adsorption not in situ photochemical production.

Table 2.2 Ice blanks tested with calibration gas and artificial bubble free ice from LGGE, France.

Artificial ice type	Weight (g)	CO blank (pmol)	$\delta^{13}C$ (‰, VPDB)	$\delta^{18}O$ (‰, VSMOW)
Polycrystalline ice	256	22	-15.8	33.2
Polycrystalline ice	385	31	-15.6	33.3
Monocrystalline ice	200	9	-14.9	33.7
Monocrystalline ice*	275	22	-15.2	32.3
Monocrystalline ice	150	31	-15.2	33.4
Monocrystalline ice	347	18	-15.9	33.3

Note: *: Dark test: glass container was wrapped with aluminum foil during the experiment.

2.3 Flow Rate Analysis

In order to determine the optimal flow rate when processing samples, an ambient air sample (395ICE) was processed with four different flow rates: 25, 50, 75, and 100 mL min^{-1}. For the same amount of air sample (100 mL at STP), running with high flow rate will shorten the collection time and reduce Schütze blank, however stripping of CO_2 in the cleanup traps may not be complete and yield may decrease. Due to the tiny amount of CO_2 (5-15 nL at STP) in the samples, the precise amount of CO_2 is difficult to be determined volumetrically with the method in [*C. A. M. Brenninkmeijer*, 1993]. Consequently, quantification for the yield of this new extraction line shows its challenge. There are two reasons making us believe yield is not a concern in this study: first, the

measured [CO] at different flow rates between 25 mL min^{-1} and 100 mL min^{-1} has a good linearity with flow rate, indicating yield does not change with this range of flow rate; second, the retention time of derived CO_2 through the collection trap (trap 3) with flow rate of 25 mL min^{-1} in this new extraction line is large than that in [*J. E. Mak and Brenninkmeijer*, 1994] and the glass wool and glass beans in trap 3 also increased the trapping efficiency, supporting the evidence that yield is not a concern at this flow rate.

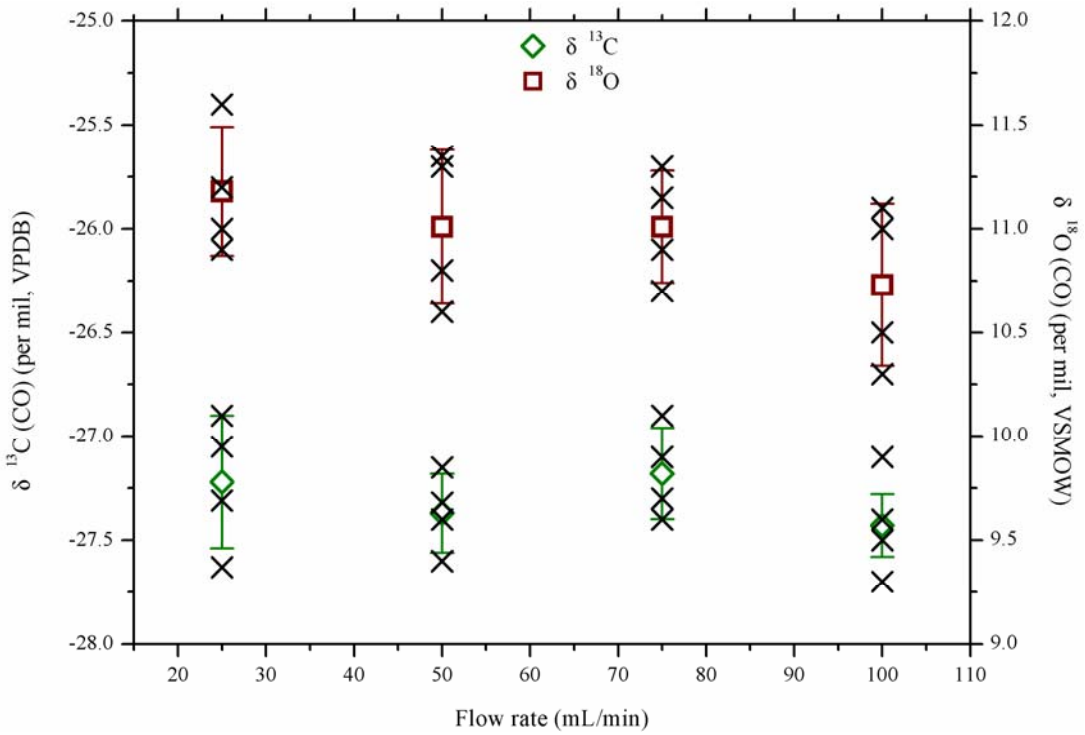

Figure 2.2 The isotopic ratios of Iceland air sample (395ICE) measured based on different flow rate and the same sample size (100 mL at STP). Details on field sample processing are presented in section 2.7.

Fig 2.2 presents the isotopic ratios of the air sample analyzed with different flow rates. No significant different was observed among different flow rates, indicating flow rates between 25 mL min^{-1} and 100 mL min^{-1} do not affect the isotopic ratios.

2.4 Reproducibility Analysis

High analytical precision, which indicates the reliability of our analysis method, is significant for our ice core measurements. Eight Iceland field air samples were processed to give the precision of our measurements and results are shown in Fig 2.3. More than three replicates were processed for each air sample with a sample volume of 100 mL (STP).

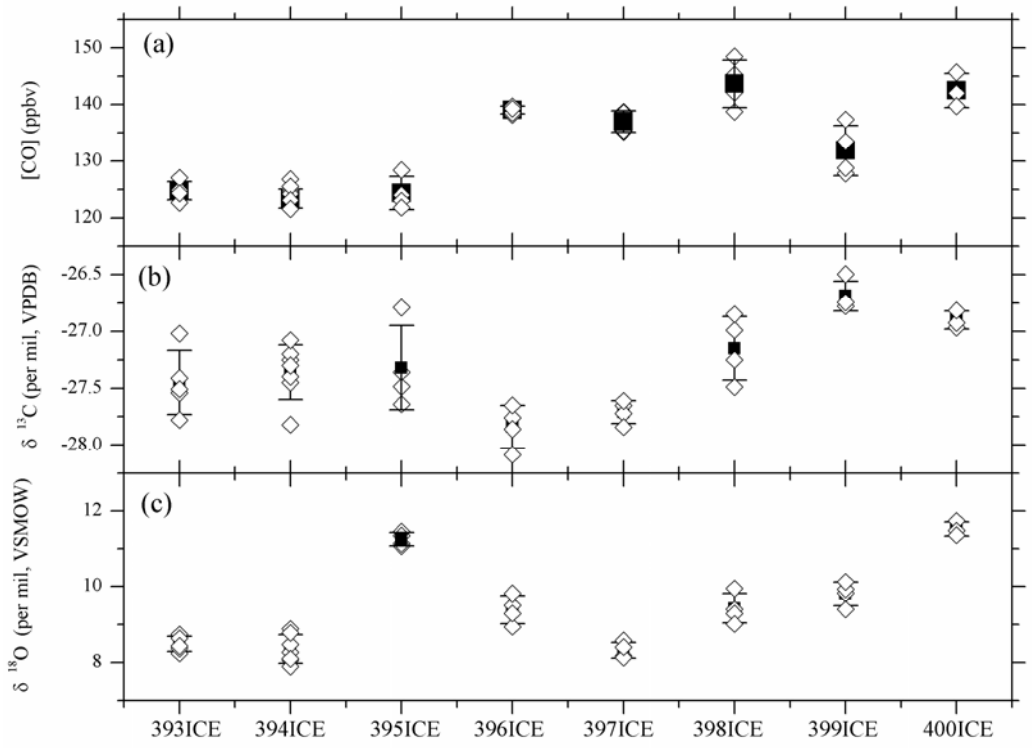

Figure 2.3 CO concentration, $\delta^{13}C$, and $\delta^{18}O$ of the eight field air samples. All sample runs are shown as open diamonds, averages of each sample are shown as close squares, and error bars are 1σ standard deviations. (a) [CO]: with average error of 2.6 ppbv; (b) $\delta^{13}C$: with average error of 0.2‰; (c) $\delta^{18}O$: with average error of 0.3‰.

The reproducibility was estimated as the ±1σ standard deviation of CO concentration

as well as both isotopic ratios. Error bars in Fig 2.3 indicate our precisions for all the eight air samples. Analytical precision of 2.6 ppb (±1σ) for CO mixing ratio, 0.2‰ (±1σ) for $\delta^{13}C$ and 0.3‰ (±1σ) for $\delta^{18}O$ can be obtained for 100 mL(STP) air with CO mixing ratio of 120-140 ppbv.

2.5 Accuracy Analysis

Field air samples were routinely processed based on the classical extraction method and dual-inlet method in IRMS to produce both mixing ratio and isotope signatures of CO [*J Mak and Kra*, 1999; *J. E. Mak and Brenninkmeijer*, 1994; *J. E. Mak and C. A. M. Brenninkmeijer*, 1998]. For this off-line method, 1σ standard deviation of [CO] is 3 ppbv with sample preparation errors, and that for $\delta^{13}C$ and $\delta^{18}O$ is 0.4‰ and 0.5‰, respectively were estimated based on 9 calibration runs in [*J. E. Mak and Brenninkmeijer*, 1994]. The eight Iceland air sample (Fig 2.4) were collected in January and February of 2007. Residual air samples in the cylinders were processed based on our cryogenic extraction plus continuous-flow IRMS method (section 2.1) [*Z H Wang and Mak*, 2009]. The isotope signatures of a calibration gas were used to calibrate the line and characterize the $\delta^{18}O$ of Schütze reagent (see details in section 2.6 and 2.7). The mixing ratio of CO for an air sample is determined by the ratio of peak areas between the sample and the calibration gas. The differences of [CO], $\delta^{13}C$, and $\delta^{18}O$ of the eight Iceland ambient air

samples between the conventional off-line method and the new on-line method are shown in Fig 2.4. Shift of [CO] ranges from +3.9 ppbv to -4.7 ppbv. Shift of $\delta^{13}C$ ranges from +0.06‰ to -0.41‰. Shift of $\delta^{18}O$ ranges from +0.31‰ to -0.95‰. Mean absolute shifts of [CO], $\delta^{13}C$, and $\delta^{18}O$ of the eight Iceland ambient air samples are 2.2 ppbv, 0.18‰, and 0.28‰, respectively, which are comparable with the uncertainties. Thus, we argue these shifts between the two different methods are of no significance and the new on-line analysis method produces reliable results. The linearity effect on [CO] is not a concern since the ambient sample (315MLCO) with lower [CO] (61 ppbv) measurement in on-line system agrees with off-line dual inlet measurement (table 2.3).

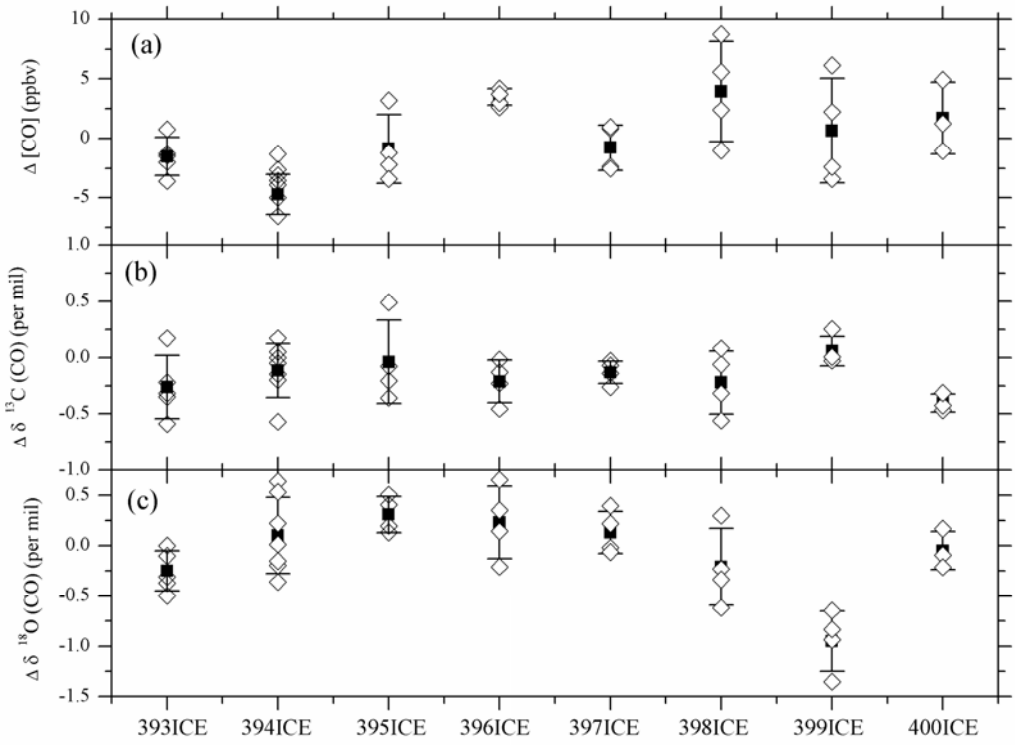

Figure 2.4 The comparison between the measurements by the conventional off-line method and our new on-line analysis method. All sample runs are shown as open diamonds, averages of shifts for each sample are shown as close squares, and error bars

are 1σ standard deviations. (a) shifts of [CO], ranging from +3.9 to -4.7 ppbv; (b) shitfs of $\delta^{13}C$, ranging from +0.06 to -0.41‰; (c) shifts of $\delta^{18}O$, ranging from +0.31 to -0.95‰.

2.6 Calibration Gas

Experiments were periodically performed to determine the reliability and precision of stable C and O isotope data using a calibration gas (secondary calibration) of known concentration and isotopic compositions calibrated by previous independent determination [*C. A. M. Brenninkmeijer*, 1993; *J. E. Mak and Brenninkmeijer*, 1994]. The secondary calibration gas is CO mixed with ultrapure air, stored in a treated aluminum cylinder with an initial pressure of 1500 psi. Concentration and $\delta^{13}C$ and $\delta^{18}O$ values were determined by using whole air extraction of several hundred liters of air for ^{14}CO analysis [*J. E. Mak and Brenninkmeijer*, 1994] followed by dual-inlet microvolume analysis with the Delta Plus IRMS [*J Mak and Kra*, 1999; *J. E. Mak and C. A. M. Brenninkmeijer*, 1998]. The CO concentration is determined volumetrically to be 141 ppbv based on a primary calibration on NOAA/CMDL CO scale and $\delta^{13}C$ is determined by the IRMS to be -45.56‰ VPDB. $\delta^{18}O$ of the secondary calibration gas is determined to be -1.94‰ VSMOW based on the $\delta^{18}O$ of derived CO_2 and the $\delta^{18}O$ of the oxygen from I_2O_5 [*C. A. M. Brenninkmeijer*, 1993]. $\delta^{18}O$ of O from I_2O_5 in the big extraction line is determined by the primary calibration runs with known concentration and isotopic ratios and equation 2.1 [*C. A. M. Brenninkmeijer*, 1993], where

$\delta^{18}O(\textit{permil}\ \text{VSMOW})_{sample}$ is $\delta^{18}O$ of CO in the secondary calibration gas, $\delta^{18}O_{CO_2}$ is measured $\delta^{18}O$ of CO_2 from the secondary calibration gas CO, $\delta^{18}O_{Cal\,CO_2}$ is measured $\delta^{18}O$ of CO_2 from the primary calibration gas CO, and $\delta^{18}O_{Cal\,CO}$ is $\delta^{18}O$ of CO in the primary calibration gas.

Once the concentration and isotopic ratios of the secondary calibration gas are determined, this secondary calibration gas is periodically processed in our new cryogenic extraction system to check its performance. Any compromise of $\delta^{13}C$ by the extraction process will be evident since $\delta^{13}C$ of CO in the secondary calibration gas has already been determined [*J. E. Mak and Brenninkmeijer*, 1994]. The measured $\delta^{18}O$ of the derived CO_2 from the secondary calibration gas is used to calculate the $\delta^{18}O$ of Schütze reagent in our new cryogenic extraction system based on the following equation:

$$\delta^{18}O(\textit{permil}\ \text{VSMOW})_{sample} = 2\delta^{18}O_{CO_2} - \left(2\delta^{18}O_{Cal\,CO_2} - \delta^{18}O_{Cal\,CO}\right) \quad \text{eq 2.1}$$

where $\delta^{18}O_{CO_2}$ is the measured $\delta^{18}O$ of CO_2 from sample CO, $\delta^{18}O_{Cal\,CO_2}$ is the measured $\delta^{18}O$ of CO_2 from calibration gas (0.42‰), and $\delta^{18}O_{Cal\,CO}$ is $\delta^{18}O$ of CO in calibration gas (-1.94‰, VSMOW).

The results of $\delta^{13}C(CO)$ and $\delta^{18}O(CO_2)$ are plotted as a function of voltage mass 44 (Fig 2.5). The mean value of $\delta^{13}C(CO)$ is -45.40‰ (VPDB) with a standard deviation of 0.33‰ (±1σ), for 47 runs of the measurements with CO amount ranging from 232 pmol to 4 nmol, and the mean value of $\delta^{18}O(CO_2)$ is 0.42‰ (VSMOW) with a standard deviation of 0.32‰ (±1σ). $\delta^{13}C$ shows an offset of +0.16‰, which is smaller than the

standard deviation of 0.33‰ (±1σ). However the shift of $\delta^{18}O$ is hard to be assessed because the $\delta^{18}O$ values themselves are used to determine the $\delta^{18}O$ of Schütze reagent [*C. A. M. Brenninkmeijer*, 1993].

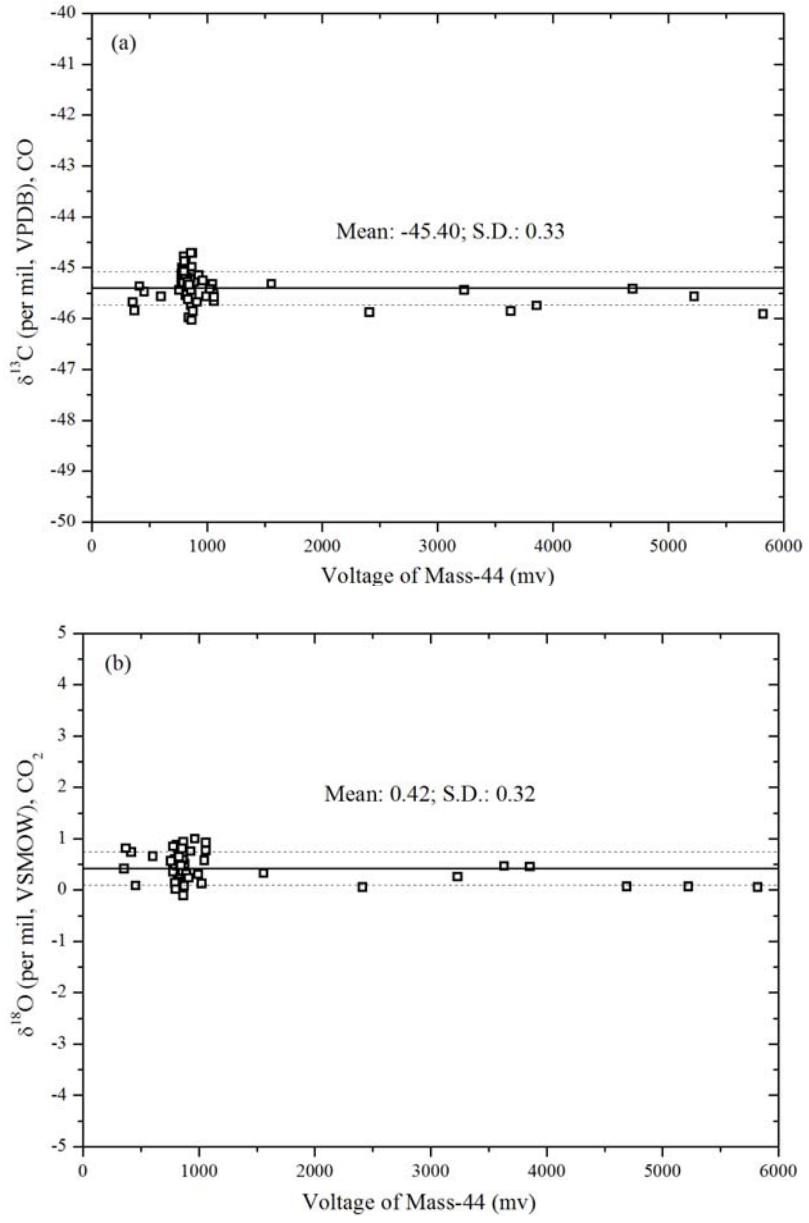

Figure 2.5 Measurements of (a) $\delta^{13}C$ and (b) $\delta^{18}O$ for calibration gas as a function of voltage for mass-44 ranging from 400mv to 6 V. Mean value of $\delta^{13}C(CO)$: -45.40‰ (with standard deviation 0.33‰); mean value of $\delta^{18}O(CO_2)$: 0.42‰ (with standard deviation

0.32‰). Sample size is linear with voltage of mass-44 and 700 pmol CO gives 1V for the signal of voltage mass-44. We show $\delta^{18}O(CO_2)$ in (b) instead of $\delta^{18}O(CO)$ because the calibration run values of $\delta^{18}O$ themselves are used to determine the $\delta^{18}O$ of I_2O_5 [*C. A. M. Brenninkmeijer*, 1993].

2.7 Field Sample Measurement

Field samples were processed with both conventional extraction and dual-inlet method and this new analysis technique (section 2.4 and 2.5). The primary calibration gas used for the off-line extraction has a [CO] of 212.7±2.1 ppmv (balanced with zero air), $\delta^{13}C$ of -39.94±0.1‰ (VPDB), and $\delta^{18}O$ of 11.36±0.2‰ (VSMOW). Comparisons indicate the performance of this new method. Air samples from two sites: the Mauna Loa Observatory and Westmann Islands, Iceland, with the whole volume on the order of 600 liters (STP) were collected into high pressure aluminum air cylinders using a previously published protocol [*J. E. Mak and Brenninkmeijer*, 1994]. These field samples were first processed with off-line extraction and analyzed with conventional dual inlet microvolume method [*J Mak et al.*, 2003]. Aliquot of remaining samples were then processed with the new on-line analysis. Measurements based on the on-line extraction CF-IRMS are compared with the off-line extraction dual-inlet results (Table 2.3).

The sample of 315MLCO has a CO concentration close to that of air samples from Antarctic ice core [*Haan et al.*, 1996]. The 0.2‰ standard deviation for $\delta^{13}C$ and 0.6‰ standard deviation for $\delta^{18}O$ obtained from the new on-line analysis method for

315MLCO indicate reliable reproducibility. Moreover, no significant difference for $\delta^{13}C$ or $\delta^{18}O$ appears between the off-line dual inlet microvolume analysis and the on-line extraction CF-IRMS analysis for small sample size (315MLCO), implying the reliable accuracy of the new on-line method. This reliable reproducibility and the good accuracy give us confidence for our ice core measurements.

Table 2.3 Comparison of $\delta^{13}C$ and $\delta^{18}O$ results of field CO samples obtained by off-line dual inlet microvolume analysis and on-line extraction CF-IRMS

	Off-line Dual inlet microvolume analysis					**On-line extraction CF-IRMS**			
Sample ID	Collection Date	[CO] (ppbv)¶	$\delta^{13}C$ (‰, VPDB)[1]	$\delta^{18}O$ (‰, VSMOW)[1]	Sample Volume (L, STP)	[CO] (ppbv)	$\delta^{13}C$ (‰, VPDB)	$\delta^{18}O$ (‰, VSMOW)	Sample Volume (L, STP)
315MLCO (12)[2]	28-Aug-07	61	-30.996±0.021	-1.27±0.043	286	62.0±1.3	-30.80±0.17	-1.33±0.61	0.1
393ICE(5)	24-Jan-07	126	-27.188±0.019	8.74±0.125	658	124.7±1.6	-27.45±0.28	8.49±0.20	0.1
394ICE(7)	31-Jan-07	128	-27.245±0.028	8.25±0.04	678	123.4±1.7	-27.36±0.24	8.35±0.38	0.1
396ICE(4)	17-Jan-07	137	-27.627±0.034	9.16±0.097	662	139.0±0.7	-27.84±0.19	9.39±0.36	0.1
397ICE(4)	07-Feb-07	134	-27.577±0.086	8.19±0.194	602	137.0±1.9	-27.71±0.10	8.32±0.21	0.1
398ICE(5)	28-Feb-07	139	-26.928±0.034	9.64±0.064	674	143.6±4.2	-27.15±0.28	9.43±0.38	0.1

Note [1]: this standard deviation for dual inlet is analytical error for mass spectrometric analysis only, and no sample preparation error is taken into account; [2]: the number in parentheses next to sample ID is the number of analyses by on-line extraction CF-IRMS; ¶: 1σ standard deviation of [CO] is 3 ppbv with sample preparation errors, and that for $\delta^{13}C$ and $\delta^{18}O$ is 0.4‰ and 0.5‰, respectively based on 9 calibration runs in [*J. E. Mak and Brenninkmeijer*, 1994].

2.8 Ice Cores Samples

This section only focuses on the analysis of ice core samples including ice sample preparation, ice extraction, and analysis of the released air. The core site characteristics,

results of ice core measurements, and the subsequent data interpretation will be presented in chapter 4 in this thesis. The detailed information of ice core measurements are shown in the appendix A and B.

2.8.1 D47 Ice Core Extraction and Gas Analysis

The D47 ice samples were provided by LGGE, Grenoble, France and 15 of them were prepared in LGGE in 2007. The other five D47 ice samples including 81 m, 86 m, 95 m, 109 m, and 111 m (Appendix B) were extracted and process with the same protocol discussed below in section 2.8.2 in 2009. Kerosene was used as a fluid at D47 ice core starting at depth of 87.2 m and all along below (when thermal drilling started in 1988), and above 87.2 m D47 ice core was electromechanical dry drilling [*Chappellaz*, person communication]. Tests conducted at LGGE showed that with careful cleaning of the sample, kerosene is not a problem for CO [*Chappellaz*, person communication]. In this study, special care was taken for cleaning D47 ice core samples below 87.2 m.

The basic principles of wet extraction technique are the same as [*Chappellaz et al.*, 1997]. Ice samples, with masses ranging between 500 and 1000g, were first trimmed with a band saw in a cold room held at -20ºC. The ice sample was then shaved with a disposable stainless steel scalpel during the time another 1-2 mm ice was removed. Samples were then placed into a 2-L cylindral borosilicate glass container sealed with indium wire by plastic flange [*Haan et al.*, 1996]. The container with ice was submerged into cold bath (-20˚C) and attached to the wet extraction line with 1/4" OD silco treated

stainless steel tubing (Resteck inc). The schematic diagram of the wet extraction system is shown in Fig 2.6. The ice container was evacuated with turbomolecular pump for 15 min. Most water vapor was removed by a spiral 1/2" OD glass trap held at -50ºC. Ice container was then closed and the cold bath was removed and replaced with hot water bath held at temperature of around 70˚C. Ice melted in 15-20 min, depending on the ice mass. After ice melting completed, the released air was then trapped into the pre-evacuated stainless steel sample vial with bellow sealed valve (NUPRO, volume ~ 14 mL) held at liquid helium temperature and the residual water vapor was removed by a stainless steel Russian doll trap held at a temperature of -70˚C. The ice container was cleaned with acetone and rinsed with distilled water, and dried in a clean bench overnight after each use. The valve for the ice container is high-vacuum stopcock with viton o-ring. Other valves are nupro stainless steel needle valves.

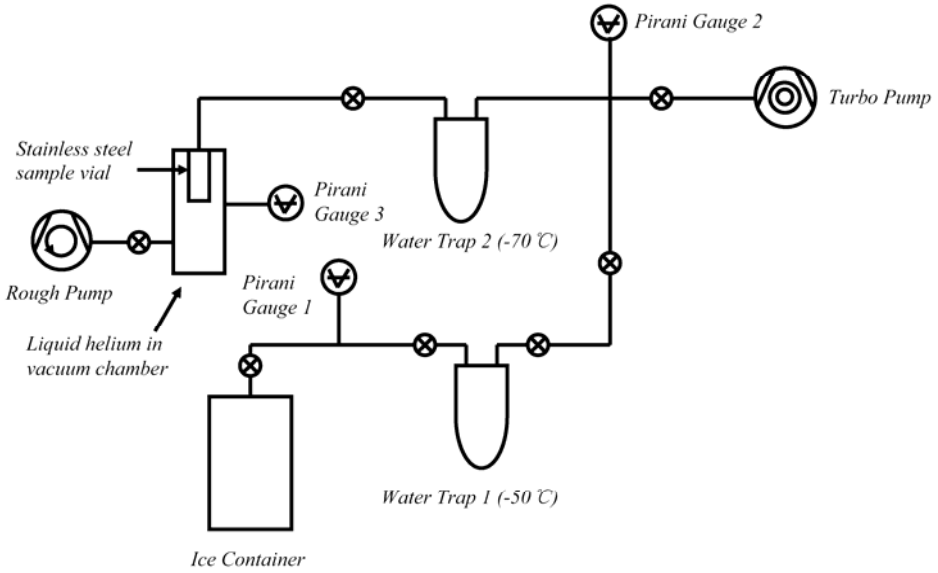

Figure 2.6 Schematic diagram for wet extraction system in LGGE [*Chappellaz et al.*,

1997]. Ice container is submerged in liquid nitrogen-alcohol cold bath (-20˚C) when evacuating and in hot water bath (70˚C) when melting.

Samples were then transferred from the vial to the preevacuated 150 mL glass flasks (wrapped with aluminum foil to prevent from light and ~10% of each sample is lost during the expansion), shipped to Stony Brook, and analyzed in our new on-line continuous-flow isotope ratio mass spectrometer (CF-IRMS) [*Z H Wang and Mak*, 2009].

To determine the ice blank, monocrystalline bubble free ice was processed in the same procedure as that for D47 ice samples and a 150 mL glass bottle filled with calibration gas (CSIRO 1636, [CO]=68 ppbv, $\delta^{13}C$=-30.9‰ VPDB, and $\delta^{18}O$=5.8‰ VSMOW). Other three ice core samples (109TOP, 95TOP, and 95BOTTOM) were stored in the 14 mL stainless steel sample vial and shipped to Stony Brook for analysis. The measurements of these three ice samples showed high [CO] (>100 ppbv, possible in-situ production occurred in the metal surface) and were rejected.

2.8.2 South Pole Ice Core Extraction and Gas Analysis

South Pole (SP) ice core samples (dry drilled in 2004, no contamination with drilling since no fluid was used) provided by National Ice Core Lab (NICL) were processed using the CF-IRMS method discussed above. The ice core samples were semi cylindrical with average length of 17cm and radius of 5cm. The ice core sample was first trimmed with a band saw to remove several mm of surface, and then scraped with a stainless steel disposable scalpel to remove additional 1-2 mm of surface. Except for five SP ice

samples (135 m, 157 m, 165.3 m, 165.7 m, and 177 m), which were processed in cold room at -20˚C, all other SP ice samples were processed in an open chest freezer (Frigidaire) with a volume of ~0.82 m^3. The depth of the freezer is ~1 m and the ice was close to the bottom when shaved. The band saw (Craftsman) was wrapped with insulation and placed upright on the bottom of the freezer. Liquid nitrogen in metal container was placed in the freezer to keep temperature low. The temperature in the 1/2 deep of the open freezer was measured periodically and confirmed to be lower than -8˚C during ice preparation.

The ice container is a 1.2 L borosilicate glass container with a 4.5 inch OD glass flange, viton o-ring and horseshoe clamp (original part from Chemglass inc and modified by General Instrument Universal). Prior to use, the bottom part of the ice container was cleaned with acetone (99.5%, Aldrich) and rinsed with deionized water (Milli-Q integral system, with resistance of 18.2 MΩ), then heated overnight at 90˚C. The cap of the ice container and the 4.5" viton o-ring was also rinsed with deionized water and heated overnight at 90˚C. The ice core sample was weighted after shaved and then sealed in the ice container and immersed in cooling bath held at –20˚C. The ice and the container were repeatedly evacuated and flushed with zero air for 30 minutes. After final pumping, the ice was melted in hot water bath held at temperature of 60-70˚C.

The on-line system for South Pole ice core samples is shown in Fig 2.7. A wet extraction line is attached to the cryogenic extraction system discussed previously in this

chapter (Fig 2.1). A four-loop coil trap (1/4" OD borosilicate glass with volume of 15 mL, both sides with hi-vacuum stopcocks and viton o-rings) between the container and the inlet of the cryogenic vacuum system is held at -70˚C and used to remove water vapor. Upon melting, the air sample released from around 1 kg ice core is around 100 mL (STP), giving an initial pressure in the headspace of about 300 mbar. This pressure drops to 60 mbar after air sample is processed for 5 min. A 150 mL glass flask filled with zero air (CO free air) is expanded to the ice container for building up pressure to around 500 mbar and is processed for another 5 minutes. The released air from the ice was then analyzed withCF-IRMS based on the procedure discussed in section 2.1.

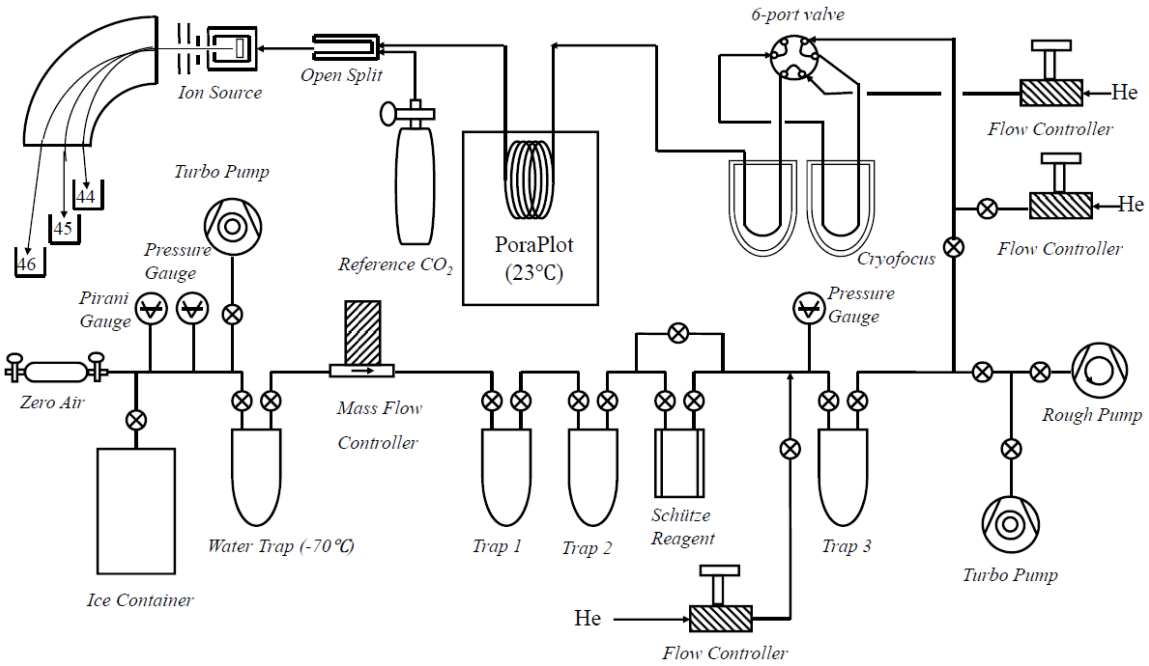

Figure 2.7 On-line analysis system for ice core samples: wet extraction system including ice container, zero air flask, pirani gauge, pressure gauge, turbomolecular pump, and 4-loop water trap attached to the cryogenic extraction line to remove water coming out from the ice container [*Z H Wang and Mak*, 2009].

Around 10% air sample is lost due to the dead volume in the ice container and the

water trap and less than 1% is lost due to solubility of CO in water [*Jauregui-Haza et al.*, 2004]. The pressure of the ice container was observed by a pressure gauge (GNS Science). The actual flow rate measured by the mass flow controller (MKS instruments) was monitored by a computer through data acquisition device (Labjack U12). The volume of the released air sample was determined by the combined pressure and flow rate monitored.

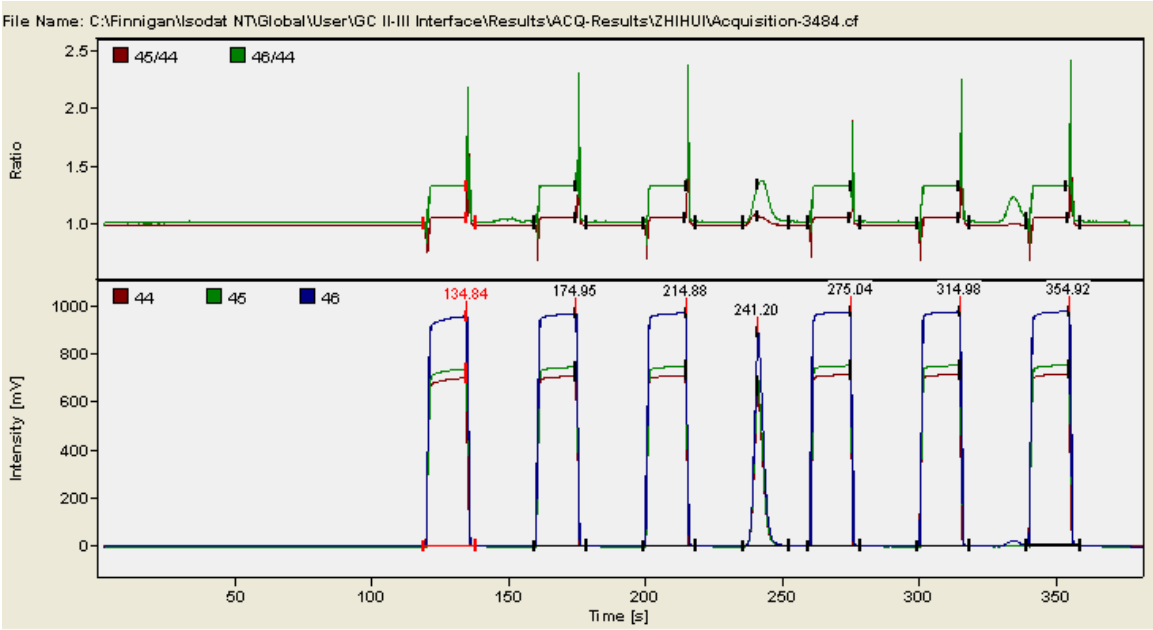

Figure 2.8 A mass spectrogram of a South Pole ice core sample. The mass spectrogram shows the measured ion intensities of m/z 44, 45 and 46 (lower) and the m/z ratios of 45/44 and 46/44 (upper). The first three peaks and the last three are the reference CO_2 gas injections. The peak at 241.20 s is the sample CO_2 peak.

A mass spectrogram of an ice core sample is shown in Fig 2.8, showing the low noise and good baseline. The third reference CO_2 peak is set to determine the m/z ratios of 45/44 and 46/44 of sample CO_2 peak. The precisions of $\delta^{13}C$ and $\delta^{18}O$ for the six reference CO_2 injections are 0.1‰ and 0.2‰, respectively.

2.9 U Trap Test

The disadvantage for the above method for South Pole ice core samples is the large blank from the Schütze reagent due to long processing times (10 min), which largely limit the precision of isotope ratios obtained with this new technique. Thus we tried a lot of approaches to reduce the processing time.

The first one is using some adsorbent to condense CO, followed by a quick elution with cryogenically purified ultrahigh pure helium flow. Different adsorbents such as HaySep D, molecular sieve 5A, and molecular sieve 13X held at liquid nitrogen temperature are used to condense air released from ice cores in order to shorten the processing time and decrease the Schütze blank.

HaySep D (80/100 mesh, Sigma-Aldrich Co.) was first tested based on its good performance as an adsorbent for ice core CH_4 [*Sowers et al.*, 2005a]. HaySep D was placed into a borosilicate glass U shape tube with ¼ inch OD, with glass wool on both ends to prevent the powder moving. A thermocouple (Watlow Inc) was wrapped around the glass to produce heat for baking out and heat desorption [*Brenninkmeijer and Hemmingsen*, 1988]. Minimum amount of HaySep D and the following molecular sieve is determined by pressure drop tests. After heating and evacuating, a glass bottle filled with air was expanded and adsorbed to the HaySep D U trap, which was held in liquid

nitrogen. The function of pressure versus time was recorded and plotted (Fig 2.9). Minimum amount of HaySep D was 1.2 mL, giving 99.1% adsorption yield in 30 min. The minimum amount of molecular sieve used to adsorb 100 mL (STP) air was 1.1 mL, indicated by the similar pressure drop.

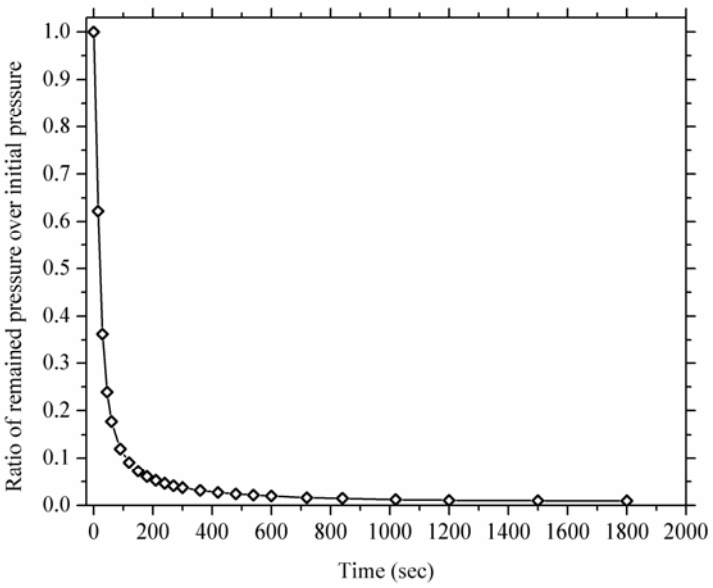

Figure 2.9 Pressure drop function for HaySep D adsorption performance. In 30 min, the pressure drops to 0.9% of the initial pressure. Pressure drop lines of molecular sieve 13X and 5A indicate the similar adsorption performance.

The HaySep D and molecular sieve U trap was then attached to the cryogenic extraction system and tested with air samples. An external cryogenically purified UHP helium flow (99.999%) was applied for elution CO during desorption. CO blank produced from HaySep D was too high and isotopic ratios cannot be reserved during this adsorption-desorption process. The results of the tests on HaySep D and molecular sieve 13X and 5A are shown in Fig 2.10. CO concentrations indicate there are high blanks from HaySep D and molecular sieve 13X, whereas CO blank from molecular sieve 5A is low.

For $\delta^{13}C$ and $\delta^{18}O$, isotopic fractionation of both carbon (2-3‰) and oxygen (1-4‰) was evident during the elution process, which prevents their use in the present study. However, this isotopic fractionation was not reported in another study [*U. Tsunogai et al.*, 2002].

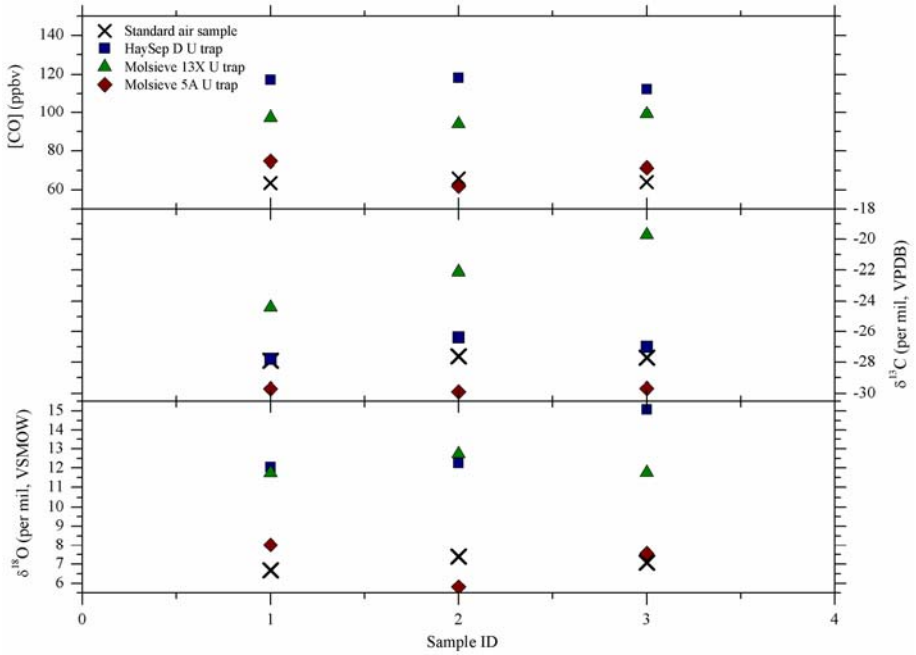

Figure 2.10 [CO], $\delta^{13}C$, $\delta^{18}O$ of the CO eluted from the HaySep D, molecular sieve 13X and molecular sieve 5A U traps. Also shown are those for the standard gas used in the tests. Isotopic fractionations occur for both $\delta^{13}C$ and $\delta^{18}O$.

2.10 Tedlar Bag Test

In order to decrease the processing time, it was realized that a collapse column might work. Use of a Teflon beaker liner (Welch Fluorocarbon Inc.) was investigated as its volume is adjustable and thus builds up pressure in the headspace by shrinking and pushing water upward. This can counteract the pressure reduction during processing. However, permeability of CO across Teflon film limits the use of this material. Similarly,

Tedlar (polyvinyl fluoride, PVF), another polyfluorocarbon but with low CO permeability, was also tested. However, it is quite difficult to engineer a Tedlar liner because of its rigidity. We first designed a pillowcase Tedlar bag attached to the aluminum flange with low vapor pressure sealant (LOCTITE Hysol 1C). Two reasons prevent its use: the vertical seam of the Tedlar tube is easy to break when shrinking and the leak problem caused by sealing. A stainless steel bellow which fits the size of our ice core samples was also attempted to design, however it was difficult to engineer this bellow due to the large diameter and small stretch length. Therefore, Tedlar bag was found to be infeasible.

In the end, while these ideas are intriguing and may warrant further study, we opted to keep our sampling protocol simple with the dilution process and characterize the Schütze blank to a high degree of precision. Clearly, an old fashioned mercury toepler pump could be ideal to solve this problem by reducing extraction time and Schütze blank.

2.11 Concluding Remarks

The purpose of this chapter is to introduce the analytical system used in this study and illustrate the diagnostic tests conducted for this system. The detailed procedure to deal with ice core samples is also addressed.

In this chapter, a new simultaneous analysis technique for stable isotope ratios ($\delta^{13}C$ and $\delta^{18}O$) of atmospheric CO from ice core samples and small air samples is presented,

based on an on-line cryogenic vacuum extraction followed by continuous-flow isotope ratio mass spectrometry (CF-IRMS). Analytical precision (±1σ) of 2.6 ppbv for [CO], 0.2‰ for $\delta^{13}C$, and 0.6‰ for $\delta^{18}O$ can be obtained for 100mL (STP) air samples with CO mixing ratios ranging from 60 ppbv to 140 ppbv (~250-650 pmol CO). Ice core samples are processed with a wet extraction method and the released air is processed in this on-line continuous-flow analysis system. Measurements based on artificial bubble free ice and calibration gas indicate this analysis system produces reliable results for ice core samples.

To reduce the process time of ice core samples and system blank, and improve the performance of our analysis system, we tried different approaches such as using adsorbents (HaySep D and molecular sieve) to condense air and using Tedlar bag to build up pressure. However, those approaches have been found infeasible. While these ideas are intriguing and may warrant further study, we opted to keep our sampling protocol simple with the dilution process and characterize the Schütze blank to a high degree of precision. Clearly, an old fashioned mercury toepler pump could be ideal to solve this problem by reducing extraction time and Schütze blank.

Chapter 3. Records of Atmospheric CO in Firn

This chapter focuses on the trends of atmospheric CO over the past several decades. As preliminary studies of this thesis, air samples trapped in firn from Arctic site (North Greenland Ice Core Project - NGRIP) and Antarctic site (Berkner Island) have been measured for CO concentration, $\delta^{13}CO$, and $\delta^{18}CO$. The atmospheric trend of CO in high-latitude Northern Hemisphere since the mid-20th century has also been reconstructed based on firn air samples from North Greenland Eemian Ice Drilling (NEEM Project, 2008) and application of firn diffusion models. CO isotopic ratios are reported for the first time in firn air in Northern Hemisphere. Because of much shorter storage time of the firn air samples and much better precisions obtained, we are more confident on the NEEM firn measurements, which we will focus on in this chapter.

3.1 Introduction

Bergamaschi et al. reported that introducing isotope data in source optimization provides relatively well constrained source strengths of CO [*Bergamaschi et al.*, 2000b]. However, essentially little observations exist from which the relative source strengths from past atmospheres can be estimated. Recently, CO isotopes in Antarctic firn air have

been studied and revealed a heavier $\delta^{13}C$ in the past [*Assonov et al.*, 2007]. However, so far there is limited information about the 20th century CO evolution in the Northern Hemisphere, and none yet from firn air except for [CO] record in Devon Island, Canada [*Clark et al.*, 2007].

Greenland ice core records have shown high-latitude CO concentration increased from ~90 ppbv to ~110 ppbv between 1800 and 1950 [*Haan et al.*, 1996], which is believed to result from anthropogenic emissions such as fossil fuel combustion [*Boden et al.*, 2009]. Today's annual mean CO concentration in high-latitude NH is ~125 ppbv based on measurements by NOAA/CMDL (http://www.esrl.noaa.gov/gmd/ccgg/iadv/). Therefore large variations of CO concentration and concurrent CO budget occurred over the last 50 years. It is very important to understand the reason of this change over the last half century, which will reveal how anthropogenic perturbations influence CO budget in NH. However, as mentioned in section 1.1, no direct systematic observations of CO exist for the past 50 years.

Air trapped in polar firn provides a way to quantify the magnitude of the atmospheric CO concentration and isotopic ratios. As the preliminary study on CO isotopes in firn air, measurements on firn air from Berkner Island and NGRIP were carried out. After that, from analysis of NEEM firn air, a more comprehensive reconstruction of combined Northern Hemispheric [CO] and its carbon and oxygen stable isotopic ratios were built up. Firn diffusion model is used to take into account physical processes occurring in firn

column and to reconstruct the atmospheric trend of CO over the past 50 years. These atmospheric scenarios of CO concentration and isotopic ratios are also tested against the measurements to reveal model validation. Then we present, based on measurements on firn air samples collected in July 2008 in the NEEM firn.

3.2 Berkner Island and NGRIP Firn

3.2.1 Physical characteristic

Samples were collected in the framework of European Project CRYOSTAT (CRYospheric STudies of Atmospheric Trends of stratospherically and radiatively important gases). The detailed field site information for NGRIP and Berkner Island such as elevation and mean annual temperature etc. is shown as table 3.1.

Table 3.1 Field site information of CRYOSTAT: CRYOspheric Studies of Atmospheric Trends in stratospherically and radiatively important gases (After [*BADC*, 2007])

Drilling Site	Lat, Long	Elevation (m)	Mean Annual Temp (℃)	Transition depth (m)	Snow accumulation rate (cm water y^{-1})	Campaign dates
NGRIP	75.1°N,42.3°W	2975	-31	78	20	Jun, 2001
Berkner Island	79°32.9'S, 45°40.7'E	900	-26	63	12	Jan, 2003

Locations of Berkner Island and NGRIP drilling site are indicated in Fig 3.1 and Fig 3.2. Location of NGRIP drilling site is on the north of GISP2 and GRIP. Firn air samples

were collected in 3 L fused-silica lined stainless steel canisters (Restek "SillcoCans") [*Sturges et al.*, 2001].

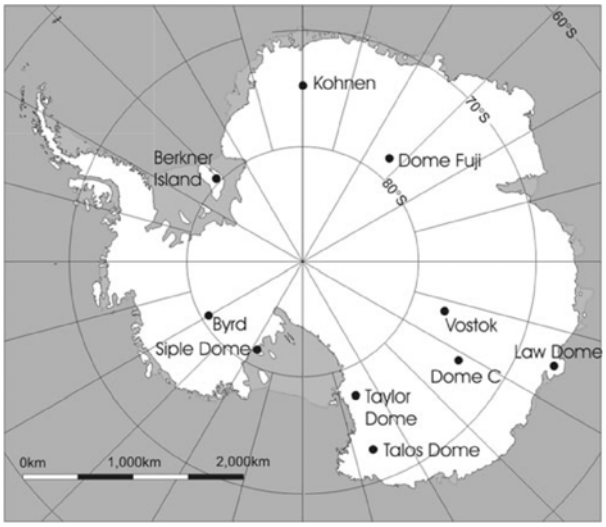

Figure 3.1 Location of Berkner Island and other deep ice-core drilling sites in Antarctica [*Mulvaney et al.*, 2007].

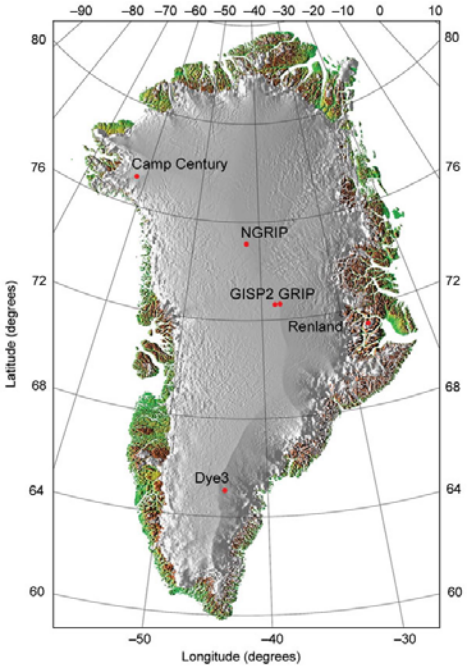

Figure 3.2 Map of Greenland, showing the locations of the deep ice core drilling sites including NGRIP (75.1°N, 42.3°W) [*Andersen et al.*, 2004].

3.2.2 Experiment

11 samples were collected from NGRIP in June, 2001 (by the CRYOSTAT team) from the surface to a depth of 78 m and other 11 samples were collected from Berkner Island in January, 2003 from surface until depth of 63 m. Firn air samples were first transferred from the original Silco cans to 150-mL glass flasks in a vacuum line.

The new analysis system discussed in chapter 2 had not been built up when these samples were analyzed. Therefore, measurements on these firn air samples were made with a continuous-flow isotopic ratio mass spectrometer (CF-IRMS) and a custom built, front end CO extraction system [*J E Mak and W Yang*, 1998]. Large errors in measured CO isotopic ratios indicate this old system was not performing well, and the NGRIP firn air samples had been stored for over 6 years when processed. Therefore, these firn air data are considered as preliminary results, on which no firn diffusion model is applied. Only depth profiles are shown and not much detail is discussed.

3.2.3 Results and Discussions

The data sets presented here include the vertical profiles of both concentration and $\delta^{13}C$ and $\delta^{18}O$ of CO in firn air samples from the both Berkner Island in Antarctica and NGRIP. Figure 2.4 shows the vertical profiles of the CO mixing ratio of the firn air samples.

Our surface CO mixing ratio for Berkner sample is close to the NOAA/CMDL CO average concentration in Jan 2003 from three different Antarctic stations (Palmer, South Pole, and Syowa: http://www.esrl.noaa.gov/gmd/ccgg/iadv/). The NOAA/CMDL average CO mixing in Antarctica in January is around 48 ppbv, and our surface CO mixing ratio from Berkner sample is 52 ppbv. The NOAA/CMDL CO mixing ration in Iceland in Jun is around 110 ppbv, which is close to our CO mixing ratio in NGRIP 120 ppbv.

As for our CO mixing ratio in Berkner Island, a slight decrease is found from 40 m to 68 m, the bottom of the firn. Above 40 m, seasonal variation affects CO mixing ratio in firn layer [*Assonov et al.*, 2007]. This slight decrease indicates that atmospheric CO has increased slightly in Southern Hemisphere over the past several decades. On the other hand, the mixing ratios of CO recorded in NGRIP shows much larger variations than those in Berkner island over the past several decades. NGRIP CO record shows a strong seasonal variation between 110 ppbv to 140 ppbv till 30 m, followed by an increase from 30 m to 72 m. CO mixing ratio peaked at 72 m with a value of around 160 ppbv, followed by a decrease to 123 ppbv at the close-off depth.

Figure 3.4 shows the isotopic ratios of CO recorded in the firn air samples. The vertical profiles of $\delta^{13}C$ show much scatter due to the large variation of Schütze blank in the old Precon system. Especially for Berkner firn air samples which have lower CO concentration and small sample signal, the measured signatures show large error bars. The surface $\delta^{13}C$ of our Berkner Island firn air sample is very close to the observation at

Scott Base in January, 2003 [*K.H. Park et al.*, in preparation]. Though both of our $\delta^{13}C$ records for Berkner island firn and those in[*Assonov et al.*, 2007]. indicate heavier isotope in the past atmospheric over Antarctica due to less contribution of CH_4 oxidation, there are large discrepancies between these two data sets. For NGRIP firn air samples which have relatively higher CO concentration, the error bars are much smaller. However, the scattering of our $\delta^{13}C$ records in NGRIP firn air hinders valuable conclusions, indicating the analysis system was not good enough and the NGRIP firn air samples might be compromised due to long storage time.

The vertical profile of $\delta^{18}O$ from the NGRIP firn air samples is shown in Fig. 3.5. The precision of $\delta^{18}O$ is much worse than that of $\delta^{13}C$. The uncertainties in this study are mainly due to analytical error, indicating a new analysis system is necessary for small air samples. Improvement of the extraction system will lead to greater accuracy in experimental results. The new cryogenic extraction system, which helps us to extend to ice core research, has been discussed in chapter 2.

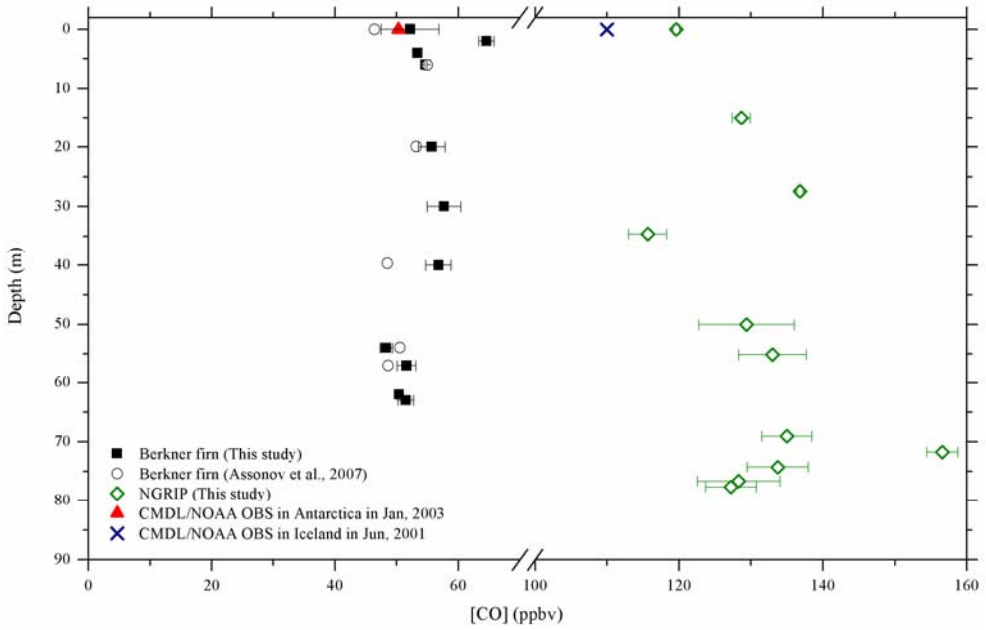

Figure 3.3 Concentration of carbon monoxide in firn air samples. Opem circles are CO concentrations for Berkner Island firn air from previous study [*Assonov et al.*, 2007]. Black squares are CO concentrations for Berkner Island firn air samples in this study. Green diamonds are CO concentrations for NGRIP firn air samples in this study. The red triangle is the CMDL/NOAA CO observation in Antarctic in Jan, 2003 and the blue cross is the CMDL/NOAA CO observation in Iceland in Jun, 2001.

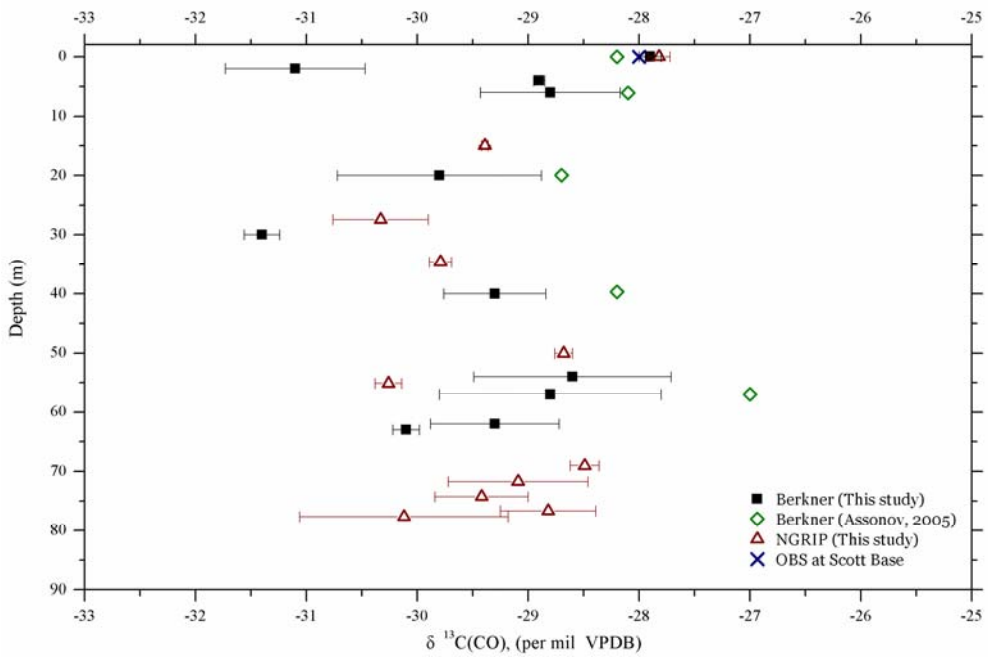

Figure 3.4 Preliminary measurements of $\delta^{13}C$ of CO in firn air samples. The black squares are results of Berkner samples in this study. The green diamonds are $\delta^{13}C$ records of Berkner island firn air from other study [*Assonov et al.*, 2007]. Red triangles are $\delta^{13}C$ records for NGRIP firn air and blue cross is the observation in Scott Base in June, 2003 by NIWA, New Zealand [*Brenninkmeijer*, personal communication].

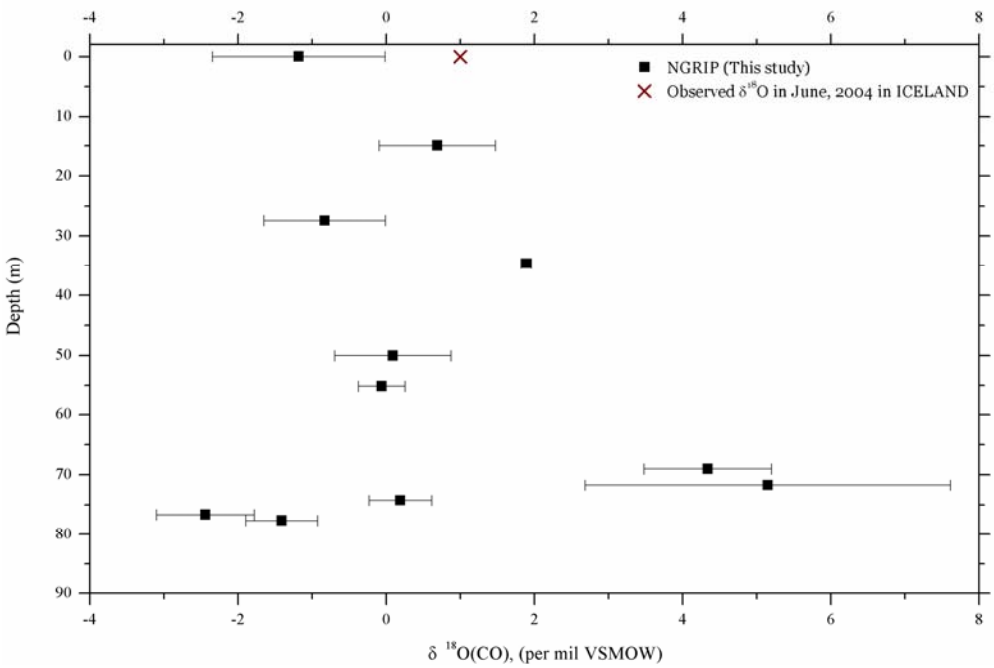

Figure 3.5 The vertical profile of $\delta^{18}O$ for NGRIP firn air samples. Black squares are $\delta^{18}O$ from NGRIP firn air samples and the red cross is observation of $\delta^{18}O$ in June, 2004, Iceland by [*J Mak*, personal communication].

3.3 NEEM Firn Air

3.3.1 Methodology

The NEEM site was pinpointed in 2007 after equipment had been transported from the NGRIP site via traverse [*Schwander et al.*, 2008]. The co-ordinates of the sites are 77.445°N, 51.066 °W, 2484 m a.s.l. The main camp infrastructure has been constructed during the 2008 season (Fig. 3.6). The prevailing wind direction is 130 degrees and other climatic data are: recent annual mean temperature: -28°C (from borehole); average ice accumulation rate: 224 mm/yr, average station pressure: approx. 745 hPa [*Schwander et al.*, 2008]. 18 firn air samples with depth ranging from 0 m to 75.9 m were collected in

3L Silco cans (Restek inc., final pressure ~40 psi) based on Uni Bern firn air sampling equipment in EU borehole from July 16, 2008 to July 27, 2008.

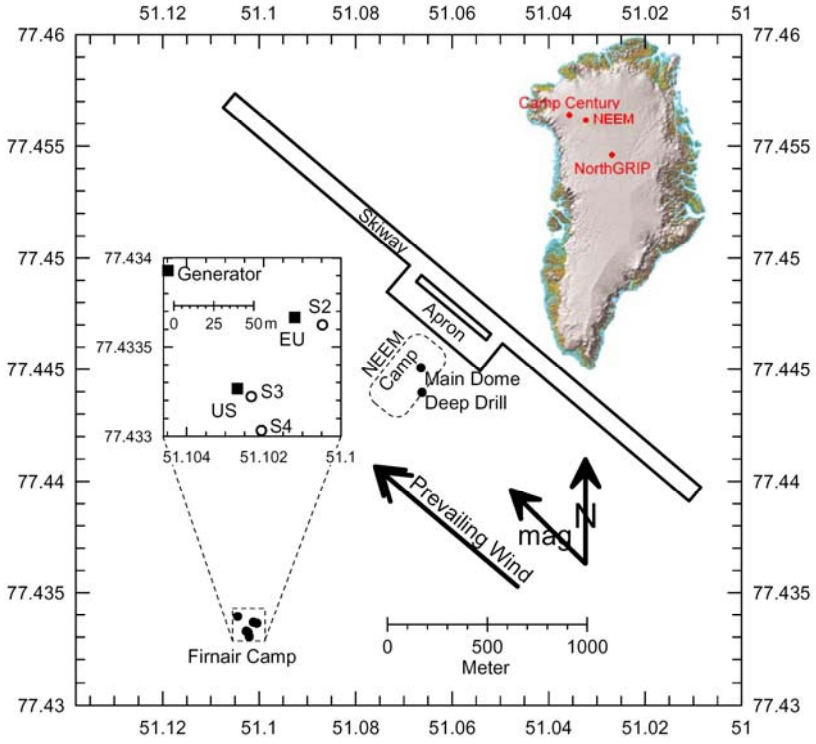

Figure 3.6 Location of NEEM and firn-air sampling sites [*Schwander et al.*, 2008].

CO concentration, $\delta^{13}C$ and $\delta^{18}O$ from trapped gases in the firn were determined by the new simultaneous analysis technique based on on-line cryogenic vacuum extraction followed by continuous-flow isotope ratio mass spectrometry (CF-IRMS) [*Z H Wang and Mak*, 2009]. The 3-L sample canister was directly attached to the inlet of the cryogenic vacuum system. 100 mL sample (STP) was processed for each run and 3 to 12 replicates were conducted for each sample. Calibration gas (CO mixing ratio 141 ppbv; $\delta^{13}C$= -45.56‰ VPDB; $\delta^{18}O$=-1.94‰ VSMOW) was processed frequently between firn air

samples, and the measurement results are shown in Fig. 3.7, which are very consistent with those for long-term calibration runs (Fig 2.5). The mixing ratio of CO for an air sample is determined by the ratio of peak areas between a sample and the calibration gas. Analytical precision of 3 ppbv (±1σ) for CO concentration, 0.3‰ (±1σ) for $\delta^{13}C$ and 0.8‰ (±1σ) for $\delta^{18}O$ have been obtained for 100 mL air sample (STP).

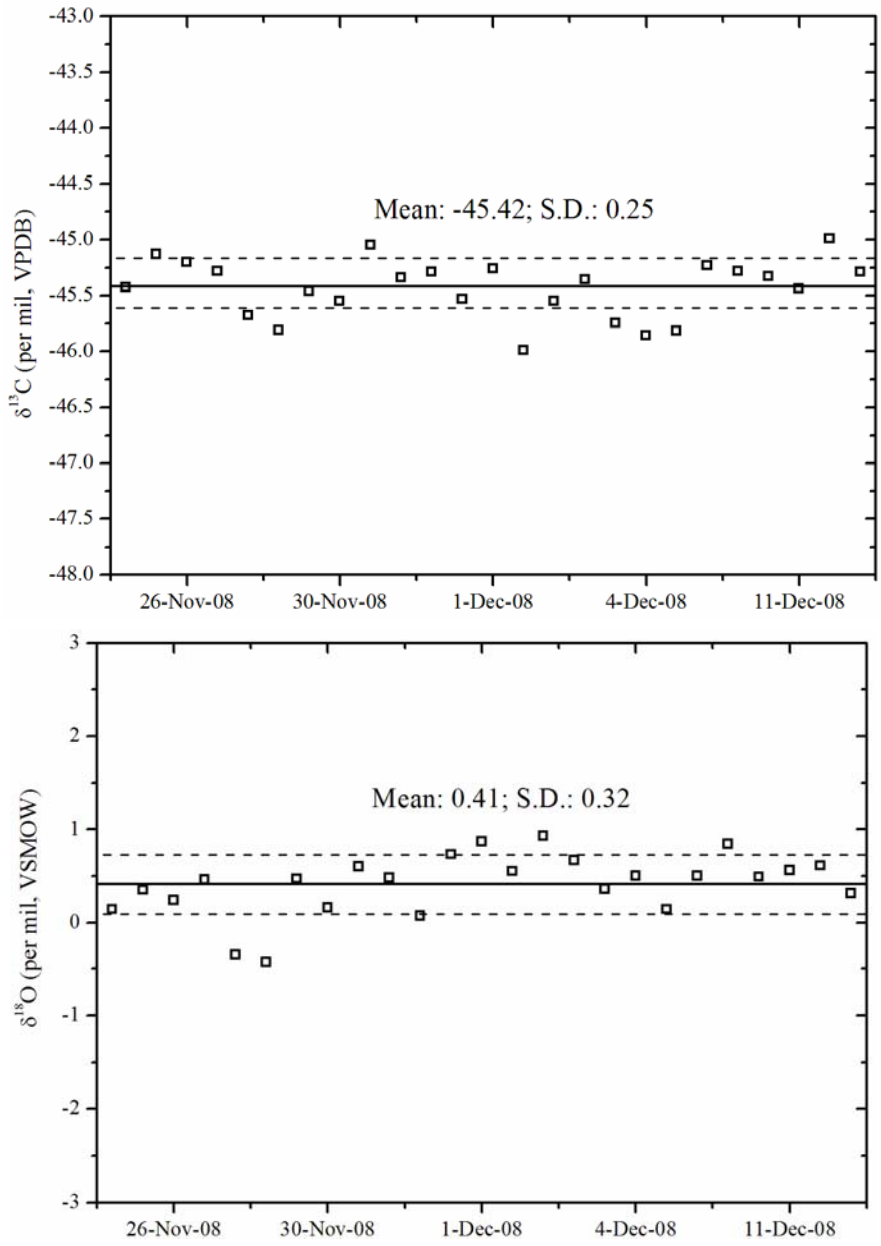

Figure 3.7 Measurements of (a) $\delta^{13}C$ and (b) $\delta^{18}O$ for calibration gas. Mean value of $\delta^{13}C(CO)$: -45.42‰ (with standard deviation 0.25‰); mean value of $\delta^{18}O(CO_2)$: 0.41‰ (with standard deviation 0.32‰). Solid lines are show the mean values and dashed lines indicate mean value plus and subtract 1σ standard deviation. $\delta^{13}C(CO)$ of calibration gas indicates good performance of the extraction system. $\delta^{18}O(CO)$ of calibration gas is used to calculate the $\delta^{18}O$ of Schütze reagent and derive the $\delta^{18}O$ of CO in air samples (see details in chapter 2).

3.3.2 Results

CO concentration and isotope profiles from NEEM firn air are shown in Fig 3.8. Good agreement of [CO] was observed among three independent labs (Fig 3.8 top panel). The concentration profiles indicate that [CO] increase from 85 ppbv to 140 ppbv between the surface and 20 m, followed by a relatively constant value of around 130 ppbv till 60 m. The first feature results from the seasonal variation of atmospheric CO concentrations, which ranged from 70 ppbv in August 1997 to 180 ppbv in February 1998 in both Alert (Canada, 81ºN) and Spitsbergen (Norway, 79ºN) [*Rockmann et al.*, 2002]. A strong increase of [CO] was then observed from 60 m to 70 m, with measured peak value of ~155 ppbv at 70 m, followed by a strong decrease down to the bottom of the firn. Furthermore, the CO peak at the bottom of NEEM is reproduced in NGRIP, with similar peak values (Fig 3.3).

The measured mixing ratio profiles for other trace gases such as CO_2, CH_4, N_2O, SF_6, CH_3Cl_3, and CCl_4 indicate the NEEM firn air is free of contamination with ambient air (Fig 3.9). The smooth trends with depth of both $\delta^{13}C$ and $\delta^{18}O$ support more evidence that there is no contamination in our samples. A seasonal imprint of both $\delta^{13}C$ and $\delta^{18}O$ in the first 10-20 m is also observed. $\delta^{13}C$ of atmospheric CO Alert was -29‰ in September 1997 and -24‰ in May 1998, where $\delta^{18}O$ ranged from -2‰ in August 1997 to 10‰ in February 1998 [*Rockmann et al.*, 2002]. Our isotopic ratio data then exhibit enriched values for both $\delta^{13}C$ and $\delta^{18}O$ below about 55 m The amplitude of this

enrichment with depth is larger than expected from gravitational fractionation (0.28‰ of $\delta^{15}N$ for NGRIP [*Landais et al.*, 2006]), and thus reflects isotope diffusion gradients in the NEEM firn and potential atmospheric changes of the CO isotopic ratios over the last several decades.

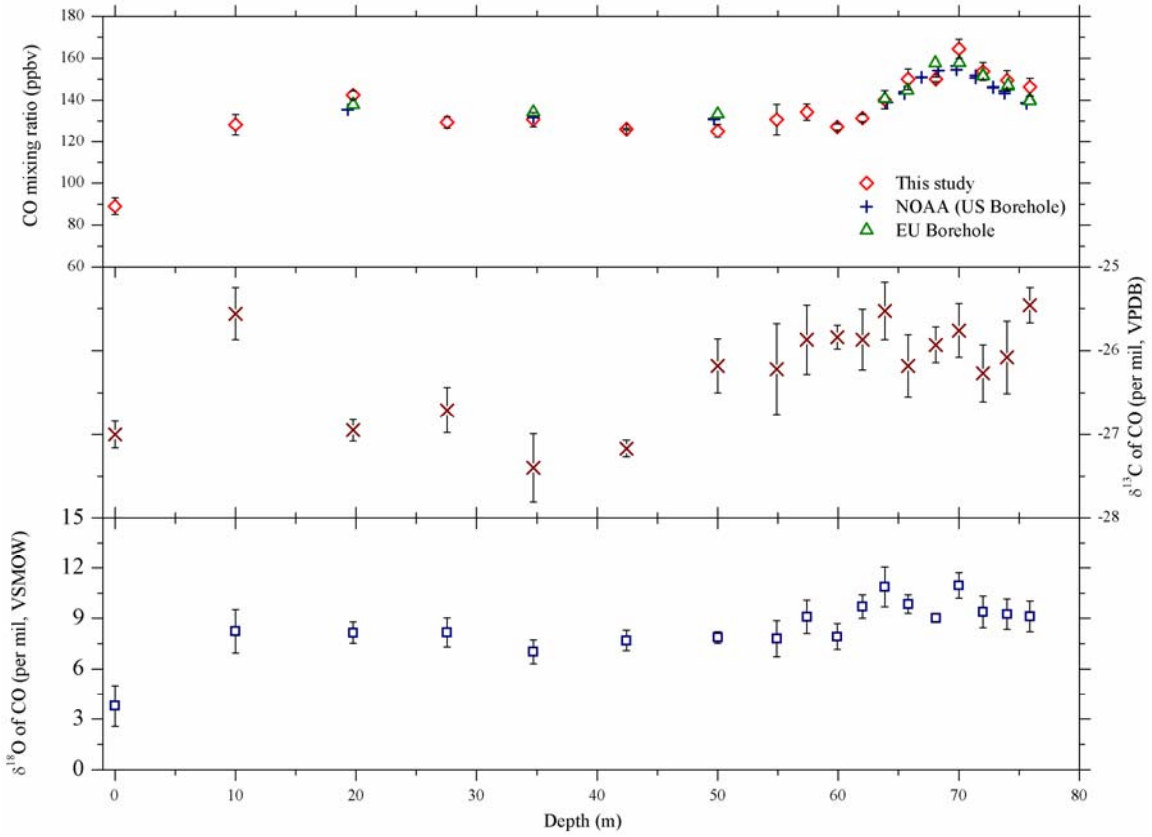

Figure 3.8 Observations for the mixing ratio and isotopic ratios of CO in NEEM firn air. Top panel: [CO] in this study (red diamonds), [CO] by NOAA based on US borehole (cross) and [CO] by University of Bern based on EU borehole (triangle); middle panel: $\delta^{13}C(CO)$ in this study (cross); bottom: $\delta^{18}O(CO)$ in this study. Error bars are ±1σ standard deviatons.

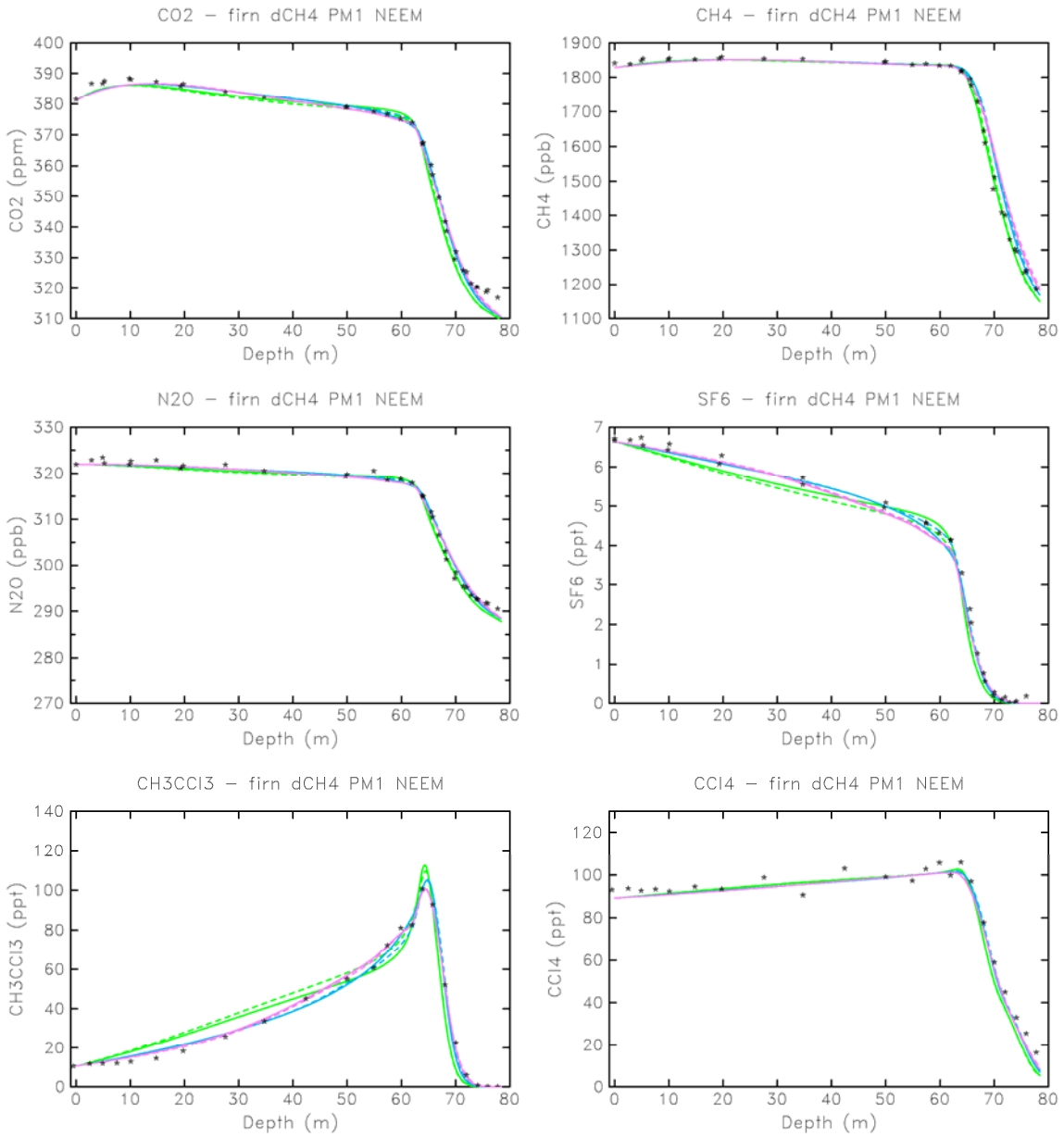

Figure 3.9 Depth profiles of observed mixing ratios (symbols) for CO_2, CH_4, N_2O, SF_6, CH_3Cl_3 and CCl_4 in NEEM firn air, along with LGGE firn diffusion model simulations (curves). For symbols: Black: NOAA observations; Blue: CSIRO observations; Pink: University of Heidelberg observations. Crosses: EU borehole; triangles: US borehole. Curves: forward model simulations from LGGE firn diffusion model, green: diffusivity tuned with CH_4; blue: diffusivity tuned with CO_2; purple: diffusivity tuned with CH_3Cl_3.

3.3.3 LGGE Firn Diffusion Model

A 1-D gas diffusion model developed by [*Rommelaere et al.*, 1997] was employed based on our CO data to reconstruct the atmospheric trend of CO in NEEM firn air by [*Martinerie*, personal communication]. The procedures include: the direct model to simulate a firn concentration profile from an atmospheric trend scenario and calculate trace gas age distribution, the inverse diffusivity model for diffusivity calculation, and the inverse scenario model for atmospheric trend calculation. The details of physical and mathematical principles in the models have been discussed in the above paper, so the methodology is briefly introduced here.

Fig 3.10 illustrates the methodology used to calculate and evaluate firn diffusivity profiles. The diffusivity is calculated on a reference gas with well-know trend scenario. The inverse diffusivity model is applied with this scenario and the measured depth profile of the reference gas to produce the diffusivity of the reference gas. The calculated diffusivity combined with a scenario of other reference gas is employed in the direct diffusion model to produce the depth-profile of other gas. This calculated depth profile is compared with that measured in the firn to show the systematic biases at the specific depth.

Fig 3.11 shows the methodology for scenario reconstruction. A Green function is calculated with the direct diffusion model with input of firn diffusivity and Dirac time trend scenario. The dirac scenario is used to derive statistics on how it propagates in the

firn, by constraining the direct model with a single time-step concentration pulse [*Martinerie*, personal communication]. The Green function and the measured data with uncertainties are then input to the inverse scenario diffusion model and produce the calculated atmospheric trend for the target gas (CO in this study). To validate this atmospheric trend, the calculated scenario with firn diffusivity is then used as input to the direct diffusion to produce a calculated depth profile. This calculated depth profile of CO is compared with the measured depth profile and provides a validation for the results. All of the results from these model simulations are shown in Fig 3.12, which will be discussed below.

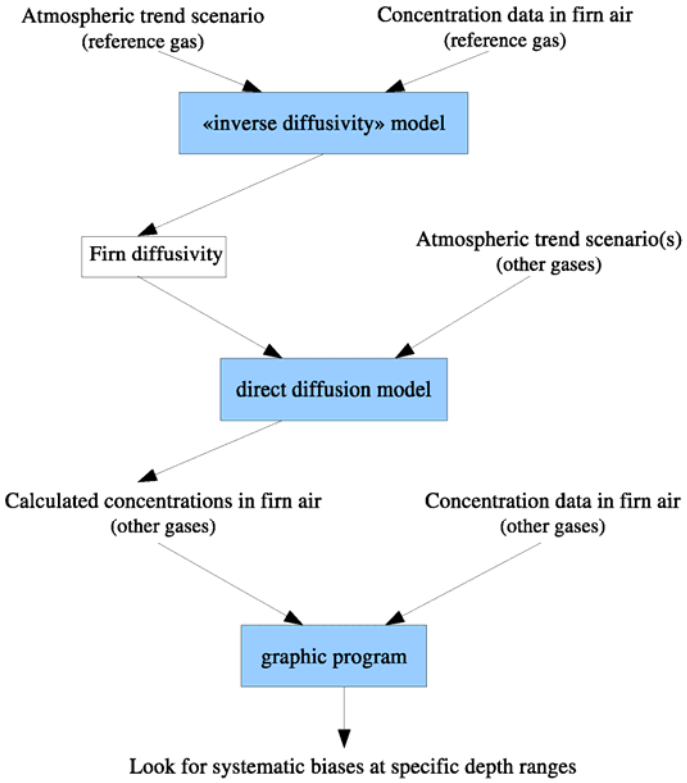

Figure 3.10 Flow chart for diffusivity calculation and depth-profile in firn diffusion model [*Martinerie*, personal communication].

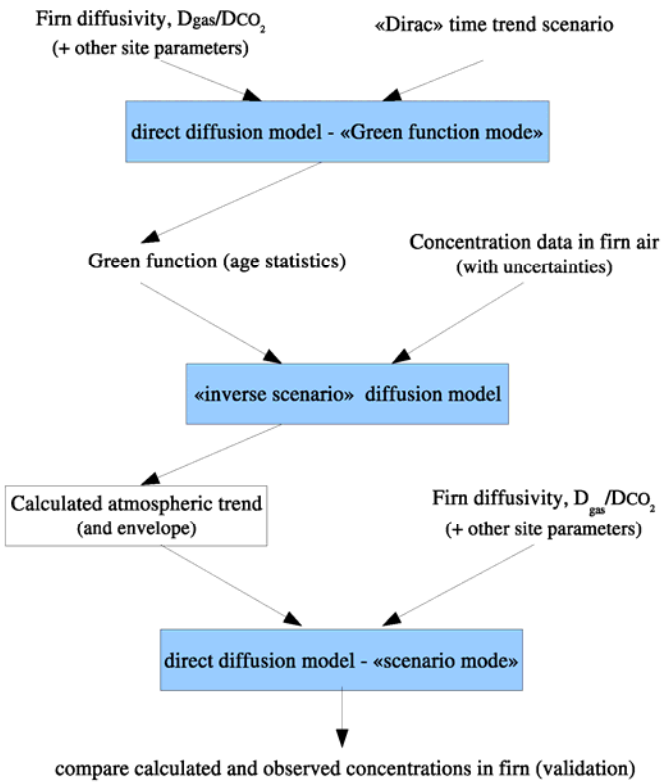

Figure 3.11 Flow chart for atmospheric trend calculations in firn diffusion model [*Martinerie*, personal communication].

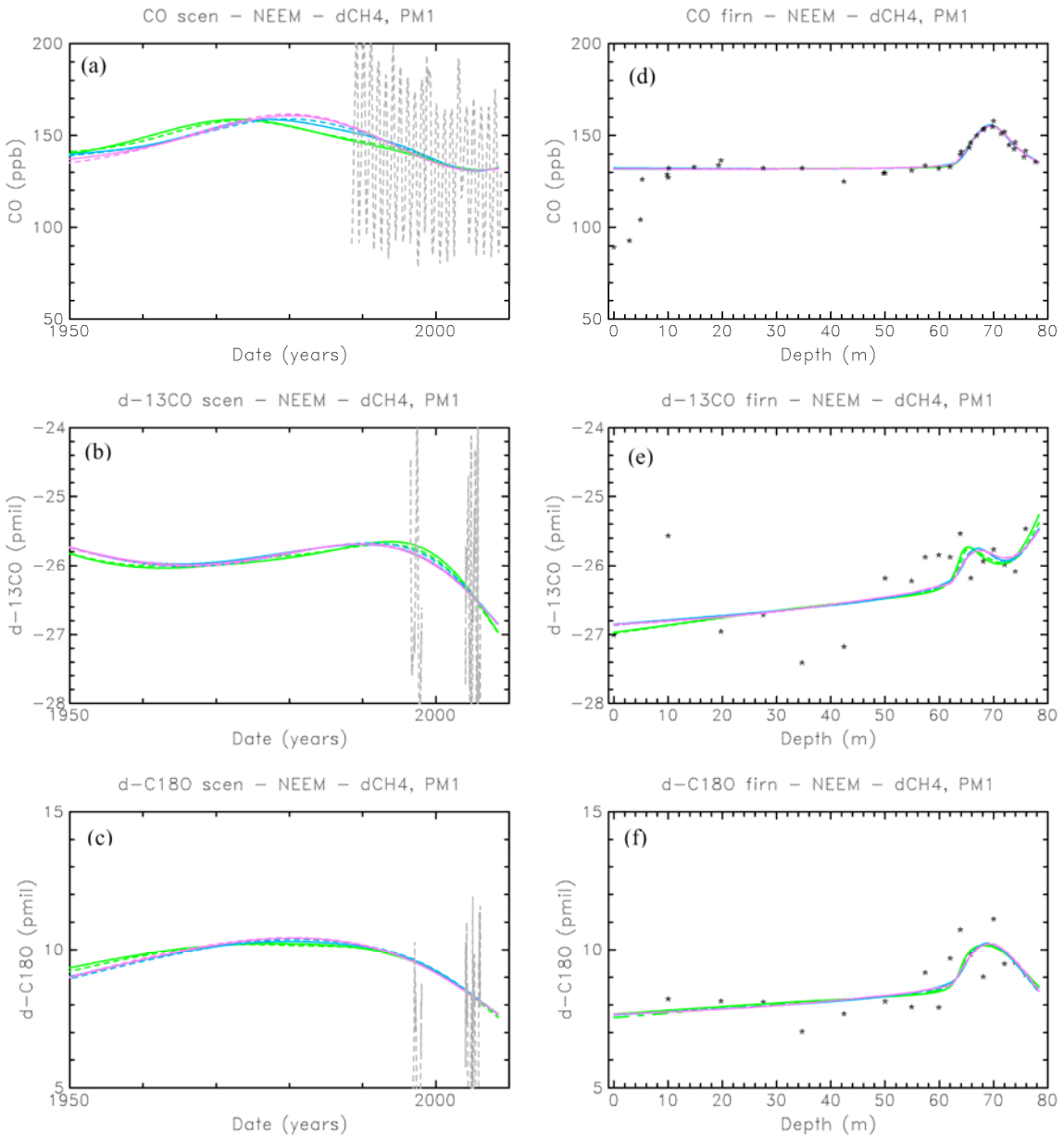

Figure 3.12 LGGE firn diffusion model simulation performed on NEEM firn air. (a)-(c): Reconstruction of atmospheric trend for [CO] and isotopic ratios since 1950 based on diffusivities derived from the direct model and our measurements on the NEEM firn air samples. (a): CO mixing ratio; (b): $\delta^{13}C$ of CO; (c): $\delta^{18}O$ of CO. Green lines: diffusivity tuned with CH_4; blue lines: diffusivity tuned with CO_2; purple lines: diffusivity tuned with CH_3Cl_3. Also shown (grey dashed lines) are: (a) NOAA atmospheric data (GAW database) at Barrow (71.32ºN 156.61ºW) in 1988-2008; (b) and (c): observations at Alert (82º27'N 62º31'W) in 1996-1998 by [*Brenninkmeijer*, personal communication] and observations at Iceland (63º15'N 20º09'W) in 2003-2004 [*J Mak*, personal

communication]. (e)-(f): Calculated depth profiles of [CO] and isotopic ratios for NEEM firn air samples based on direct diffusion model with firn diffusivity and the calculated atmospheric trend in (a)-(c), compared with our observations. Colors of the lines stand for the same as in (a)-(c).

3.3.4 Discussions

First of all, due to the limitations of firn models, more attention should be paid for the upper firn (above 20 m, Fig 3.12 a-c). It should be noted that the rugosity factor [*Rommelaere et al.*, 1997] controlling the smoothness of the solution has the same effect at all depths [*Martinerie*, 2009], whereas the physics of firn diffusion implies faster gas exchanges near the surface than in the deep firn [*Colbeck*, 1989; *Landais et al.*, 2006; *Sowers et al.*, 1992]. Thus a large rugosity factor avoiding oscillations of the solution does not allow to simulate fast near-surface variations such as the impact of large seasonal variations for CO [*Martinerie*, 2009]. The inverse problems are multiple solution problems, thus a best model solution is not necessarily to be the real solution [*Rommelaere et al.*, 1997]. The Rommelaere et al. (1997) model aims at finding the smoothest solution (defined by using the highest acceptable rugosity factor) which fits measurements in firn within a user-defined error criteria [*Martinerie*, 2009].

. The atmospheric trend of CO concentration shows a peak of ~155 ppbv in the past 50 years in (Fig 3.12 a), however there exists discrepancy for the exact year of the [CO] peak between CH_4 tuned simulation and CO_2/CH_3CCl_3 tuned simulation. The CH_4 tuned simulation indicates a peak in 1970, whereas CO_2/CH_3CCl_3 tuned simulation shows [CO]

peaked in 1980. This is explained by the fact that CH_4 diffuses faster than CO_2, resulted from higher diffusion coefficient for a smaller molecule [*Martinerie*, personal communication]. Our modeled atmospheric trend of [CO] in the recent past is consistent with NOAA observations at Barrow, Alaska, United States. Both show a decrease of [CO] from late 1980s and relatively stable trend after 2000.

Our reconstructed CO concentration indicates [CO] in 1950 was ~140 ppbv (Fig 3.12a), which is inconsistent with 110 ppbv in 1950 from Greenland ice core CO record [*Haan et al.*, 1996]. This apparent disagreement is not really a concern at this point [*Chappellaz*, person communication]. First, it is hard to attribute a specific date to the deepest firn air sample, with a large range of time contribution, covering potentially several decades. Second, the dating of a single point in Eurocore ice is also not determined at better than 10-20 years on average [*Chappellaz*, person communication].

$\delta^{13}C$ decreased around 1‰ since 1950, compared with present-day annual average value of ~ -27‰ in Iceland. And $\delta^{13}C$ was relatively constant before 1990. The modeled $\delta^{13}C$ in the recent past is comparable with Alert (1996-1998) and Iceland (2003-2004) observations. Discrepancies appear between the calculated $\delta^{13}C$ and observed $\delta^{13}C$, which arises from the uncertainties of our measurements as well as the errors from the firn diffusion model. The inconsistence between 30 m to 50 m, where the seasonal impacts disappear, is unexplained so far and more model tests are required [*Martinerie*, personal communication].

Our modeled $\delta^{18}O$ increased ~1‰ from 1950 to 1980, followed by a decrease of 2‰ to present-day. Larger discrepancies are observed between the calculated $\delta^{18}O$ and observed $\delta^{18}O$, which are believed to come from the large uncertainties of our measurements as well as the errors from the firn diffusion model. Similar to $\delta^{13}C$, the inconsistence between 20 m to 50 m is unexplained so far and more model tests are required [*Martinerie*, personal communication].

The variations of atmospheric trend of [CO] as well as the shifts of both isotope compositions since 1950 indicate a variation of CO budget in high-latitude NH: a [CO] peak occurred in 1970s-1980s To explain the atmospheric trend of CO over the past half century, we first discuss high-latitude NH CO budget in modern atmosphere. MOZART-4 simulations have been performed on Iceland in 1996-2004 to produce the relative contribution of different CO sources [*K.H. Park et al.*, in preparation]. CO sources in high-latitude NH are complicated. Model simulations indicate that there are five major sources which contribute more than 10 ppbv CO: fossil fuel combustion, NMHC oxidation, CH_4 oxidation, biogenic, and biofuel. ^{18}O enriched sources are fossil fuel combustion, biomass burning and biofuel [*K.H. Park et al.*, in preparation]. $\delta^{13}C$ isotope fraction of fossil fuel combustion is very close to the total $\delta^{13}C$ [*L K Emmons et al.*, in preparation], indicating change of fossil fuel CO has little impact on the total $\delta^{13}C$ of CO. However, the calculated $\delta^{18}O$ isotope fractions of different sources in Iceland indicate fossil fuel, biomass burning, and biofuel are the three major sources providing heavy

$\delta^{18}O$ of CO [*K.H. Park et al.*, in preparation]. Thus we believe the $\delta^{18}O(CO)$ increase from 1950 to 1980s accompanying with [CO] increase possibly resulted from these three sources. The high-resolution ammonium and formate profiles are used to reconstruct the frequency and the intensity of high-latitude biomass burning input having reached central Greenland between 1193and 1980, indicating a decrease of fire frequency from the beginning of the 20th century to 1980 [*Savarino and Legrand*, 1998]. Woodfuel consumption increases with population, thus we believe biofuel CO emission also increased over the past half century.

The $\delta^{13}C$ isotope fraction in Iceland was estimated to be ~-23.5‰ [*L K Emmons et al.*, in preparation], which is 2.5‰ heavier than reconstructed $\delta^{13}C(CO)$ before 1980. If biofuel emission dominated CO level increase from 1950 to 1980, $\delta^{13}C$ of CO would show a greater increase during this period. So we conclude fossil fuel combustion most likely caused this [CO] and $\delta^{18}O(CO)$ peaks.

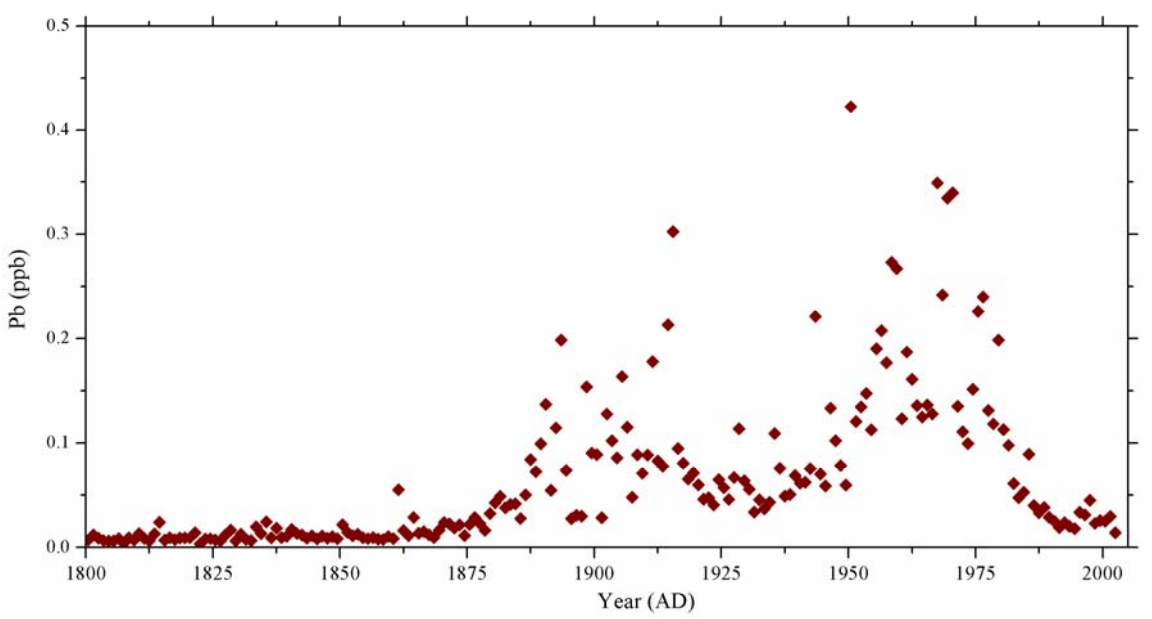

Figure 3.13 High-resolution, continuous measurements of Pb concentration in an ice core from Summit, Greenland from 1750 to 1998 [*McConnell et al.*, 2002].

Fig 3.13 shows the Pb concentration in mid-high latitude NH since 1800 based on Greenland ice core measurements, showing the decrease of Pb occurred from 1970 to 1985 [*McConnell et al.*, 2002]. This decrease of Pb concentration is believed to result from the invention of catalytic converter and application in vehicles since late 1970s [*Kummer*, 1980; *Young and Finlayson*, 1976]. The catalytic converter also effectively reduces the CO emission [*Tsunogai et al.*, 2003] based on the oxidation reaction of 2CO + O_2 -> CO_2. Therefore, we believe CO emission from fossil fuel combustion has dropped since 1980, which counteracts the CO growth due to CH_4 increase (Fig 3.14) and is at least partly responsible for [CO] peak in 1980. Furthermore, the most important fossil fuel CO contributor is West Europe, where the diesel engine vehicles market started to grow in early 1980s and about 50 percent of all new car sales in Europe are diesel

based as of 2007 [*Smolinska*, 2008]. With the three-way functional catalytic converter and the oxygen storage capacity [*Brandt et al.*, 2000], diesel engine vehicles have much higher efficiency to convert CO in exhaust to CO_2 [*Tsunogai et al.*, 2003], supporting a decrease of CO emission from fossil fuel combustion since 1980.

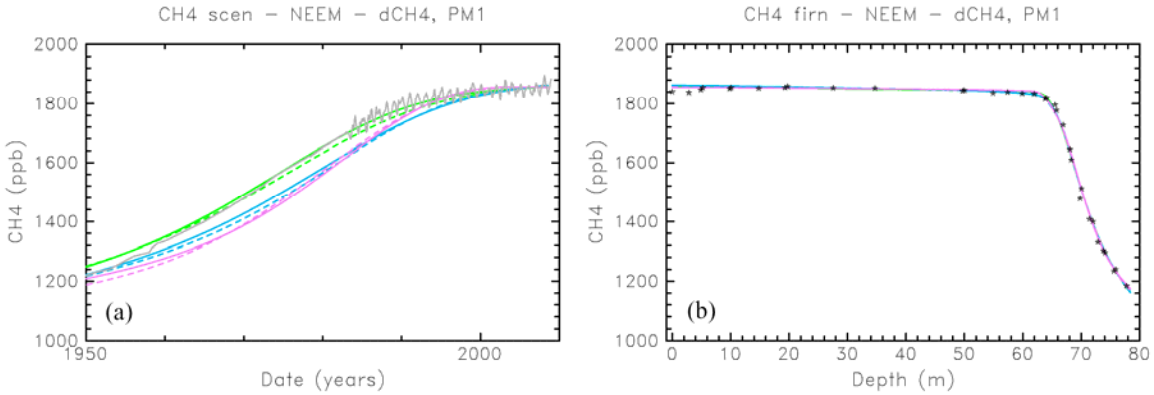

Figure 3.14 LGGE firn diffusion model performed on NEEM fir nair. (a): Evolution of the atmospheric CH_4 concentration since 1950. (b) Calculated depth profile and observations of [CH_4] in NEEM firn air. Colors of the lines stand for the same as in Fig 3.12.

Figure 3.13 shows the $\delta^{18}O$ isotope fraction is a good tracer of fossil fuel combustion since its $\delta^{18}O$ is very different from others. Furthermore, its $\delta^{18}O$ signature is as high as 23.5‰ [*C. A. M. Brenninkmeijer*, 1993; *Stevens et al.*, 1972]. Annual average of $\delta^{18}O$ of CO in Iceland is around 5‰ [*K.H. Park et al.*, in preparation], and only ocean and fossil fuel $\delta^{18}O$ is heavier than this (Fig 3.13). Ocean source is tiny and its influence on the total $\delta^{18}O$ is considered negligible. Furthermore, both ammonia and formate records [*Savarino and Legrand*, 1998] and records of ^{17}O in sulfate and nitrate [*Alexander et al.*, 2004] in Greenland ice core show a decrease of biomass burning from 1880 to 1980. Therefore,

$\delta^{18}O$ peak in 1980 supports that fossil fuel might be part of the reason for [CO] peak in 1980. As mentioned above, $\delta^{13}C$ is not sensitive to the [CO] derived from fossil fuel combustion since they have very close $\delta^{13}C$ values. Consequently, even fossil fuel dominated atmospheric CO trend since 1950, $\delta^{13}C$ was relatively stable.

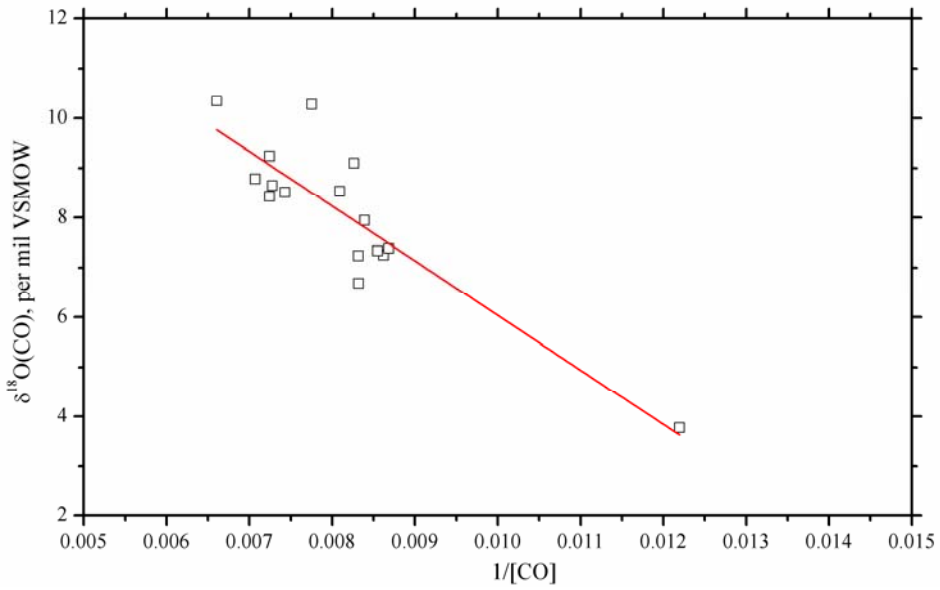

Figure 3.15 The linear correlation between $\delta^{18}O$ and 1/[CO] for NEEM firn air (known as a keeling plot). $R^2 = 0.77$ is obtained, indicating a strong correlation. Data has already been corrected by gravitational fractionation based on NEEM $\delta^{15}N$ data [*Landais and Capron*, personal communication].

A linear regression is obtained based on $\delta^{18}O$ and inverse of [CO] (Fig 3.15). First of all, this linear correlation shows increase of [CO] will drive an increase of $\delta^{18}O$, indicating some heavy $\delta^{18}O$ source dominated CO evolution since 1950. Intercept of 17‰ is exactly the $\delta^{18}O$ isotope fraction of fossil fuel combustion in Iceland [*K.H. Park et al.*, in preparation], showing fossil fuel combustion source dominated the $\delta^{18}O$ change. Based on the [CO] increase from 140 ppv to 160 ppbv between 1950 and 1980, $\delta^{18}O$ will

increase 1.15‰, which is consistent with the model simulation (~ 1 per mil increase). From 1980 to 2000, [CO] dropped from 160 ppbv to 130 ppbv, resulting in a 1.9‰ decrease for $\delta^{18}O$, which is also consistent with the modeled $\delta^{18}O$ decrease of ~ 2‰.

Future work will be Monte-Carlo simulation: using a large number of hypothetical trend scenarios and selecting those consistent with measurements in firn. This will give us the envelope of the temporal scenarios [*Braunlich et al.*, 2001; *Sowers et al.*, 2005b]. Once we are confident with the temporal scenarios, an atmospheric model can be applied on our reconstructed CO records of the three tracers: the mixing ratio and the two stable isotopes and the change of CO budget since 1950 can be determined [*Braunlich et al.*, 2001].

3.4 Concluding Remarks

This chapter focuses on the atmospheric CO records over the last several decades. These records have been produced based on measurements of firn air samples collected from both hemispheres: Berkner Island in Antarctica, NGRIP and NEEM in Greenland.

Air samples from NGRIP firn and Berkner Island firn have been analyzed to reconstruct atmospheric CO concentration and isotopic compositions during the past half century in high-latitude Northern Hemisphere and over Antarctica. As the preliminary work of this study, and since the new cryogenic extraction system was not ready at that

time, we are not very confident about these data and no diffusion model is applied on them.

The atmospheric trend of CO in Northern Hemisphere since the mid-20th century has also been reconstructed from firn air of North Greenland Eemian Ice Drilling (NEEM Project, 2008). CO concentrations, $\delta^{13}C$, and $\delta^{18}O$ have been determined. The LGGE firn diffusion models have been applied to reconstruct past atmospheric trend in CO, where its concentration and isotope composition is constrained by our observations of CO concentration and isotopic ratios. The depth profiles show the concentration of CO peak at around 70 m with a value of 160 ppbv, whereas isotopically heavy peaks for both $\delta^{13}C$ and $\delta^{18}O$ occurred below 60 m. Firn diffusion model simulation indicates that the maximum of atmospheric CO in high latitude Northern Hemisphere occurred in 1970s. The peak of $\delta^{18}O$ reflects the large contribution of fossil fuel combustion in 1970s.

By future application of an atmospheric model, changes in CO sources and OH sink are compatible with the past atmospheric trends will be explored. This will definitely help understand the causes of CO change and the atmospheric chemistry in NH.

Chapter 4. Records of Atmospheric CO in Antarctic Ice Cores

Though not directly a greenhouse gas, atmospheric CO is known to play a significant role in atmospheric chemistry and have a close link with OH and CH_4 [*Crutzen and Zimmermann*, 1991; *Logan et al.*, 1981; *A.M. Thompson*, 1992]. CH_4 oxidation by OH is an important source of CO especially in the SH [*Bergamaschi et al.*, 2000b; *Manning et al.*, 1997], meanwhile CO reaction with OH is the major sink of CO [*C. A. M. Brenninkmeijer*, 1993; *IPCC-SAR*, 1996] and also the major sink of OH [*Crutzen and Zimmermann*, 1991]. The coupling of CH_4-CO-OH is complex and has been discussed in [*Crutzen and Zimmermann*, 1991; *Isaksen*, 1987; *A. M. Thompson and Cicerone*, 1986], which shows the strong correlation among these three species. Atmospheric OH determines the oxidation efficiency of the atmosphere and it is, therefore, of the utmost importance for maintaining the chemical composition of the atmosphere [*Crutzen and Zimmermann*, 1991].

Ice core records have indicated substantial increase in the concentrations of CH_4 during the past 200 years due to anthropogenic emissions [*Etheridge et al.*, 1998; *Meure et al.*, 2006]. It is also speculated that human activities have led especially to increasing CO, O_3, and NO_x, which will thus change the atmospheric oxidizing capacity [*Crutzen*

and Zimmermann, 1991]. As a key player of atmospheric chemistry, preindustrial CO enhances understanding the change of atmospheric oxidizing capacity and how anthropogenic emissions have driven the change of atmospheric chemical compositions and atmospheric chemistry since preindustrial times.

The main reason to determine preindustrial CO abundances is thus to examine natural variations in the CO budget without human perturbations, which is then used to extrapolate the overall stability of tropospheric chemistry basics: CH_4-CO-OH cycle. Previous studies indicate CO concentration was relatively stable in high-latitude SH between 1840 and 1920 [*Haan et al.*, 1996] and between 235 to 1375 [*Haan and Raynaud*, 1998]. There are no data in the intervening period, spanning between 1375 and 1840, in their CO record, and the limited information on CO budget can be obtained only based on CO concentration. Thus, further more comprehensive study on preindustrial CO budget is necessary and important.

In this chapter, we will present new high precision measurements of atmospheric CO concentration and isotope composition during the past 700 years accomplished by analyzing the air trapped in Antarctic ice. A mass balance model is applied to the ice core data and allows for addressing the biogeochemical causes of atmospheric CO variations before preindustrial times.

4.1 Introduction

Previous studies show that isotope ratios of trace gases such as CH_4 and N_2O in ice cores assist in determining the various sources and sinks in the past and their historic relative magnitudes [*Ferretti et al.*, 2005; *Rockmann et al.*, 2003a]. It was observed that $\delta^{13}CH_4$ was at least 2‰ enriched during 0-1000 A.D. compared to expected values, and an about 2‰ depletion occurred during the following 700 years [*Ferretti et al.*, 2005]. The authors suggest that both human activities and natural climate change influenced preindustrial biomass burning emissions, which drove the unexpected variability of the methane budget over the last 2,000 years [*Ferretti et al.*, 2005]. Records of isotopic composition of atmospheric N_2O from Berkner Island ice core help a better understanding of the biogeochemical cycles involving atmospheric N_2O [*Bernard et al.*, 2006]. The 2.8‰ depletion for $\delta^{15}N$ and 1.6‰ depletion for $\delta^{18}O$ since 1700 indicates the increasing importance of agriculture for the present anthropogenic N_2O budget [*Bernard et al.*, 2006]. However, little is known about CO in ice core and none on isotope ratios of CO in ice core has been reported yet because of the experimental difficulties such as limitation of sample size and contamination due to in situ production [*Haan and Raynaud*, 1998; *Haan et al.*, 1996].

This chapter focuses on atmospheric CO isotope records since preindustrial times (1360-1900 A.D.). New decade-scale records of CO concentration as well as $\delta^{13}C$ and $\delta^{18}O$ have been produced from 40 Antarctic ice core samples. 20 of them are from the

D47 ice core (67˚23'S 154˚03'E 1550 m a.s.l.) and the other 20 samples are from near the South Pole (89˚57'S 17˚36'W 2800 m a.s.l.).

4.2 Drilling site and ice core characteristics

Antarctic ice cores samples in the present study are from two different drilling sites: D47 (67˚23'S 154˚03'E) and South Pole (89˚57'S 17˚36'W). D47 ice core was drilled in 1988-1989 by LGGE (Laboratoire de Glaciologie et Géophysique de l'Environnement) [*Barnola et al.*, 1995]. As mentioned (section 2.8.1), D47 ice core was dry drilled before 87.2 m and drilled with kerosene as fluid below and tests conducted at LGGE showed that kerosene is not a problem for CO with careful cleaning of the sample [*Chappellaz*, person communication]. Our CO measurements prove that our D47 ice core samples were not affected by kerosene at all (section 4.5.1). South Pole ice core (Bore Hole 5) was drilled in 2004 with electromechanical method by Jihong Cole-Dai from NICL-MSO (National Ice Core Laboratory-Science Management Office). No fluid was used during drilling so that there was minimum amount of contamination for CO. The detailed ice core characteristics were listed in the table 4.1 and the location of the cores is shown in Fig 4.1. Apparently, South Pole ice core is located on the central plateau with low accumulation rate of 7.6 cm ice yr^{-1}, whereas the D47 ice core is from a coastal site of east Antarctica with high accumulation rate of 30 cm ice yr^{-1}.

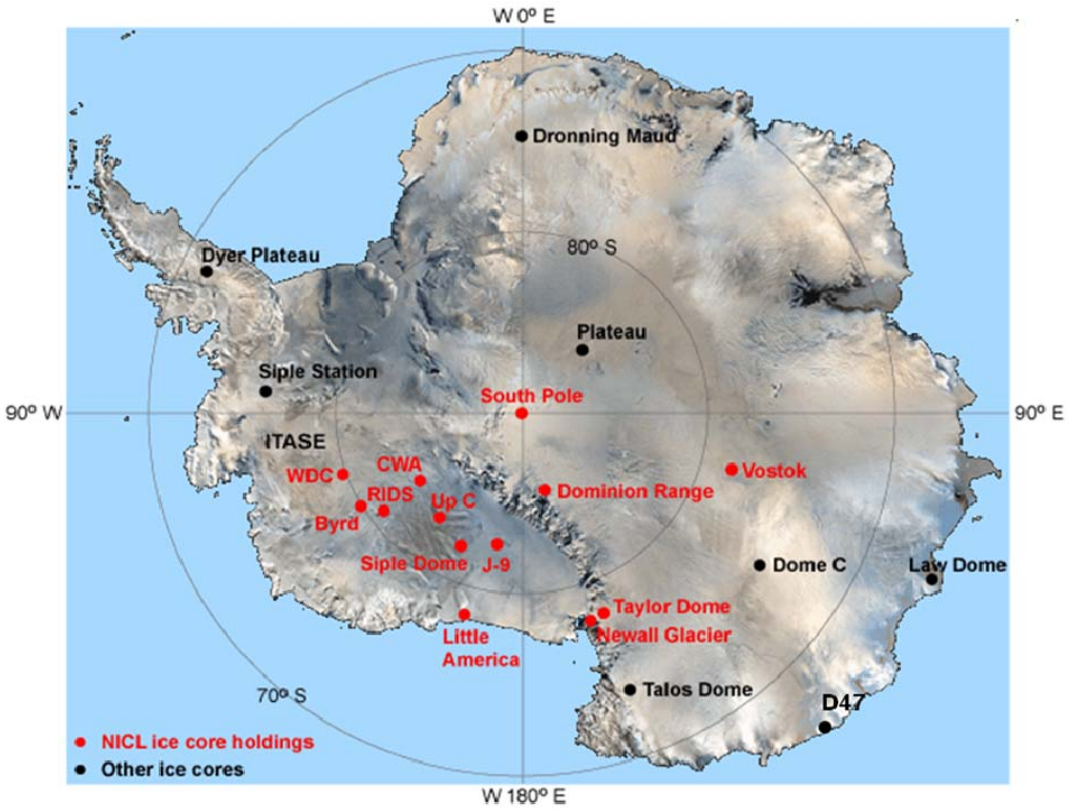

Figure 4.1 Location of D47 (67˚23'S 154˚03'E 1550 m.a.s.l.) and South Pole (89˚57'S 17˚36'W 2800 m a.s.l.) ice core drilling site, together with other core sites including Law Dome (66°44' S, 112°50' E, 1390 m a.s.l.) ice core [*Ferretti et al.*, 2005] which will be discussed in section 4.5. Map is edited based on that from NICL Science Management Office website: nicl-smo.unh.edu/icecoresites/antarctica.html.

Table 4.1 Present-day physical characteristics for D47 ice core and South Pole ice core.

Site	D47[1]	South Pole
Location	67˚23'S 154˚03'E	89˚57'S 17˚36'W
Altitude (m)	1550	2800[2]
Year of drilling	1988-1989	2004
Mean annual temperature	-25	-51[2]
Accumulation rate	30 cm ice / year	7.6 cm ice / yr[¶]
Air/ice difference in age	165	950[2]
Width of age distribution	10-15	220[2]

[1]: Data from [*Chappellaz et al.*, 1997]; [2]: data from [*Schwander and Stauffer*, 1984]; [¶]: [*Battle et al.*, 1996].

The D47 ice core samples were full cylinders with a diameter of around 10 cm and length of around 27 cm (some pieces are shorter and some consist of couple of small pieces), whereas South Pole ice core samples were longitudinal half core sections, approximately 30 cm in length. The mass of D47 ice samples ranged from 500-1200 g, and that of South Pole ice samples ranged from 900-1100 g.

D47 ice core samples were provided from the archived collection at LGGE by Dr. Jérôme Chappellaz. As discussed in section 2.7.1, D47 ice samples were processed in the wet extraction system in LGGE based on the principles in [*Chappellaz et al.*, 1997] and released air was analyzed based on the protocol for small air samples in [*Z H Wang and Mak*, 2009]. South Pole ice core samples were cut and prepared in NICL. South Pole ice samples were measured based on the protocol in [*Z H Wang and Mak*, 2009].

4.3 Dating of D47 and South Pole ice cores

4.3.1 D47 ice core

Dating of D47 ice core has been discussed in [*Barnola et al.*, 1995; *Haan et al.*, 1996]. We briefly summarize here. This core has been dated using different volcanic horizons revealed by the Electrical Conductivity Measurement (ECM) records as no continuous record of seasonal variation have been obtained [*Barnola et al.*, 1995]. The age distribution of each D47 sample was characterized by a standard deviation of 12

years around the mean and the uncertainties were suggested as ±15 years [*Haan et al.*, 1996], which will be taken as the dating error for our D47 ice core samples. Ice age-gas age difference was estimated to be 162-214 years [*Barnola et al.*, 1995]. As pointed out in [*Barnola et al.*, 1995], the accuracy of the chronology for D47 dating is good down to the last volcanic horizon, which correspond for the age to around 1630 (~ 154 m). A linear function between D47 ice core depth ranging from 70.48 m to 154 m and the mean gas age [*Barnola et al.*, 1995; *Haan et al.*, 1996] is plotted in Fig 4.2 and our D47 ice core samples have been dated by extrapolation. The slope, intercept, and correlation is given by the table on the top right. The mean gas ages calculated based on the linear function and sample depths are shown in table 4.2.

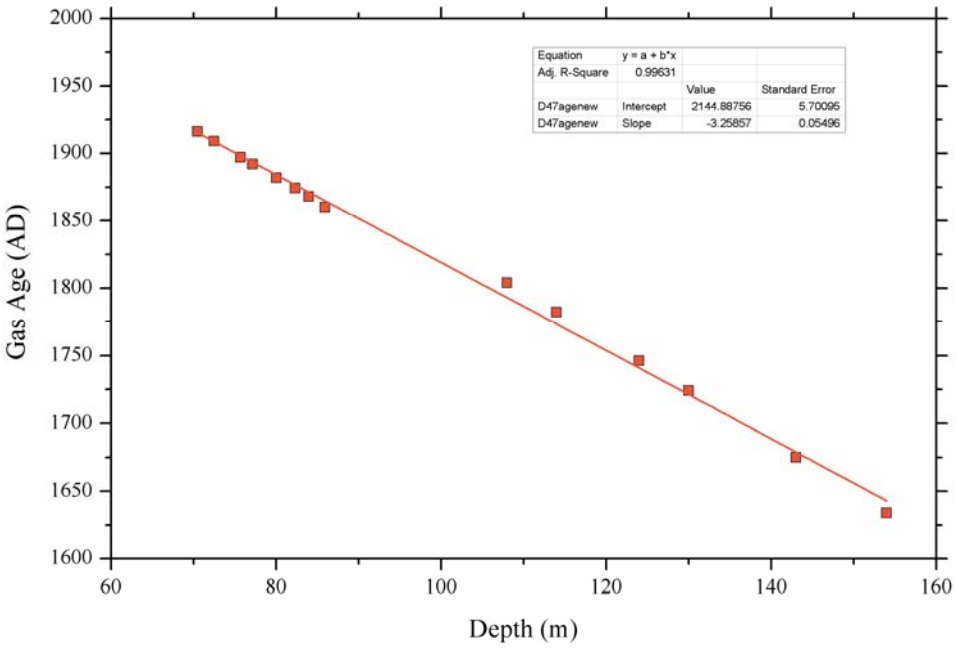

Figure 4.2 Linear regression curve used for D47 ice core dating, data from [*Barnola et al.*, 1995; *Haan et al.*, 1996].

Table 4.2 Calculated mean gas age for D47 ice core samples based on the linear regression in Fig 4.2

Depth(m)	Mean Gas Age (year AD)
76	1897
79	1887
80	1884
81	1881
86	1865
89	1855
95	1835
98	1826
100	1819
109	1790
111	1783

4.3.2 South Pole ice core

Dating of South Pole ice core is still in progress. In this study, dating South Pole ice core is based on gas age data reported in [*Friedli et al.*, 1984; *Neftel et al.*, 1985; *Schwander and Stauffer*, 1984], which is based on the Tambora volcanic horizon (1816) revealed by the ECM record [*Barnola et al.*, 1995]. The ice age-gas age difference was estimated to be 950 years [*Schwander and Stauffer*, 1984]. A linear regression is obtained with all depth-gas age data reported in these studies (Fig 4.3) and our South Pole ice core samples have been dated by extrapolation. The slope, intercept, and correlation is given

by the table on the top right. The age width of South Pole ice core is estimated to be 100 years, which is suggested by the firn densification model [*Schwander et al.*, 1993]. The mean gas ages calculated based on the linear function and sample depths are shown in table 4.2.

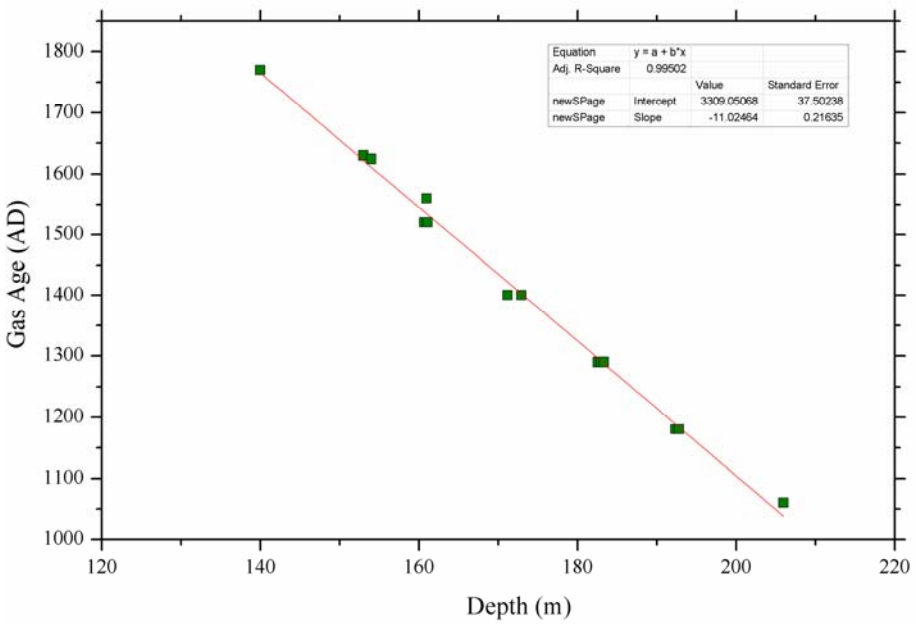

Figure 4.3 Linear regression curve for South Pole ice core dating, data from [*Friedli et al.*, 1984; *Neftel et al.*, 1985; *Schwander and Stauffer*, 1984].

Table 4.3 Calculated mean gas age for South Pole ice core samples based on the linear regression in Fig 4.3

Depth(m)	Mean Gas Age (year AD)
130	1876
132	1854
135	1821
139	1777
141	1755
144	1722
147	1688
150	1655
152	1633
153	1622
157	1578
160	1545
162	1523
165	1490
168	1457
170	1435
173	1402
177	1358

4.4 Corrections for Ice Core Isotopes

The measured ice core data should be corrected for gravitational fractionation,

which can be estimated with the $\delta^{15}N$ data obtained on firn air of the corresponding core sites [*Bender et al.*, 1997; *Bender et al.*, 1994; *Landais et al.*, 2006; *Sowers et al.*, 1989].

The pressure of some species (trace gas or isotope) in the firn increases with depth below the surface according to the barometric equation:

$$P_z / P_0 = \exp(mgz/RT)$$

Where P is the pressure, z is the depth (z =0 at the surface of the firn), m is molar mass, g is gravitational acceleration constant, R is the ideal gas constant, and T is the absolute temperature [*Battle et al.*, 1996; *Craig et al.*, 1988a; *Sowers et al.*, 1989]. As a result, the heavier gases and isotopes enrich with depth. The relative enrichment with depth for different species is directly proportional to the mass difference, which means correction of our $\delta^{18}O$ as twice as that of $\delta^{13}C$. The correction of $\delta^{13}C$ and $\delta^{18}O$ is thus derived based on the following equation:

$$\delta^{15}N = \delta^{13}Cc = \delta^{18}Oc / 2 = (g \times z) / (R \times T) \times 1 \text{ kg mol}^{-1}$$

where $\delta^{15}N$ is the value reached at the close-off depth, $\delta^{13}Cc$ and $\delta^{18}Oc$ is the correction for our ice core data, g is the gravitational acceleration, z is the thickness of the diffusive column, R is the gas constant, and T is the mean firn temperature, with all parameters being expressed in SI [*Landais et al.*, 2006].

Fig 4.4 shows the firn isotopic measurements of $\delta^{15}N$, $\delta^{40}Ar$, and $\delta^{18}O$ performed on Berkner Island, Antarctica. $\delta^{15}N$ shows a 0.25‰ shift between the surface and the close-off depth. No firn air experiment was performed at the time of D47 ice core drilling

in 1988, and no such measurements have been performed on D47 ice so far. Consequently, no $\delta^{15}N$ measurement appears from the D47 ice core yet. However, as the climactic conditions in D47 are very close to those of Berkner Island, both of which are coastal core sites, the $\delta^{15}N$ value in Berkner Island is adopted as the correction for our $\delta^{13}C$ in this study [*Chappellaz*, person communication]. Consequently, the correction for D47 ice core $\delta^{13}C$ is -0.25‰ and that for $\delta^{18}O$ is -0.5‰.

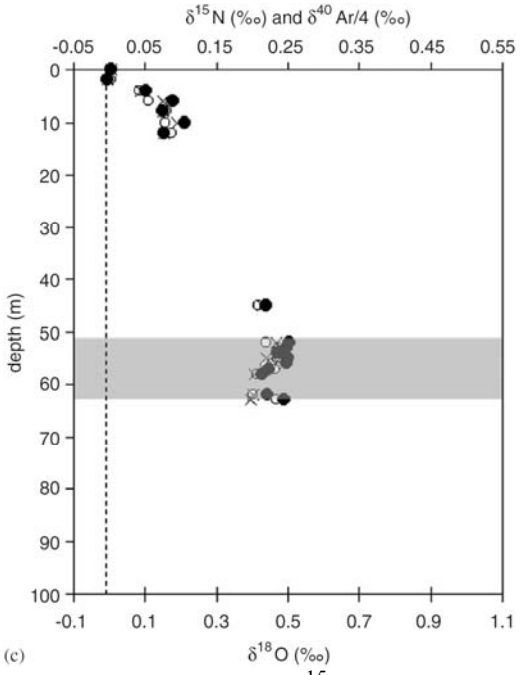

Figure 4.4 Firn air isotopic measurements of $\delta^{15}N$ (black circles), $\delta^{40}Ar$ (open circles), and $\delta^{18}O$ (crosses) performed on Berkner Island [*Landais et al.*, 2006]. Shading strip stands for the non-diffusive zone and the dashed line is 0‰.

As for South Pole, firn air $\delta^{15}N$ measurement has already been performed [*Battle et al.*, 1996]. The $\delta^{15}N$ at close-off depth is around 0.6‰, which is taken as the correction of our isotopic measurements on South Pole ice core samples. Consequently, the correction for South Pole ice core $\delta^{13}C$ is -0.6‰ and that for $\delta^{18}O$ is -1.2‰.

4.5 Results and Discussions

4.5.1 CO concentration

First of all, it must be determined whether the trends observed in the record are real, and if the CO measurements were enhanced, by how much and whether the cause of this enhancement may be identified [*Meure*, 2004]. Studies on CO production from organic compounds in fresh snow [*Haan et al.*, 2001] and ammonia and formate in Greenland ice core [*Savarino and Legrand*, 1998] have shown the possibilities of in-situ CO production in polar ice core. Modeled global distribution of biogenic Volatile Organic Compounds (VOC) indicates a much higher level in Northern Hemisphere than in Southern Hemisphere [*Guenther et al.*, 1995], supporting less possibility of in-situ production of CO in Antarctic ice core. The concentrations of organic compounds in the ice at Law Dome are not expected to be significant, so in situ production of CO is unlikely [*Meure*, 2004].

Colussi and Hoffmann proposed a new mechanism for CO production in deep ice: in-situ photodecarbonylation of chromophoric organic matter due to Çerenkov radiation fluxes generated by penetrating muons of cosmic origin [*Colussi and Hoffmann*, 2003; *Guzman et al.*, 2007]. This in-situ photodecarbonylation has been shown to be quantitatively consistent with the elevated CO concentrations in Greenland ice [*Haan and*

Raynaud, 1998], but not in the cleaner Antarctic ice [*Colussi and Hoffmann*, 2003]. The CO production in Greenland Summit ice core records correlate significantly with the occurrence of boreal fires and the associated release of organic aerosol [*Savarino and Legrand*, 1998]. It has been pointed out that this photodecarbonylation reaction would drive an increase in CO concentration with depth, consistent with the Greenland CO measurements [*Meure*, 2004]. However, this correlation does not appear in our ice core CO records.

The in situ production of CO_2 in ice also depends on the presence of organic compounds, which have also been shown to elevate CO_2 in the ice sheet, where organic compounds may be oxidized by H_2O_2, or other acids [*Meure*, 2004; *Tschumi and Stauffer*, 2000]. The CO_2 records from D47 ice core [*Barnola et al.*, 1995] and South Pole [*U. Siegenthaler et al.*, 2005] produce reasonable atmospheric CO_2 histories (Fig 4.6a) and show good agreements over the last millennium, indicating no in-situ production of CO_2 in these two cores. Therefore there is no evidence of enhanced CO in the D47 and South Pole ice cores and the trends observed in the presented records are deduced to be free from significant artifacts.

Observations of atmospheric CO concentration in different locations of Antarctica including Scott Base (77º51'S 166º46'E) [*Brenninkmeijer*, personal communication], South Pole Station (SPO: 89.98ºS, 24.80ºW, 2810 masl), Palmer Station (PSA: 64.92ºS, 64.00ºW, 10 masl), Halley Station (HBA: 75.58ºS, 26.50ºW, 30 masl), and Syowa Station

(SYO: 69.00ºS, 39.58ºE, 11 masl) (http://www.esrl.noaa.gov/gmd/ccgg/iadv/) show good consistence in 1993-2008, indicating homogeneous distribution of CO in this plateau, which is what we expect. Therefore, it is safe to combine our D47 ice core data with South Pole ice core data to produce a continuous CO record since preindustrial times.

Our ice core data are shown in Fig 4.5, along with the [CO] record from D47 and Vostok ice core published previously [*Haan and Raynaud*, 1998; *Haan et al.*, 1996]. Haan et al. 1996 indicates a fairly constant [CO] of 56.9 ppbv (±1σ standard deviation: 1.1 ppbv) in D47 ice core between 1860 and 1916. Our data also indicate a fairly constant [CO] of 55.2 ppbv (±1σ standard deviation: 2.3 ppbv) between 1865 and 1897. T-test was performed on these two data sets and indicated no significant difference between them, which shows good agreement between our D47 [CO] data and those in [*Haan et al.*, 1996]. CO mixing ratio shows a gradual decrease from 53 ppbv in 1360 A.D. and reached its minimum of 36 ppbv in 1600 A.D., which is within LIA. CO mixing ratios then increased from 40 ppbv in 1700 A.D. to a relatively constant mixing ratio of 50-60 ppbv in late 19th century. Observations of atmospheric CO at Scott Base by the National Institute of Water and Atmospheric Research (NIWA, New Zealand) from 2000-2003 are also shown in Fig 4.5 to show present CO [*Brailsford*, personal communication]. Annually averaged [CO] of 50-55 ppbv was observed at Scott Base, which is close to the CO levels in the 13th century and the 19th century. These observations indicate the CO budget has changed significantly during the past 700 years.

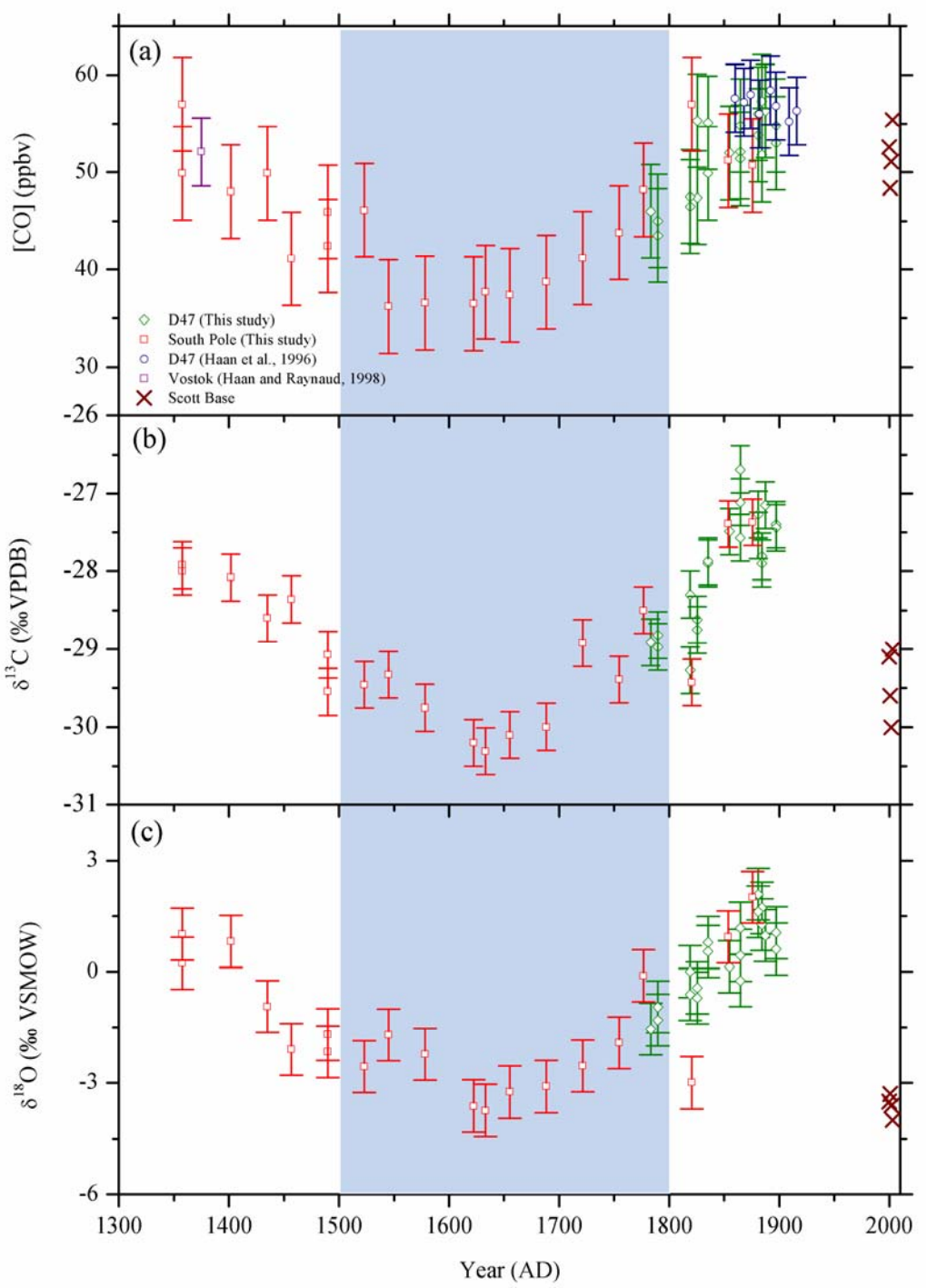

Figure 4.5 The D47 ice core (triangles) and South Pole ice core (diamonds) records from 1360 to 1900. (a) CO mixing ratio; (b) $\delta^{13}C$ of CO; (c) $\delta^{18}O$ of CO. Error bars show the analytical uncertainties (±1σ) of [CO], $\delta^{13}C$ and $\delta^{18}O$ as 4.8 ppbv, 0.3‰ and 0.7‰, respectively. Shading area shows the little ice age (1500-1800). Also shown are

observations of annually averaged atmospheric CO (crosses) in Scott Base (77° 51′S, 166° 46′E) in 2000-2003 [*L K Emmons et al.*, in preparation]. The ice core analytical method is discussed in previous study [*Z H Wang and Mak*, 2009] and chapter 2 of this thesis. The original ice core data are shown in appendix A and B.

The signal/noise ratio for our [CO] data is around 4 (20ppbv/5ppbv), that for $\delta^{13}C$ is around 10 (3‰/0.3‰), and that for $\delta^{18}O$ is around 7 (5‰/0.7‰). These high signal/noise ratios show these results are robust and the variations are significant.

Our observations of [CO] for D47 ice core and South Pole ice core agree well with previous [CO] observations in both the 13th century and the 19th century (Fig 4.5a). While uncertainties of [CO] are relatively high, they are still smaller than our [CO] variation and we still believe there is a real decrease of [CO] between 1500 and 1800. The saddle-shaped [CO] spanning the time period from 1360 to 1850, indicates a strong variation on CO source evolution.

Other trace gases recorded in Law Dome ice core and CO_2 from Dronning Maud Land and South Pole ice core during the past millennium are shown in Fig 4.6. The first feature is that [CH_4] was relatively constant before 1800 and the trend of [CH_4] did not coincide with the trend of NH temperature anomaly, which reached its minimum during the past two millennia [*Mann and Jones*, 2003; *Moberg et al.*, 2005]. As the CH_4 emission from wetland increased during little ice age, the decrease of CH_4 from biomass burning was thus compensated [*Ferretti et al.*, 2005]. Both [CO_2] and [N_2O] show a slight decrease during the little ice age, followed by a strong increase accompanying with the industrialization [*Barnola et al.*, 1995; *Meure et al.*, 2006; *U. Siegenthaler et al.*,

2005]. Compared with greenhouse gases, the correlation between CO and temperature is even more robust.

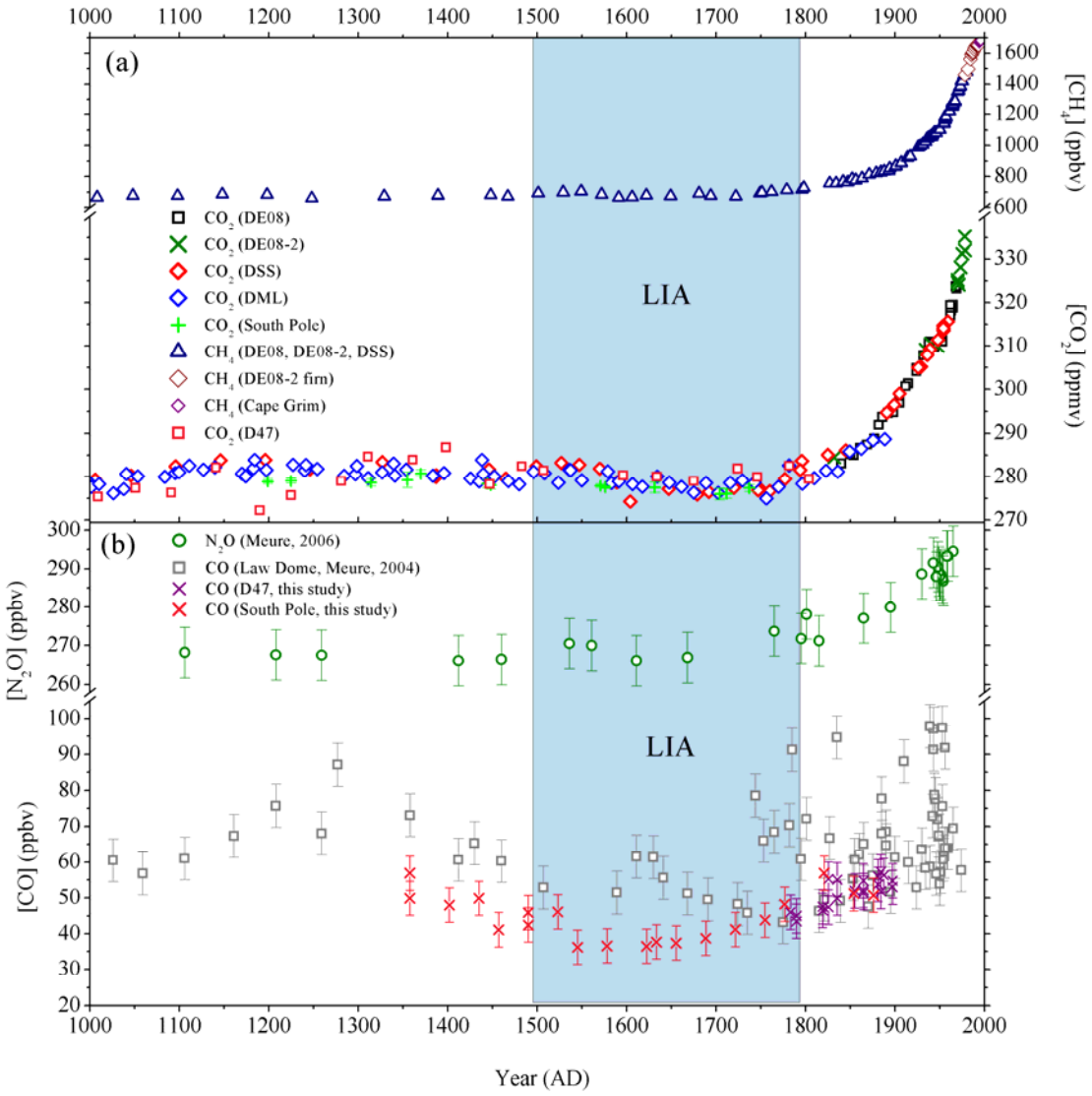

Figure 4.6 The 1000-year Law Dome ice core records for CH_4, CO_2, N_2O and CO [*Meure*, 2004; *Meure et al.*, 2006], also shown is CO_2 records in Dronning Maud Land (DML), South Pole (SP) and D47 ice cores [*Barnola et al.*, 1995; *U. Siegenthaler et al.*, 2005]. Shading area stands for the Little Ice Age (LIA).

The [CO] record from Law Dome [*Ferretti et al.*, 2005; *Meure*, 2004] is shown in Fig 4.6b. [CO] shows high concentrations and with large variabilities because of

occasional contamination within ice core samples and during extraction of the air from the samples, however it can be used as an indication of atmospheric changes in the high latitude southern hemisphere [*Etheridge*, personal communication]. It has been pointed out that improvements had been made to the Law Dome CO measurements for the period AD 0 to 1800, where there were fewer outliers and the majority of measurements were within the analytical uncertainty of the adjacent samples [*Meure*, 2004]. Consequently, we have more confidence on the trends of Law Dome [CO] and relative variations from AD 0 to 1800. More importantly, the trend of gradual decrease of [CO] from 1300 to 1700 is reproduced in our CO records, which shows a pronounced a decrease from 1300 to 1500 and a relatively stable level between 1500 and 1700 [*Ferretti et al.*, 2005].

4.5.2 CO Isotopes

Isotope ratios of CO in our ice core records are shown Fig 4.5b and Fig 4.5c. This is the first report of isotopic ratios of CO in ice. Isotopic ratios and concentrations of CO in firn air from Berkner Island has been measured and a CO record for the past 100 years has been produced [*Assonov et al.*, 2007]. Assonov et al. 2007 argued that an increase of [CO] along with a decrease of $\delta^{13}C$ in the past century resulted from CH_4 growth and possible increase in biomass burning.

Both isotopic ratios show a decrease from the 14th century to the 17th century and an increase from the 18th century to late 19th century. $\delta^{13}C$ decreased from ~ -27‰ in 1360

to ~ -30‰ in 1600-1700, followed by a strong increase to -27‰ by late 19th century. Meanwhile, $\delta^{18}O$ decreased from ~ 2‰ in 1360 to -3‰ in 1700, followed by an increase to 1.5‰ by late 19th century. Scott Base observations indicate present-day annual mean $\delta^{13}C$ is ~ -29~-30‰ and $\delta^{18}O$ is ~ -3~-4‰, which are close to the minimum values for the past 700 years.

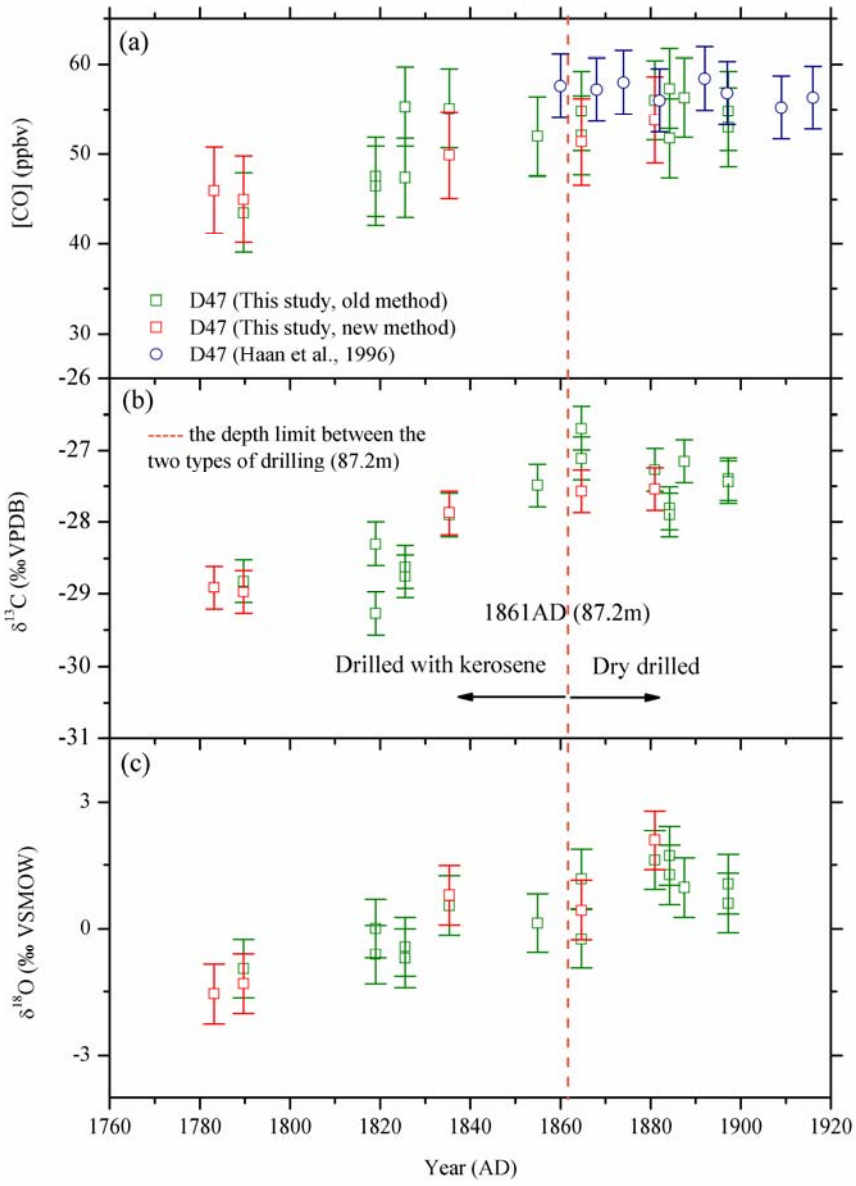

Figure 4.7 D47 ice core records (the same data as those in Fig 4.5), shown as new method (red squares, on-line analysis system, section 2.8.2) and old method (green squares) prepare with wet extraction in LGGE and analyze in Stony Brook University, section 2.8.1). Dashed line indicates the depth below which thermal drilling started and kerosene was used.

. To show the good agreements of our ice core measurements based on different processing methods, the D47 ice core CO records are separated based on different methods and shown in Fig 4.7. Five samples (red squares) were processed with the new on-line analysis method (section 2.8.2) and all others fifteen samples (green squares) were wet extracted in LGGE and analyzed in Stony Brook University (refer as old method, section 2.8.1). First, our CO levels agree well with contemporary measurements in previous study [*Haan et al., 1996*]. Second, the results of both CO concentration and isotopic ratios by new method are consistent with those by old method. This is very important, indicating the reliability of our new on-line analysis system. Third, our results above and below 87.2 m (gas age: 1861 AD) indicate that kerosene does not contaminate CO in ice core if care is taken for cleaning ice. Furthermore, for the eight replicates on given D47 depth levels (Appendix B), the maximum ±1σ standard deviation of [CO], $\delta^{13}C$, and $\delta^{18}O$ is 5.6 ppbv, 0.7‰, and 0.7‰, respectively, which is still comparable with the precision of our on-line analysis system. This is a strong case showing the overall uncertainty of the system, from gas extraction to CF-IRMS analysis, has been well evaluated.

4.5.3 Mass Balance Model

The current major sources of atmospheric CO in high-latitude Southern Hemisphere such as Scott Base (77º51'S 166º46'E) are identified as CH_4 oxidation, non-methane hydrocarbon (NMHC) oxidation, and biomass burning based on MOZART-4 (Model for Ozone And Related chemical Tracers) simulation (Table 4.4) [*L K Emmons et al.*, in preparation; *K.H. Park et al.*, in preparation].

Table 4.4 MOZART-4 simulations on CO at Scott Base in Jan 1, 1997-Dec 31, 2004 [*K.H. Park et al.*, in preparation]

Sources	$[CO]_{source}$	[CO] percentage	Source $\delta^{18}O$ (‰)*	$\delta^{18}O$ at Scott Base (‰)#
Oceanic	1.6	3.0%	15	9.2
Biofuel	2.2	4.1%	17.5	0.6
Biogenic	2.9	5.4%	0	-10.5
Methane	24.7	46.3 %	0	-9.4
NMHC	12	22.5%	0	-11.8
Biomass Burning	7.4	13.9%	17.5	5.3¶
Fossil Fuel	2.5	4.7%	23.5	9.3

Note: *: these are original $\delta^{18}O$ signatures used for each type of emission in the model, references are the same as Table 1.1 in chapter 1, and biofuel can be combined to biomass burning and its $\delta^{18}O$ signature is thus considered the same as that for biomass burning; #: $\delta^{18}O$ at Scott Base is the isotopic ratio calculated in the model based on the ratio between $[C^{16}O]$ and $[C^{18}O]$ at Scott Base [*K.H. Park et al.*, in preparation]. ¶: a measurement of 4.5‰ was derived from observations and a dilution model [*Brenninkmeijer and*

Rockmann, 1997]. See details in text.

MOZART-4 is a 3-D global chemical transport model developed by NCAR, MPI for meteorology, and NOAA/GFDL and is used to simulate the global CO concentration and its isotopic signature [*L K Emmons et al.*, in preparation; *K.H. Park et al.*, in preparation]. The detailed description of MOZART-4 is presented in [*L K Emmons et al.*, 2009]. A tracer version of MOZART-4 which is tagged for $C^{16}O$ and $C^{18}O$ from each region and each source was developed to determine the contribution of each source to the atmosphere [*K.H. Park et al.*, in preparation]. Bayesian inversion techniques have also been used to estimate the global CO budget. To maximize the strengths of using isotope data in the inverse modeling analysis, various coupling schemes combining [CO], $\delta^{18}O$ and $\delta^{13}C$ have been investigated to enhance the credibility of the CO budget optimization [*K.H. Park et al.*, in preparation].

To better understand the CO source evolution during the past 700 years, an observation-driven zero dimensional chemistry model (mass balance model) is applied to our ice core data and the source compositions of CO in Antarctica since preindustrial period can be determined based on the following equations [*J Mak and Kra*, 1999].

$$[CO_A]+[CO_B]+[CO_C]+[CO_D]+[CO_E]=[CO_T]$$

$$[\delta^{13}C_A]\times[CO_A]+[\delta^{13}C_B]\times[CO_B]+[\delta^{13}C_C]\times[CO_C]+[\delta^{13}C_D]\times[CO_D]+[\delta^{13}C_E]\times[CO_E]=[\delta^{13}C_T]\times[CO_T]$$

$$[\delta^{18}O_A]\times[CO_A]+[\delta^{18}O_B]\times[CO_B]+[\delta^{18}O_C]\times[CO_C]+[\delta^{18}O_D]\times[CO_D]+[\delta^{18}O_E]\times[CO_E]=[\delta^{18}O_T]\times[CO_T]$$

where A, B, C, D, and E stand for the three major CO sources in Southern Hemisphere in

preindustrial times: biomass burning, CH_4 oxidation, NMHC oxidation, and two minor sources : biogenic and ocean, respectively. T stands for total CO and is our ice core observation. Biofeul emission is assumed to have the same isotopic signatures as biomass burning and thus classified as biomass burning in preindustrial times. A major issue has to be addressed is that assumption of steady state conditions have to be made since the entire KIE is subtracted from left sides of the above equations (see details below). As isotopic equilibration of atmospheric CO after a source change should be several times longer than the CO lifetime (~3 months on global average [*C. A. M. Brenninkmeijer*, 1993]) but still shorter than the time resolution. Considering the time scale of our ice core record study (~ years on average) and the short lifetime of CO (~months), assumption of steady state of CO mixing and isotopic ratios can be made through the studied time period.

MOZART-4 simulations show the minor sources in the high-latitude SH are fossil fuel combustion, biogenic and ocean emissions. CO derived from these minor sources in the modern atmosphere at Scott Base is on the order of few percent [*K.H. Park et al.*, in preparation]. Model simulation also indicates CO derived from fossil fuel combustion at Scott Base in present-day is only 2.5 ppbv and dominated by Southern Hemisphere emissions [*K.H. Park et al.*, in preparation]. SH CO_2 emission from fossil fuel combustion in later 19^{th} century, where the record started, is smaller than 0.1% of that in 2000 and SH CO_2 emission from fossil fuel combustion in 1900 is less than 3% of that in

2000 [*Boden et al.*, 2009]. Fossil fuel combustion during preindustrial times was much less than present day due to smaller population and much less industrial activities [*Boden et al.*, 2009]. Particularly in the SH, CO derived from fossil fuel combustion is thus considered negligible in this study.

Model simulations estimate oceanic CO emissions account for about 3% in today's atmosphere at Scott Base [*K.H. Park et al.*, in preparation]. Previous studies indicate oceanic CO emissions are dependent on the intensity of radiation [*Nakagawa et al.*, 2004; *Seiler*, 1974] and CO in seawater is mainly produced by the photochemical oxidation of dissolved organic matter (DOM) [*Bauer et al.*, 1980; *Conrad and Seiler*, 1980]. Considering the stable solar insolation [*Bard et al.*, 2000] and relative stable abundance of phosphorus in Southern Ocean (a proxy of oceanic productivity) [*Filippelli et al.*, 2007] during the past 700 years, we assume the oceanic CO source has been fairly stable since preindustrial times. Model simulation indicates present-day [CO] from oceanic source at Scott Base is around 1.6 ppbv (Table 4.4) [*K.H. Park et al.*, in preparation]. $\delta^{13}C$ and $\delta^{18}O$ isotope fraction at Scott Base were estimated to be -23.5‰ by [*L K Emmons et al.*, in preparation] and 9.2‰ [*K.H. Park et al.*, in preparation] respectively based on model simulation and the original source signatures in section 1.2 (Table 1.2).

The direct biogenic source of CO is dominated by emission from vegetation [*Guenther et al.*, 2000] and is 2.9 ppbv at Scott Base in present-day [*K.H. Park et al.*, in preparation]. We assume the biogenic CO emission is proportional to the global

vegetation area. A reduction of global forest cover has accompanied human history from the start of the agricultural revolution 8000 years ago, but only around 7% of global forest area had been lost by 1700 [*Goldewijk*, 2001; *Malhi et al.*, 2002; *Ramankutty and Foley*, 1999]. The rate of deforestation had accelerated since the industrial revolution due to human activities, and the global preindustrial forest area has been reduced by about 20-30% by 1990 [*Malhi et al.*, 2002]. A more comprehensive estimate of total vegetation area including forest area and grassland and shrub area history for different regions in the world has been presented [*Pongratz et al.*, 2008]. Since VOC emissions from forests account for more than 70% of the total VOC emissions [*Guenther et al.*, 1995] and to simplify the calculation, we only consider the forest area change over the past millennia in [*Pongratz et al.*, 2008], which should be reasonable since biogenic source is very small. Their reconstruction indicates SH forest area had been fairly constant before 1800, and had reduced 30% between 1800 and 2000 and 20% between 1900 and 2000, respectively. This results are very consistent with those in [*Malhi et al.*, 2002]. Today biogenic CO is 2.9 ppbv, therefore we assume biogenic CO was 3.8 ppbv in 1800 and earlier and was 3.5 ppbv in 1900. The $\delta^{13}C$ isotope fraction for direct biogenic emission of CO is calculated to be -21‰ for C3 plants and -9‰ for C4 plants [*L K Emmons et al.*, in preparation]. $\delta^{18}O$ isotope fraction is estimated to be -10.5‰ [*K.H. Park et al.*, in preparation].

The records of CH_4 concentration and $\delta^{13}CH_4$ in Law Dome ice core have been reported [*Etheridge et al.*, 1998; *Ferretti et al.*, 2005] (Fig 4.8). Considering the time

scale of our ice core study (~years) and the short lifetime of CO (~months), assumption of steady state of CO can be made and CH_4 derived [CO] is consequently proportional to the [CH_4]. Modeled [CO] from CH_4 oxidation at Scott Base in present-day is ~ 25 ppbv [*K.H. Park et al.*, in preparation]. The $\delta^{13}C$ of CO from CH_4 oxidation is based on this $\delta^{13}CH_4$ record and a constant KIE (3.9‰) for CH_4+OH [*Saueressig et al.*, 2001]. $\delta^{18}O$ isotope fraction is calculated to be -9.4‰ [*K.H. Park et al.*, in preparation].

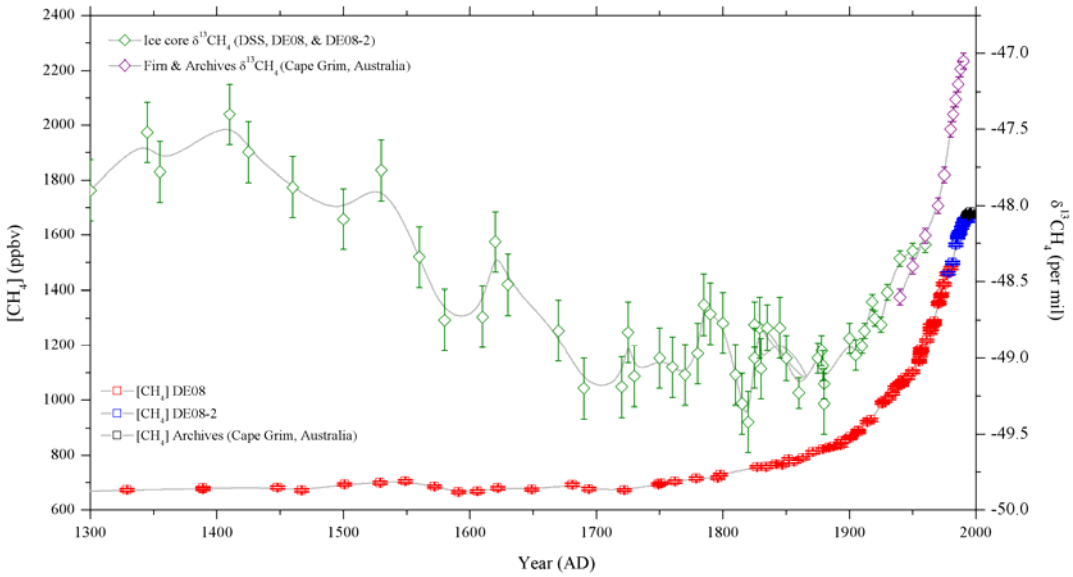

Figure 4.8 The 700-year Law Dome records for [CH_4] and $\delta^{13}CH_4$, based on air measurements from ice cores (DSS, DE08, and DE08-2), firn, and archives (Cape Grim, Australia and Baring Head, New Zealand) [*Etheridge et al.*, 1998; *Ferretti et al.*, 2005].

The terms of CH_4 oxidation (B), biogenic (D) and ocean (E) can be solved based on concentrations and isotopic ratios data given above and thus subtracted from left sides of these three equations, therefore the left unknowns are only biomass burning (A) and NMHC oxidation (C). The calculated residual $\delta^{13}C$, $\delta^{18}O$, and [CO] (combine biomass burning and NMHC oxidation as one source) thus indicate the CO variation caused by

biomass burning and NMHC oxidation. Once the $\delta^{18}O$ signatures of biomass burning and NMHC oxidation are assigned with numbers in Table 4.4, the CO derived from biomass burning and that from NMHC oxidation can be calculated based on the first and the third equation. The reason we assign $\delta^{18}O$ signatures of biomass burning and NMHC oxidation into the equations is because $\delta^{13}C$ signatures have much large uncertainties, though we do not know exactly how large they are. First, there are large uncertainties in $\delta^{13}C$ signature for biomass burning (section 1.2) This $\delta^{13}C$ signature is dependent on the burned C3/C4 plants ratio, which has been confirmed to vary temporally [*Huang et al.*, 2001]. Second, $\delta^{13}C$ signatures for different NMHC are different [*Rudolph et al.*, 1997] and particularly the kinetic isotope effects for NMHC + OH have a large range for different NMHCs [*Iannone et al.*, 2009; *Iannone et al.*, 2003; *Rudolph et al.*, 2000]. Therefore, we would rather assign $\delta^{18}O$ signatures of biomass burning and NMHC oxidation into the equations to derive CO partitioning.

To solve contribution of CH_4 oxidation, we assume contribution of CH_4 oxidation to CO is proportional to the mixing ratio of atmospheric CH_4 and modern [CH_4] is 1728 ppbv over South Pole based on the ground based measurements [*Dlugokencky et al.*, 2005] (also on: http://www.esrl.noaa.gov/gmd/dv/ftpdata.html, NOAA globally averaged in 2004, in 2000-2005 1730 ppb at SPO, 1725 ppb at HBA, 1728 ppb at PSO, 1725 ppb at SYO) and simulated [CO] partition in Scott Base is 25 ppbv from 1994-2000 based model simulation [*K.H. Park et al.*, in preparation]. [CH_4] and $\delta^{13}C$ isotope fraction from

CH_4 oxidation used in the mass balance calculation is based on the data of CH_4 concentration from [*Etheridge et al.*, 1998] and the $\delta^{13}CH_4$ from [*Ferretti et al.*, 2005] (both shown in Fig 4.8) and a constant KIE of 3.9‰ for CH_4+OH [*Saueressig et al.*, 2001]. $\delta^{18}O$ of CO from CH4 oxidation is assumed to be constant as -9.4‰ [*K.H. Park et al.*, in preparation].

For the model inputs of different isotopic signatures, ongoing isotopic fractionation that occurs in CO+OH reaction during long-range transport should be considered, which means the signatures for certain sources at Scott Base may be different from the original signatures (Table 4.4). MOZART-4 simulations of atmospheric CO have been studied for Scott Base (77º51'S 166º46'E) and the isotopic ratios from different sources at that site have been calculated [*L Emmons*, personal Communication; *K. H. Park*, personal Communication].

The uncertainties of these values are very important to our model calculations. Unfortunately, due to technique difficulties (extensive sensitivity tests are required) [*L Emmons*, personal Communication; *K. H. Park*, personal Communication], the uncertainties of these source derived [CO] or isotope fractions cannot be determined so far and we assume no error arising from them. An example is listed here to give a basic ideal for the uncertainty of $\delta^{18}O$ for biomass burning. This value was calculated to be 5.3‰ at Scott Base from model simulation, whereas it was estimated to be 4.5‰ based on aircraft measurements [*Brenninkmeijer and Rockmann*, 1997]. The $\delta^{18}O$ of CO from

air samples collected in the upper troposphere and lowermost stratosphere between Christchurch, New Zealand, and Scott Base, Antarctica, during aircraft flights in October 1993. The $\delta^{18}O$ was plotted versus the inverse CO concentration (dilution model), and the intercept returns a value of 4.5‰ for infinite dilution of the tropospheric air masses with, presumably, biomass burning derived CO of which the isotopic composition as changed during transport [*Brenninkmeijer and Rockmann*, 1997].

Table 4.5 MOZAR simulation on $\delta^{13}C$ isotopic ratio at Scott Base [*L K Emmons et al.*, in preparation]

CO Source	Source $\delta^{13}C$ (‰)	$\delta^{13}C$ at Scott Base (‰)*
Biomass burning	-25[1]; -12[2]	-9¶, -21¶
CH_4 oxidation	-49	-48
NMHC oxidation	A	-27[3]
Ocean	-25	-23.5
Biogenic	-25[1]; -12[2]	-25

Notes: *: $\delta^{13}C$ at Scott Base is calculated in the model based on ratio between [^{12}CO] and [^{13}CO]; [1]: forest burning (C3); [2]: savanna burning (C4); ¶: estimated based on C3 (-21‰) and C4 (-9‰) burning [*L Emmons*, personal Communication]; [3]: based on $\delta^{13}C$ signature of NMHC oxidation [*Stevens and Wagner*, 1989] and ~ 5‰ KIE of CO + OH reaction [*Stevens et al.*, 1980]; A: $\delta^{13}C$ has been assigned to different organic compounds [*L Emmons*, personal Communication]. Other $\delta^{13}C$ values are from [*L Emmons*, personal Communication].

The major source regions of biomass burning that impact Scott Base include tropical Africa, tropical America, and tropical Asia. Isotopic fractionation occurs due to the CO-OH loss reaction during transport, resulting in a ~ +4‰ shift for $\delta^{13}C$ (Table 4.5) [*L K Emmons et al.*, in preparation] for C3 plants burning compared with the source

signature of ~-25‰ [*Manning et al.*, 1997] and ~ +4‰ shift [*L K Emmons et al.*, in preparation] for C4 plants burning compared with the source signature of -12‰ [*Marino and McElroy*, 1991]. Meanwhile, an inverse kinetic isotope effect results in the enrichment of ^{18}O in CO, resulting in a shift in $\delta^{18}O$ of 5.3‰ [*K.H. Park et al.*, in preparation] compared with the source signature of 17.5‰ (Table 4.4) [*Stevens and Wagner*, 1989]. This same isotopic fractionation occurs for CH_4 oxidation as well as NMHC oxidation. Table 4.4 and 4.5 give the isotopic ratios used in our mass balance model in terms of the difference sources listed.

4.5.4 Residual results

To understand why CO isotopes behave like the trends shown in Fig 4.5 and how CO sources evolve in the past, a mass balance model is performed, which includes biogenic, ocean, oxidation of CH_4 and NMHC, and biomass burning sources and the corresponding [CO] and isotopic ratios in the ice core.

We first subtract the source of CH_4 oxidation, biogenic, and ocean sources from the isotope box model (section 4.5.3), yielding residual sources of biomass burning and NMHC oxidation. The reason we do this is that CH_4 oxidation is already known based on Law Dome ice core records [*Etheridge et al.*, 1998; *Ferretti et al.*, 2005] and biogenic and ocean source have been plausibly determined based on our assumptions. Since there are no accurate estimates of preindustrial ocean and biogenic emissions, we perform

different scenarios to test the model sensitivity to these two minor sources. These scenarios include: taking into account on both ocean and biogenic source (scenario 1), only taking into account on ocean (scenario 2), ignoring both ocean and biogenic source (scenario 3), and only taking into account on biogenic source (scenario 4). The solved concentration and isotopic ratios (plug in ice core data into the right side of the equations and subtract the terms containing B, D, and E on the left side of equations) are called residual [CO], residual $\delta^{13}C$ and residual $\delta^{18}O$, which show how CO varied with change of biomass burning and NMHC.

First of all, there exist errors for different parameters in the mass balance model. For example, there is no clue how isotopic signature changed over time [*Schaefer and Whiticar*, 2008]. Also for the isotopic signature itself, for example biomass burning, large range was observed [*Kato et al.*, 1999] even without considering the errors arising from mixture of C3 and C4 plants [*Ehleringer*, 1993]. Quantification of the errors is crucial for our data interpretation, but meanwhile is difficult. Error propagation even makes this more complex. Due to limited information about tiny sources, we assume no error arising from them. For errors relating to $[CH_4]$ (5 ppbv [*Etheridge et al.*, 1998]) and $\delta^{13}CH_4$(~0.2‰ [*Ferretti et al.*, 2005]), we determine them as following steps.

As mentioned, [CO] derived from CH_4 is proportional to $[CH_4]$, giving $[CO]_{CH4} = [CH_4]\times 25.3/1728$, where 25.3 ppbv is modern $[CO]_{CH4}$ at Scott Base (Table 4.4) [*K.H. Park et al.*, in preparation] and 1728 ppbv is the modern $[CH_4]$ in South Pole

[*Dlugokencky et al.*, 2005]. Thus the error from $[CO]_{CH4}$ is negligible. Consequently, error of $[CO]_r$ is 4.8 ppbv, the same as that of $[CO]_T$. Similarly, error propagated from $\delta^{13}CH_4 \times [CO]_{CH4}/[CO]_r$ is estimated to be smaller than 0.07‰, which is taken into account in determining error for $\delta^{13}C_r$. $\delta^{13}C_T \times [CO]_T/[CO]_r$ gives an error of 0.45‰ based on the calculated $[CO]_T/[CO]_r$ and the uncertainty ($\pm 1\sigma$) of 0.3‰ for $\delta^{13}C_T$. The error combining this 0.45‰ and the 0.07‰ gives a total error is 0.456‰ for $\delta^{13}C_r$. For error of $\delta^{18}O_r$, we assume no error arises from $\delta^{18}O$ of CH4 oxidation due to limited information. Consequently, $\delta^{18}O_T \times [CO]_T/[CO]_r$ gives an error of 1.05‰ based on the calculated $[CO]_T/[CO]_r$ and the uncertainty ($\pm 1\sigma$) of 0.7‰ for $\delta^{18}O_T$.

The residual CO concentration and residual isotopic ratios are presented in Fig 4.9. More attention should be paid for the interpretations on this residual [CO] data because of the large uncertainties. The upper limit of uncertainty including the uncertainties from replicates and the error propagation during the mass balance model calculation even gives range as large as 20 ppbv, which is comparable with the maximum [CO] variation over the past 700 years and possibly obscure the real preindustrial [CO] variation. Even with this limitation, we still would like to interpret the [CO] data based on the averages of each sample and give the possible scenarios for preindustrial CO budget evolution. Moreover, the more pronounced variations for both isotopes (Fig 4.8b and c) give us more confidence for the residual [CO] variation in preindustrial times.

For all scenarios, both residual [CO] and residual $\delta^{18}O$ show a saddle-shaped curve,

with higher values in the 14th century and the 18th century and minimum values occurred in the 16th century. Residual [CO] decreased around 15 ppbv from 1360 to 1700, and increased about 15 ppbv from 1700 to 1900. Meanwhile, residual $\delta^{18}O$ is depleted about 5‰ from 1360 to 1700, and enriched about 6‰ from 1700 to 1900. Unlike the trend of residual [CO] and residual $\delta^{18}O$, residual $\delta^{13}C$ fluctuated between -21‰ to -24‰ from 1360 to 1800, and enriched about 4‰ from 1800 to 1900. The large variations of residual [CO], residual $\delta^{13}C$, and residual $\delta^{18}O$ indicate biomass burning and/or NMHC oxidation significantly changed and drove the variation of atmospheric CO over the past 700 years.

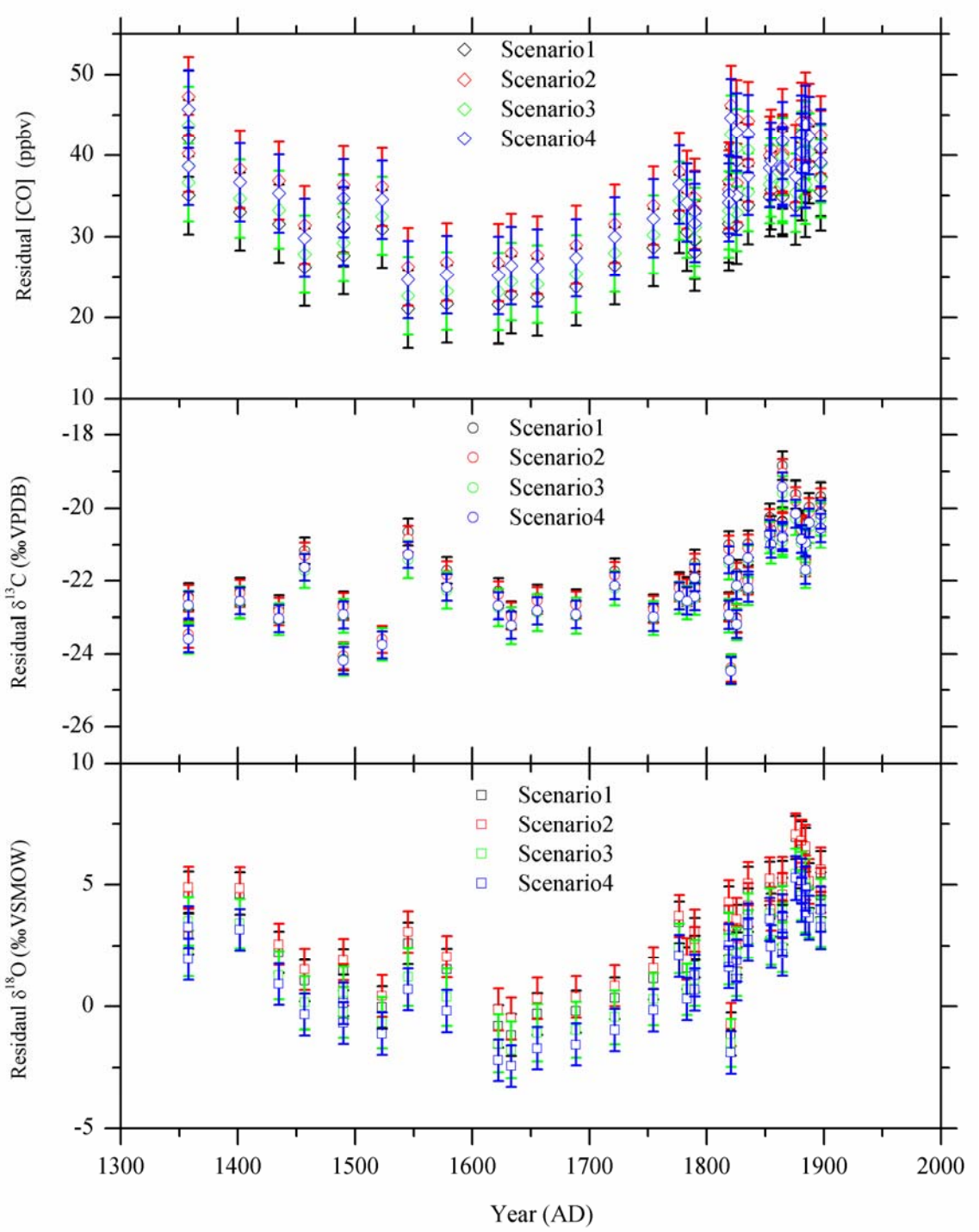

Figure 4.9. Records of $\delta^{13}C$ (circles) and $\delta^{18}O$ (squares) and [CO] (triangles) for residual sources of CO based on different scenarios of mass balance model simulation. Scenario 1: model with ocean and biogenic source; scenario 2: model with biogenic source but without ocean source; scenario 3: model without ocean or biogenic source; scenario 4:

model with ocean but without biogenic source. Discrepancies among different scenarios indicate sensitivities of ocean and biogenic source to the model simulations. Uncertainties of residual [CO], residual $\delta^{13}Cr$, and residual $\delta^{18}O$ are 4.8 ppbv, 0.46‰, and 1.05‰, respectively. See the details on the uncertainty determination in text.

4.5.5 Discussions

4.5.5.1 Residual data

There are discrepancies among difference scenarios, especially for residual [CO] (maximum difference: ~5 ppbv) and residual $\delta^{18}O$ (maximum difference: ~2.5‰), indicating the model errors arising from these minor sources. The different scenarios give parallel trends, indicating variations of CO budget are not sensitive to the minor sources during the period of this study. Of course this is because we treat minor source as relatively constant throughout the whole period of the present study based on our assumptions (section 4.5.3), which might not be true. But this is not a concern in our data interpretation since the trend of residual [CO] (Fig 4.9a) show very good agreement with that of total [CO] (Fig 4.5a) between 1360 and 1800, which is exactly within the preindustrial times, indicating ocean and biogenic source, and even CH_4 oxidation did not play an important role in the variation of CO budget in preindustrial times. It is also found that the increase rate of residual [CO] (Fig 4.9a) is smaller than that of the total [CO] (Fig 4.5a), which is resulted from the dramatic increase of CH_4 concentration since 1800 due to anthropogenic emissions [*Etheridge et al.*, 1998; *Meure et al.*, 2006]. Also shown here is that a large variation for biomass burning and/or NMHC oxidation

occurred in preindustrial time, which drove the large variations of CO budget. Thus this residual [CO] record gives us a clear picture of how preindustrial CO budget behaved without the anthropogenic impacts due to industrialization.

Isotopic ratios provide additional information for the sources. In modern atmosphere CH_4 oxidation is believed to dominate the seasonal variations of $\delta^{13}C$ of CO from extratropical SH (Baring head, 41°24' S, 174°54' E) [*Manning et al.*, 1997] to high latitude SH (Scott Base, 77°51' S, 166°46' E) [*L K Emmons et al.*, in preparation]. The residual $\delta^{13}C$ (Fig 4.9b) shows a very different trend from that of total $\delta^{13}C$ (Fig 4.5b), particularly in the period between 1360 and 1700, indicating CH_4 oxidation played a significant role in the $\delta^{13}C$ of CO during the same period. However, it is still not very clear if biomass burning or NMHC oxidation or both also played a key role here. The residual $\delta^{13}C$ (Fig 4.9b) between 1700 and 1900 reproduces the trend of total $\delta^{13}C$ of CO (Fig 4.5b), indicating biomass burning or NMHC oxidation or both dominated $\delta^{13}C$ of CO during the period of the present study.

MOZART-4 simulations show the seasonal variation for $\delta^{18}O$ of CO at Scott Base is not sensitive to CH_4 oxidation [*K.H. Park et al.*, in preparation]. The residual $\delta^{18}O$ (Fig 4.9c) almost reproduces the trend of total $\delta^{18}O$ of CO (Fig 4.5c), showing CH_4 oxidation did not play an important role in the variation of $\delta^{18}O$ over the past 700 years. Consequently, biomass burning or NMHC oxidation or both drove the variations of $\delta^{18}O$ over the past 700 years.

4.5.5.2 CO partitioning

To quantify the relative contribution from biomass burning and NMHC oxidation and reveal the biogeochemical causes of preindustrial CO variations, we used the mass balance model the calculated residual [CO] (Fig 4.9a) and assigned $\delta^{18}O$ data (Table 4.4) are plugged into the first and the third mass balance equations and $[CO]_r$ is separated to $[CO]_{Biomass\ Burning}$ and $[CO]_{NMHC}$, where $[CO]_{Biomass\ Burning}$ stands for [CO] from biomass burning and $[CO]_{NMHC}$ stands for [CO] from NMHC oxidation. The calculated CO partitioning is shown in Fig 4.10.

As mentioned, uncertainties of such calculation are very significant to the data interpretation. Due to limited information on the uncertainties for the source signatures, we assume that the uncertainties are negligible. The uncertainties ($\pm 1\sigma$) of $[CO]_{CH4}$,$[CO]_{Biomass\ Burning}$, and $[CO]_{NMHC}$ are thus estimated to be 0.07 ppbv, 4.8 ppbv, and 3.7 ppbv, respectively based on the similar method discussed above and the principles for error propagation calculation. It has also to be noticed that no direct measurements are available to for $\delta^{18}O$ signatures from oxidation of CH_4 and NMHC and the accepted $\delta^{18}O$ signatures in the present study are estimated to be 0‰ by CO observations and simple budget considerations [*Brenninkmeijer and Rockmann*, 1997] and may cause potential errors for mass balance calculation.

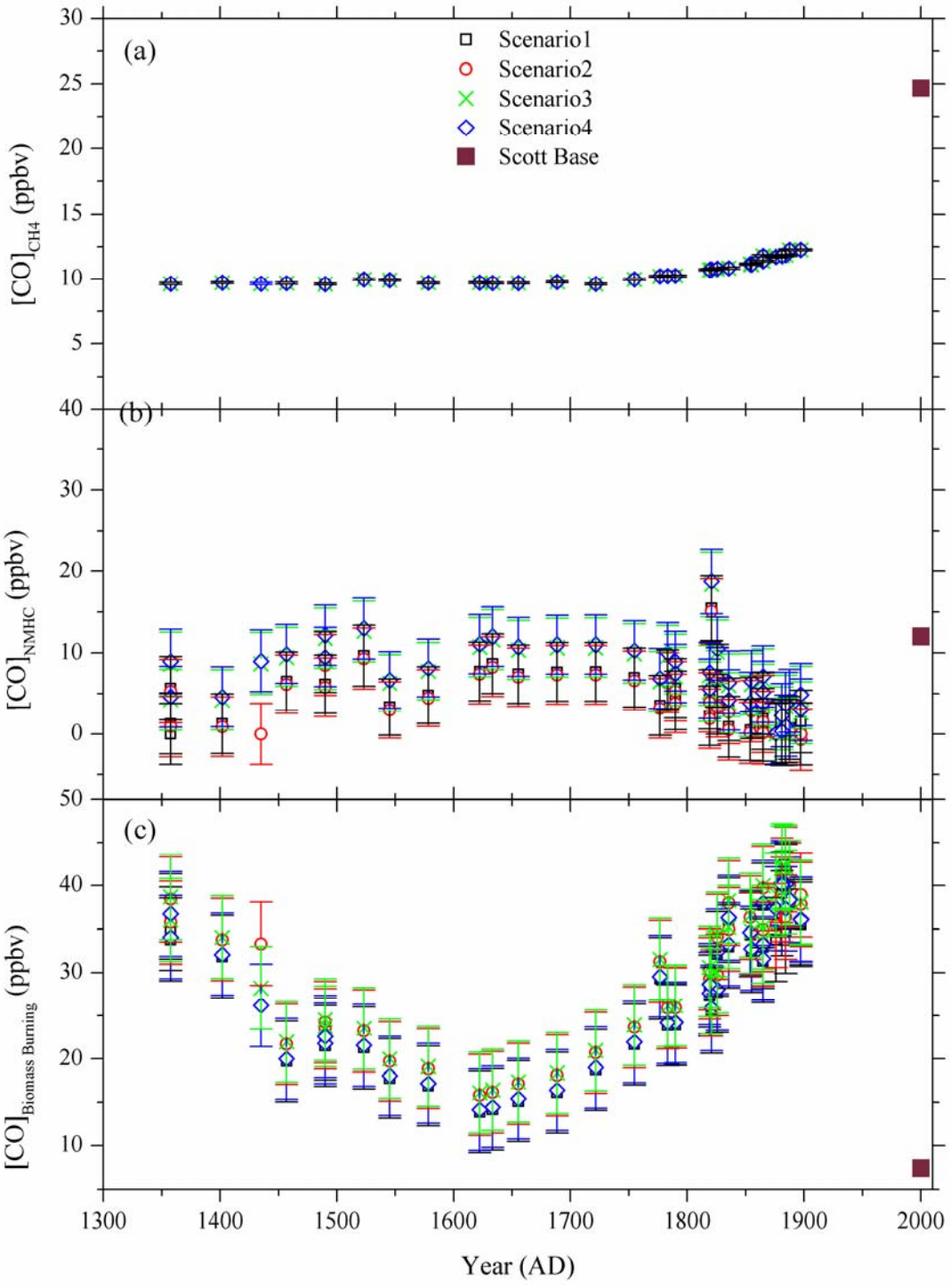

Figure 4.10 Modeled CO source partitioning based on ice core data and mass balance model. Also shown are [CO] derived from the three major sources at Scott Base in modern atmosphere (annually average in 1997-2004) at Scott Base [*K.H. Park et al.*, in

preparation]. Scenarios are the same as Fig 4.9. The uncertainties (±1σ) of $[CO]_{CH4}$,$[CO]_{Biomass\ Burning}$, and $[CO]_{NMHC}$ are 0.07 ppbv, 4.8 ppbv, and 3.7 ppbv, respectively. See details on uncertainties in text. [CO] from CH_4 oxidation was relatively stable between 1360 and 1900, however large variations are observed for [CO] from biomass burning even with large uncertainties. Due to large uncertainties, no clear trend can be found on CO from NMHC oxidation.

Similarly, four different scenarios were performed on the mass balance calculation and produced the CO budget evolution between 1360 and 1900. [CO] from CH_4 oxidation was relatively constant as around 10 ppbv between 1300 to 1800 and increased only ~2 ppbv in 1800-1900, followed by a rapid increase to around 25 ppbv by 2000, which is due to the significant increase of atmospheric methane concentration due to anthropogenic emissions [*Etheridge et al.*, 1998]. The relatively stable CH_4 oxidation provides supporting evidence that this source did not play a significant role in the preindustrial CO budget variation.

Large variations occurred in the source strengths of biomass burning between 1360 and 1900 (Fig 4.10c). Though uncertainties are large, it is still observed that [CO] from biomass burning decreased from 35 ppbv to 15 ppbv between 1360 and 1650, followed by an increase to 40 ppbv by 1900. Since then, [CO] from biomass burning dropped dramatically to 7.4 ppbv in modern atmosphere [*K.H. Park et al.*, in preparation]. CO derived from biomass burning reaching Scott Base originates mainly from the tropics [*K.H. Park et al.*, in preparation]. We believe CO derived from biomass burning over the entire Antarctic plateau originates from the tropics since there dose no exist any local wildfire in this continent. The biomass burning analysis based on our ice core (even not

close to Scott Base) data is thus reflective of the tropical biomass burning record. The close correspondence between our derived biomass burning emission (Fig 4.10c) and $\delta^{13}CO$ and $\delta^{18}CO$ data (Fig 4.5b and c) between 1300 and 1900 leading to our conclusion that tropical biomass burning substantially affected the preindustrial CO budget. Furthermore, some of the multicentury and multidecadal anomlies in reconstructed NH temperatures [*Moberg et al.*, 2005] correlate with our $\delta^{13}CO$ for the entire period of this study rather than SH temperature anomalies [*Mann and Jones*, 2003], indicating that natural climate change particularly large-scale climate change influence the high latitude SH CO budget between 1300 to 1900. It has to be noticed that the huge drop of biomass burning derived CO from 1900 to present-day, which is very intriguing but might be supported by wildfire records deduced from charcoal in lake sediments [*Marlon et al.*, 2008], ammonium and formate in ice core [*Savarino and Legrand*, 1998], and even tree trunk fire scars in giant sequoia [*Swetnam*, 1993].

Variations in temperature and humidity are believed to affect the history of wildfires. The elevated biomass burning is favorable with warmer temperatures [*Carcaillet et al.*, 2002] and dryer conditions [*Crutzen and Andreae*, 1990]. Temperature and humidity patterns show large spatial and temporal variations. Since biomass burning derived CO in Antarctica originates from tropics, we focus on the climate change over the past millennium in the tropics. Previous studies show that LIA is of global extent with slight difference in timing of its paroxysm, depending on the geographical location [*Bradley*

and Jones, 1992; *Lamb*, 1977], thus we postulate temperature decreased in LIA in the tropics based on the temperature reconstructions (Fig 4.10b) [*Mann and Jones*, 2003; *Moberg et al.*, 2005].

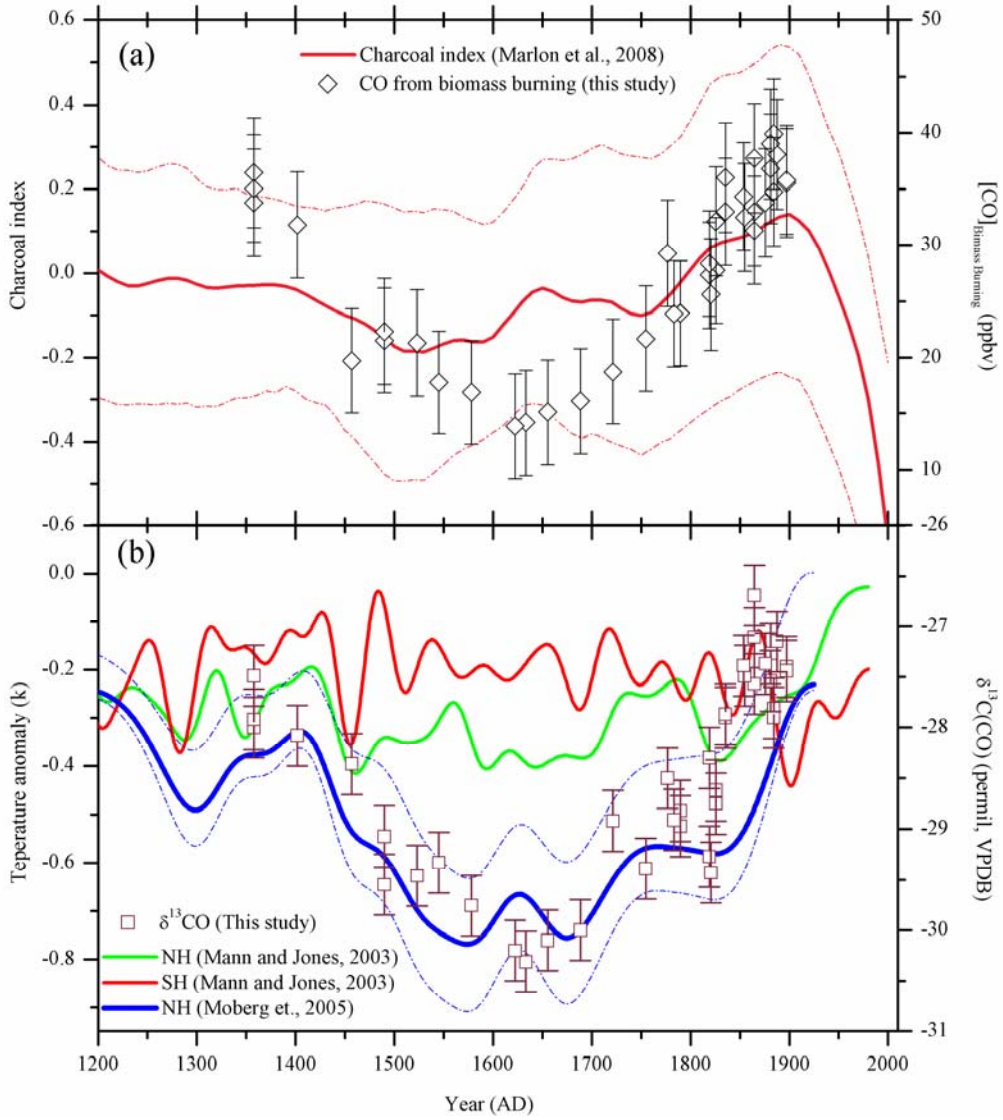

Figure 4.11. (a) Sedimentary charcoal record in tropics (solid line) (30˚N-20S) and uncertainties (dashed lines) for tropical region (30˚N- 20˚S) from 1200 to 2000 indicates biomass burning in tropics dropped from 1200 and increased from 1750 to 1900 [*Marlon et al.*, 2008]; also shown is deduced biomass burning CO in the present study (open diamonds). (b) The relation between δ^{13}CO (open squares) and NH temperature anomaly reconstructions [relative to 1961-1990 mean] (green line [*Mann and Jones*, 2003] and

blue line [*Moberg et al.*, 2005], blue dashed lines are largest errors at 95% confidence interval) as well as SH temperature anomaly reconstruction [relative to 1961-1990 mean] (red line) [*Mann and Jones*, 2003]. The multicentenial changes that the Moberg record better incorporates by use of low-resolution proxies.

Regional record of drought and rainfall over the past millennium recovered from lakes in Africa [*Verschuren et al.*, 2000] indicates equatorial east Africa has alternated between contrasting climate conditions, with significantly drier climate than today during the Medieval Warm Period (MWP, similar to AD 1000-1270) and a relatively wet climate during the Little ice Age (LIA, similar to AD 1270-1850). The wetter tropical east Africa climate is supported by [*Cohen et al.*, 1997; *Halfman et al.*, 1994], showing relatively wet from the late thirteenth century to the mid-eighteenth century. Ice core records from Southern tropics indicate a wettest period occurred in 1500-1720 interval, followed by a very dry condition in 1720-1860 interval, indicating the worldwide characteristics of the LIA [*L G Thompson et al.*, 1985; *L G Thompson et al.*, 1986]. Thus, the wetter and colder climates in tropics over the millennium provide supporting evidence that moisture is negatively correlated to temperature and that the biomass burning most likely decreased in response to cooling temperatures and increasing moisture from 1300 to 1700.

This analysis of biomass burning derived from the sedimentary charcoal record in the tropics [*Marlon et al.*, 2008] is a stronger and more direct support. The deduced biomass burning derived CO agrees well with the charcoal index record in the tropics (Fig 4.11a), giving more confidence on our deduced biomass burning trend. Their sedimentary charcoal records in the tropics (20ºS-30ºN) indicate a decrease of biomass burning from

1400 to 1750, a following abrupt increase from 1750 to 1870 and abrupt drop after 1870 (Fig 4.11a). It has found that human activities are the primary cause of biomass burning including forest clearance and savanna burning in tropics [*Delmas et al.*, 1999]. The early decrease of biomass burning deduced from their charcoal data was argued to be correlated with both global cooling trend and human activities. The biomass burning decrease in central and tropical South America from 1300 to 1600 is consistent with the population drop in the same area, [*Marlon et al.*, 2008], indicating the impact of human activities on biomass burning. However, the strong correlation between temperature and biomass burning [CO] prior to 1700 in this study (Fig 4.11b) indicates large-scale natural climate change dominated biomass burning during this period. Since then, the increase of biomass burning has been likely influenced by both natural and anthropogenic forcings. The abrupt drop of biomass burned over the past 150 results from an intensive grazing, agriculture and fire management [*Marlon et al.*, 2008].

Another two studies [*Savarino and Legrand*, 1998; *Swetnam*, 1993] on record of wildfires may not directly relate to our biomass burning analysis since they focused on fire records in middle to high-latitude NH, which are more dependent on boreal wildfires. In [*Savarino and Legrand*, 1998], three periods of enhanced biomass burning input over central Greenland are identified: 1200-1350 A.D., 1830-1930 A.D., and to a lesser extent 1500-1600 A.D based on their measurements of ammonium and formate in the ice core. They also observed a decrease of fire frequency throughout the 20th century after the

most active period of fire events (1830-1930) over the past 800 years [*Savarino and Legrand*, 1998]. The fire records deduced from tree trunk scars in giant sequoia of western North America also observed a greatly reduce of fires after about 1860, which resulted from intensive sheep grazing, a decrease in fires set by Native Americans, and fire suppression by government agencies [*Swetnam*, 1993].

The 20th century is the period of most rapid land-use change, characterized by large-scale conversion of native vegetation to croplands and the widespread introduction of domestic grazing animals such as cows and sheep [*Goldewijk*, 2001; *Pongratz et al.*, 2008; *Savage and Swetnam*, 1990]. Therefore, our deduced biomass burning derived CO drop from 1900 to present can be plausible explained by the intensive grazing and fire management [*Goldammer and De Ronde*, 2004].

The only thing differing CO from NMHC oxidation and that from biomass burning is $\delta^{18}O$ signature [*Brenninkmeijer and Rockmann*, 1997]. However, we do not know for sure what those source signatures are [*Brenninkmeijer and Rockmann*, 1997; *Rockmann et al.*, 2002]. This introduces uncertainty into the NMHC derived CO component especially. In Fig 4.10b, due to large uncertainties, it is difficult to find a clear trend on CO derived from NMHC oxidation. Based on the averages, [CO] from NMHC oxidation fluctuated slightly between 1300 and 1600 and kept relatively constant between 1600 and 1750, followed by a decrease from 1750 to less than 5 ppbv by 1900. [CO] from NMHC oxidation increased to 12 ppbv in modern atmosphere [*K.H. Park et al.*, in preparation].

The drop of CO from NMHC in the 19th century and following increase by 2000 is at present unexplained, which might cast doubt on the entire analysis such as overestimate the biomass burning derived CO. However, no direct record of NMHC in the past atmosphere exists due to their low concentration and short lifetime. As mentioned, the different species of hydrocarbons have different isotopic signatures (biogenic or anthropogenic) [*Rudolph et al.*, 1997] and different kinetic isotope effects with OH [*Iannone et al.*, 2003; *Rudolph et al.*, 2000], which imposes the complexity. Therefore our deduced NHMC oxidation derived CO records have limited use for understanding the NMHC variation in the past in the present study.

As discussed, it seems most likely biomass burning drove CO budget variations in preindustrial times. However, possible higher OH level in preindustrial times [*Martinerie et al.*, 1995; *Y H Wang and Jacob*, 1998] could also caused a drop of CO level.

Ferretti et al. reconstructed the CH_4 source evolution over the past 2000 years by using an atmospheric box model that includes global biogenic, pyrogenic, and fossil sources and accommodates the dynamics of $[CH_4]$ and $\delta^{13}CH_4$ responses to budget changes [*Ferretti et al.*, 2005]. They found pyrogenic emissions of CH_4 decrease by ~40% in 1700 relative to the emissions from 0 to 1000, which is comparable with our ~50% drop for biomass burning emissions of CO.

Another issue has to been addressed is the possible change of atmospheric circulation over the past 1000 years, which could potentially influence the long-range transport of

CO in biomass burning plume from the tropics to the high-latitude SH [*Edwards et al.*, 2006a; *Edwards et al.*, 2006b; *Pradier et al.*, 2006]. Previous studies have shown the close correlation between atmospheric circulation and solar energy output [*Maasch et al.*, 2005; *Mayewski et al.*, 2005] and increased (decreased) solar irradiance is associated with increased (decreased) zonal wind strength near the edge of the Antarctic polar vortex [*Mayewski et al.*, 2005]. This polar vortex possibly prevents biomass burning CO transporting to the surface of this plateau. It has shown that variability of solar irradiance over the past 1000 years is relatively small [*Jones and Mann*, 2004]. Mayewski et al. also pointed out that the last period of intensification of southern circumpolar westerlies and accompanying relatively cooler conditions over East Antarctica [*Masson et al.*, 2000] and West Antarctica occurred ~1200-1000 years ago [*Mayewski et al.*, 2009], indicating a relatively stable atmospheric circulation in SH over the period of our study. Thus we believe the atmospheric dynamics did not play an important role in these preindustrial CO variations.

4.6 Implications to Atmospheric Chemistry

Atmospheric carbon monoxide strongly affects the oxidative capacity of the atmosphere, being the main reactant with OH in the troposphere. Little is known about its variability in the past and about the size of the anthropogenic impact, although both affect

e.g. the CH_4 and O_3 atmospheric budgets and thus the climate/chemistry interactions.

Numerical models have been performed to understand the change of atmospheric oxidizing capacity since preindustrial times [*A.M. Thompson*, 1992; *Y H Wang and Jacob*, 1998] or since last glacial maximum (LGM) [*Martinerie et al.*, 1995; *Pinto and Khalil*, 1991]. Wang and Jacob (1998) demonstrated the model simulation on O_3 and OH since preindustrial times and showed preindustrial CO played an important role in paleoatmospheric chemistry. Only CO data of [*Haan and Raynaud*, 1998; *Haan et al.*, 1996] were available to compare with their simulation results and great discrepancies appeared. Our decade-scale CO record dating back to 1360 will provide a good constrain and greatly improve such model simulation, providing very useful information on O_3, OH, CH_4, and other NMHC since preindustrial times and enhance understanding paleoatmospheric chemistry.

In the simulations of [*Martinerie et al.*, 1995; *Pinto and Khalil*, 1991; *A.M. Thompson*, 1992], input data of CO are based on some assumptions, which will add large uncertainties to their estimates and thus diminish the importance of their conclusions. Our ice core CO data will absolutely help improve the model with strong constrain and reduce their uncertainties.

Thompson et al. (1993) has performed a multi-box photochemical model and studied the effect of changing CH_4 fluxes on global tropospheric oxidant levels including O_3, OH, H_2O_2. In their study, the preindustrial CO data is constrained by ice core H_2O_2 record. Our

preindustrial CO data will add an independent constrain to such model and also provide a validation for the model as well.

CO is a very good indicator for biomass burning, particularly in Southern Hemisphere [*Ferretti et al.*, 2005; *Manning et al.*, 1997]. Though sedimentary charcoal records in lakes provide useful biomass burning history [*Marlon et al.*, 2008], they cannot give biomass burning information in high-latitude SH due to short lifetime and fast deposition of particles. Our ice core CO records enhance understanding how biomass burning evolve and influence the atmosphere in high-latitude SH since preindustrial times.

4.7 Outlooks

Based on our findings on preindustrial CO in high-latitude SH, I believe the following work will also be very interesting and significant for us to understand the atmospheric CO budget in the past:

1) CO variations during the past 1000 years in the northern hemisphere. Since CO in NH has a higher level than SH in industrial era and it is dominated by fossil fuel combustion in modern atmosphere, Greenland ice core CO will provide a good picture on how human activities, particularly fossil fuel combustion, influence the CO budget in NH.

2) CO change since the last glacial maximum (LGM). In the LGM, [CH_4] was only ~350 ppbv and the temperature was ~8ºC lower than present-day [*Petit et al., 1999*]. Study on CO in this abrupt climate transition will enhance our understanding on atmospheric CH_4 budget and atmospheric chemistry.

3) Other possible isotopmers: $^{17}O(CO)$ and ^{14}CO. The $\Delta^{17}O$ (^{17}O excess) is a direct measure for the exposure of CO to OH and ^{14}CO provides a very detailed picture of effects due to transport combined with its removal by OH [*Brenninkmeijer et al., 1999*]. However, both measurements are challenging and need large sample of ice. Future study on CO in blue ice from Antarctica could make these measurements feasible and provide valuable information on OH level in the paleoatmosphere.

4.8 Concluding Remarks

In order to determine the CO budget in the past atmosphere and reveal the biogeochemical reasons for CO budget change, we have reconstructed the CO concentration and its major sources since preindustrial period based on measurements of CO concentration as well as $\delta^{13}C$ and $\delta^{18}O$ from 40 Antarctic ice core samples.

CO concentration in the 13th century was ~50 ppbv, close to the annual mean CO concentration in high-latitude Southern Hemisphere (SH). During the following 300

years, CO concentration gradually dropped to 38 ppbv during the little ice age (LIA), followed by an increase to 55 ppbv in 1900. $\delta^{13}C$ and $\delta^{18}O$ both decreased by about 3‰ and 5‰ respectively from 1380 to 1700, then increased by about 3‰ and 5‰ respectively by 1900.

Mass balance model calculation indicates biomass burning dominated the CO budget variation in preindustrial times. [CO] from biomass burning decreased from 35 ppbv to 15 ppbv between 1360 and 1650, followed by a rapid increase to 40 ppbv by 1900. These variations of biomass burning are caused by the climate change such as dryness and temperature change. Since then, [CO] from biomass burning dropped dramatically to 7.4 ppbv in modern atmosphere. This suppression of wildfires is plausible due to the intensive grazing and fire management in the tropics over the last century. The correlation between NH temperature anomalies and biomass burning [CO] in 1300-1900 indicates natural climate change drove biomass burning emissions. We thus conclude that biomass burning strongly modulated the CO budget during preindustrial time and considerably decreased since the early 20th century. This decrease was nearly compensated by the concomitant CH_4 increase, bringing back CO mixing ratio close to its maximum level observed over the last 700 years.

Our ice core CO data will absolutely help improve the numerical model on past atmospheric chemistry, understand CH_4-CO-OH-O_3 chemistry from past to present, and predict the future oxidizing capacity.

Chapter 5. CO Records in the Pakitsoq Ice of Greenland

5.1 Introduction

This chapter focuses on atmospheric CO records in two climatic transitions during the last glacial termination based on Greenland ice margin. Previous work has demonstrated that large quantities of ice dating to the last glacial termination are exposed at the surface at an ice-margin ablation site called Pakitsoq in West Greenland [*Petrenko et al.*, 2008; *Reeh et al.*, 1991]. This ice is believed to originate near Greenland Summit, about 190 km south and 40 km west of the GISP2 site, based on an ice sheet flow model [*Reeh et al.*, 2002].

$\delta^{13}CH_4$ in Pakitsoq ice spanning the Younger Dryas - Preboreal (YD-PB) transition has been studies and constrain the CO budget during the last glacial termination [*Schaefer et al.*, 2006]. Observed constant $\delta^{13}CH_4$ during the rise in methane concentration at the YD-PB transition is consistent with additional emissions from tropical wetlands, or aerobic plant CH_4 production, or with a multisource scenario, and this rules out the marine clathrate source [*Schaefer et al.*, 2006].

The Paskitsoq ice is an outcropping blue ice instead of conventional ice core, which provides plenty of ice [*Nisbet and Chappellaz*, 2009]. By mining large amounts of ice (~ 1000 kg) from the Pakitsoq ice margin for $^{14}CH_4$ analysis, Petrenko et al. elucidate some

of the processes behind a rapid climate transition of YD-PB that began about 11,600 years ago [*Nisbet and Chappellaz*, 2009; *Petrenko et al.*, 2009]. The results in their study suggest that wetland sources were likely responsible for the majority of the YD-PB CH_4 rise instead of the clathrate breakdown [*Petrenko et al.*, 2009].

To better understand cosmogenic ^{14}C production in Pakitsoq ice and correct the measurements of $^{14}CH_4$, ^{14}C of CO in remaining sample air was also measured [*Petrenko et al.*, 2009]. The number of ^{14}CO molecules expected in each sample from occluded ancient air was calculated based on sample size, [CO], expected paleo [CO], ^{14}C activity of paleoatmospheric CO and gas age [*Petrenko et al.*, 2009]. Model simulation suggested preindustrial [CO] is around 50 ppbv [*Haan et al.*, 1996].

CO concentrations of the Pakitsoq ice samples were first analyzed at the National Institute of Water and Atmosphere (NIWA), New Zealand and very high concentrations of CO (> 500 ppbv) were observed [*Petrenko et al.*, 2009]. An independent Pakitsoq ice sample measured in Washington State University also indicated a [CO] higher than 800 ppbv [*Petrenko et al.*, 2009]. Based on this consistence of high [CO] and the relatively low CO blank (10-38 ppbv) from the wet extraction method, the elevated CO in Pakitsoq ice is believed to come from the ice itself [*Petrenko et al.*, 2009].

Since in situ production of CO has already been observed in Greenland ice [*Haan and Raynaud*, 1998], we speculate some in-situ CO production in Pakitsoq ice probably had already occurred before the ice reached the Pakitsoq margin. Furthermore, Petrenko

et al. also argued in situ CO production might also happen near the Pakitsoq margin, given the likely presence of organic matter scraped from the glacier bed as well as relatively warm ice temperatures near the margin (0 to -7 °C) [*Petrenko et al.*, 2009].

To better understand how and where this elevated CO comes from and better understand the chemical processes in the ablating glacier ice, the stable isotopes of CO in Pakitsoq ice were analyzed to provide more information on the CO sources in the rapid climatic transitions during the last glacial termination.

5.2 Methodology

The large Pakisoq ice samples were cut with oil-free electric chainsaws near the surface instead of drilling deep into the ice [*Petrenko et al.*, 2006]. YD-PB samples were collected in 2004 and Oldest Dryas-Bølling (OD-Bølling) samples were collected in 2005 [*Petrenko et al.*, 2006]. Characteristics of the drilling site have already been described [*Schaefer et al.*, 2006], and the extraction and dating techniques for the air samples have been discussed [*Schaefer et al.*, 2009]. The ages for Pakitsoq ice samples dating back to the last glacial termination are determined by correlating Pakitsoq surface ice records of $\delta^{15}N$ of N_2, $\delta^{18}O$ of O_2, $\delta^{18}O_{ice}$ and $[CH_4]$ with records from GISP2 [*Petrenko et al.*, 2006].

After completion of $^{14}CH_4$ and $^{14}CO_2$ measurements, the pressure in the Pakitsoq

sample air tanks dropped to ~0.3 bar [*Petrenko et al.*, 2009]. To raise the tank pressure for more reliable [CO] and stable isotope measurements, the air samples were diluted with CO-free ultrahigh pure air (zero air) to raise the tank pressures to 3 bars [*Petrenko et al.*, 2009]. This was done by flowing CO-free ultrahigh pure air through Sofnocat to remove any traces of CO, into the sample tanks [Petrenko, p. comm.]. The diluting air stream was monitored by gas chromatography for [CO] to ensure that it was CO-free [Petrenko, p. comm.]. The CO concentrations in the diluted samples were first measured in NIWA. The remaining samples were transferred into 50 mL glass bottle with Teflon stopcock and measured for CO stable isotopes in Stony Brook University based on the method in [*Z H Wang and Mak*, 2009]. The dilution factors and some measurements of [CO] in the tanks prior to dilution are shown in Table 5.1.

Table 5.1 Pakitsoq ice samples preparation and dilution information

Sample Name	[CO] before dilution* (ppbv)	Dilution Factor	[CO] after dilution (ppbv)	Subsample Name
Younger Dryas 1	671.4	8.64	77.71	KL46
Younger Dryas 2	583.9	8.647	67.52	kl41
YD-PB Transition 1	636.4	8.773	72.54	KL6
YD-PB Transition 2	735.5	8.648	85.05	KL7
Preboreal 1	566.7	8.618	65.76	kl16
Preboreal 2	879.2	8.577	102.5	kl81
Contaminated PB	672.0	8.65	77.69	kl25
Oldest Dryas 1	998.2	9.005	110.85	bottle 5
Oldest Dryas 2	967.9	8.961	108.01	bottle 6
Bølling Sample 1	569.3	8.607	66.15	bottle 16
Bølling Sample 2	734.0	9.112	80.56	Bottle27
Contaminated OD	1286.1	9.384	137.05	kl11

Note: *: [CO] before dilution is calculated with the dilution factor and diluted [CO].

Calibration gas was processed frequently between Pakitsoq ice samples to ensure the analysis system was working well and provide $\delta^{18}O$ values [*C. A. M. Brenninkmeijer*, 1993; *J. E. Mak and C. A. M. Brenninkmeijer*, 1998; *Z H Wang and Mak*, 2009]. 1σ errors for [CO], $\delta^{13}C$, and $\delta^{18}O$ during the period of measuring Pakitsoq ice samples were 1.6 ppbv, 0.1‰ and 0.43‰ respectively, in terms of 100 mL (STP) calibration gas. These errors were then applied to all Pakitsoq ice samples.

5.3 Results and Discussions

Results of CO concentrations measured in this study are shown in Fig 5.1, along with the original CO concentrations prior to dilution, CO concentrations measured in NIWA and CH_4 concentrations in [*Petrenko et al.*, 2008]. Rapid [CH_4] increase and abrupt warm event occurred during both YD-PB transition and OD- Bølling transition [*Petrenko et al.*, 2008], which is consistent with that in GISP2 [*Brook et al.*, 2000].

For the diluted [CO], our concentrations are comparable with those from NIWA except for two samples (YD-PB Transition 1 and Oldest Dryas 2). Due to different dilution factors, diluted [CO] could not provide much information. The original CO concentrations in this study are calculated based on diluted [CO] measured in this study and the dilution factors in Table 5.1. The original [CO] data indicate [CO] decreased in

OD- Bølling transition and increased afterwards, whereas [CO] increased in YD-PB transition and dropped since then.

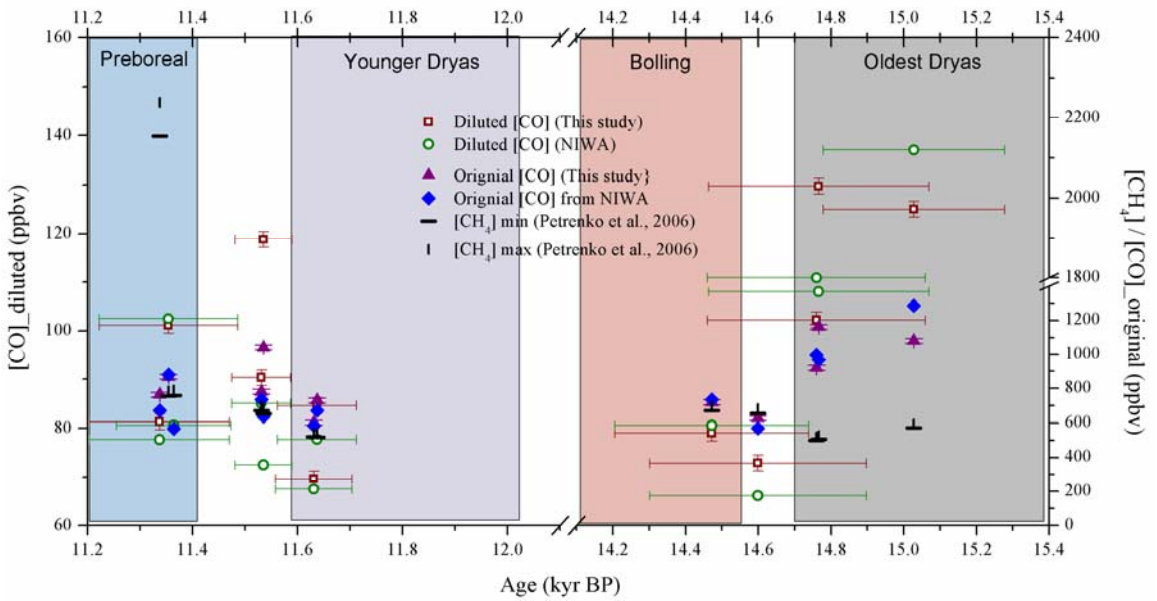

Figure 5.1 Diluted CO concentrations (left scale) of the Pakitsoq ice samples in this study (green circles) and given by NIWA (red squares). Also shown (right scale) are the original CO concentrations in this study (purple triangles) and those from NIWA (blue diamonds) and concentrations of CH_4 (black dashes and bars) [*Petrenko et al.*, 2006]. [CO] error (±1σ) in this study is 1.6 ppbv based on calibration runs. Errors (±1σ) for original [CO] are calculated to be 13-15 ppbv based on errors for subsamples and dilution factors in Table 5.1. Gas age and age errors are derived from $\delta^{15}N$ and $\delta^{18}O_{atm}$ and GISP2 timescale [*Petrenko et al.*, 2006; *Schaefer et al.*, 2006]. Kyr BP is thousand years before present, with present defined as 1950 AD.

Observations of stable isotopes of CO in Pakitsoq ice samples are shown in Fig 5.2. $\delta^{13}C$ varied between -26.5‰ and -29.5‰, which is comparable with present-day $\delta^{13}C$ seasonal variability in Spitsbergen (78.54ºN) [*Rockmann et al.*, 2002]. $\delta^{18}O$ fluctuated between -7‰ and +3‰, which is much lighter than modern $\delta^{18}O$ of CO (-2‰ to 10‰) in Spitsbergen (78.54ºN) [*Rockmann et al.*, 2002]. Due to the large difference between some adjacent samples, it is difficult to find a very clear trend. $\delta^{13}C$ shows a 1‰ increase in

OD-Bølling transition, followed by 1.4‰ decrease from the transition to Bølling. $\delta^{18}O$ shows a 4‰ increase in both OD-Bølling transition and YD-PB transition.

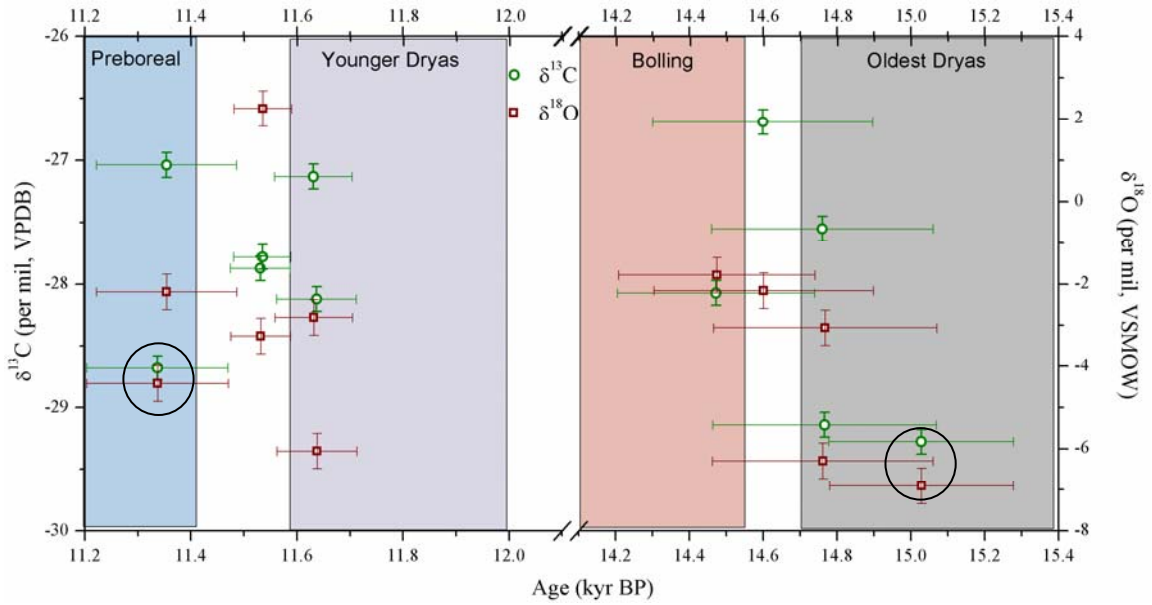

Figure 5.2 Isotopic ratios of CO in Pakitsoq ice samples. Green circles denote $\delta^{13}C$ (left scale) and red squares are for $\delta^{18}O$ (right scale). Error bars for $\delta^{13}C$ and $\delta^{18}O$ are 1σ standard deviations: 0.1‰ and 0.43‰ respectively. The two circles stand for the two contaminated samples (contaminated PB and contaminated OD in Table 5.1). Kyr BP is thousand years before present, with present defined as 1950 AD.

We believe the elevated CO in Pakitsoq is from in situ production. However the mechanisms of CO production in ice are not very clear, though several mechanisms have been suggested. We discuss the possibilities of CO production below and rule out some of them base on our [CO] and isotope data.

The first mechanism is photochemical production of organics by ultraviolet radiation generated by fast muons passing through deep ice [*Colussi and Hoffmann*, 2003]. The result of this photodecarbonylation reaction would result in an increase of [CO] with depth [*Meure*, 2004], which is consistent with the Greenland CO measurements [*Haan*

and Raynaud, 1998]. However, this relationship was not observed in the Pakitsoq ice samples. Thus this possibility may plausibly be ruled out.

A second possibility is oxidation of organic impurities in snow [*Haan et al.*, 2001] and ice [*Haan and Raynaud*, 1998]. The elevated [CO] in snow pack is correlated with the concentrations of total organic carbon in snow, snow temperature and solar radiation [*Haan et al.*, 2001]. As suggested by [*Haan et al.*, 2001], the in situ production of CO in snow should not alter the CO preserved in air bubbles. Therefore, we argue the elevated [CO] in Pakitsoq ice is from oxidation of organic compounds in ice. We assume the elevated [CO] in ice is also dependent on these factors. Temperature dropped in both transitions based on the $\delta^{18}O_{ice}$ measurements in Pakitsoq ice [*Petrenko et al.*, 2008]. Solar activity also dropped in both transitions based on the ^{10}Be concentration record in GISP2 [*Finkel and Nishiizumi*, 1997]. Unfortunately, the information of amount of total organic carbon in Pakitsoq ice is not available. We do not have enough proof to rule out this possibility.

The third possibility is CO production from microbial activity [*Tsunogai et al.*, 2005]. CO production from this mechanism was found to take place in a hydrothermal water plume, but it cannot be concluded that this will also happen in ice. Furthermore, the $\delta^{13}C$ of CO in the plume exhibited highly ^{13}C-depleted values: -110‰ VPDB to -60‰ VPDB, which was not observed in Pakitsoq ice.

The last one is that CO is produced via photolysis of organics such as formaldehyde

by UV penetrating the near-surface ice [*Haan et al.*, 2001]. $\delta^{13}C$ of atmospheric formaldehyde is around -31‰ to -25‰ in urban air [*Rice and Quay*, 2009], but the $\delta^{13}C$ of formaldehyde in ice is still unknown. However the strong isotope fractionation ($j(H^{13}CHO)/j(H^{12}CHO)=0.894$, where j is the photodissociation coefficient of HCHO) occurs during the photolysis of formaldehyde [*Feilberg et al.*, 2005], therefore the produced CO will be much more depleted in ^{13}C compared with our $\delta^{13}C$ range of -26.5‰ to -29.5‰. This mechanism is also plausibly impossible.

As a summary, we argue that oxidation of organic impurities in snow and ice is the most possible reason for this high elevated CO in Pakitsoq ice. Compared with the ~50 ppbv of modeled preindustrial [CO], the original [CO] is more than 10 times larger. Thus our measurements of $\delta^{13}C$ and $\delta^{18}O$ of CO reflect the isotopic signatures of the organics and isotopic fractions in the chemical process. Unfortunately, due to limited information on the ice such as total organic carbon amount and the details of the chemical reactions etc., the trends of isotopic ratios in both transitions are unexplained so far.

To figure out if the in situ production occurred before the ice reached the Pakitsoq margin or after, we can measure the contemporary CO from other Greenland ice core. If [CO] in Greenland ice core is much lower than that in Pakitsoq, the in situ production should occur after the ice reach the margin. If this is the case, there should exist some chemical process, which only occurs in the near-surface ice.

As mentioned previously in this thesis (chapter 4), elevated CO_2 will also be

observed if in situ production of CO is from oxidation of organics since organic material may be oxidized in ice sheet by hydrogen peroxide, formaldehyde and other acids [*Tschumi and Stauffer*, 2000]. CO_2 concentrations in Pakitsoq ice were 5 times higher than expected values [*Petrenko et al.*, 2009]. This supports our argument that in situ production of CO is from the oxidation of organic compounds in Pakitsoq ice.

The sky-high CO concentrations make the data interpretation very difficult. Based on the above discussions, we suggest in situ production of CO is from the oxidation of organic compounds in Pakitsoq ice, but this does not eliminate other possibilities.

5.4 Concluding Remarks

This chapter focuses on the CO records in two abrupt climatic transitions during the last glacial termination: Younger Dryas - Preboreal (YD-PB) transition and Oldest Dryas-Bølling (OD-Bølling) transition based on ablating glacier from Greenland. Sky-high [CO] is observed in Pakitsoq ice. CO concentration in all of the Pakitsoq ice samples were 500-1300 ppmv, indicating huge in situ production. To better understand how and where this elevated CO comes from and better understand the chemical processes in the ablating glacier ice, the stable isotopes of CO in Pakitsoq ice are analyzed. Based on the stable isotopic ratios of CO, we argue this elevated [CO] is from the oxidation of organic compounds in ice sheet, but this does not eliminate other

possibilities. Due to limited information from the ice, the trends of isotopic ratios in both transitions and their causes are still unexplained. Future measurements of contemporary CO in conventional ice cores of Greenland or in blue ice in Antarctica will provide valuable information.

References

Alexander, B., J. Savarino, K. J. Kreutz, and M. H. Thiemens (2004), Impact of preindustrial biomass-burning emissions on the oxidation pathways of tropospheric sulfur and nitrogen, *Journal of Geophysical Research-Atmospheres*, *109*(D8).

Alley, R. B. (2000), Ice-core evidence of abrupt climate changes, *PNAS*, *97*, 1331-1334.

Andersen, K. K., et al. (2004), High-resolution record of Northern Hemisphere climate extending into the last interglacial period, *Nature*, *431*(7005), 147-151.

Assonov, S. S., and C. A. M. Brenninkmeijer (2003), On the ^{17}O correction for CO_2 mass spectrometric isotopic analysis, *Rapid Communications in Mass Spectrometry*, *17*(10), 1007-1016.

Assonov, S. S., C. A. M. Brenninkmeijer, P. J. Jockel, R. Mulvaney, S. Bernard, and J. Chappellaz (2007), Evidence for a CO increase in the SH during the 20th century based on firn air samples from Berkner Island, Antarctica, *Atmospheric Chemistry and Physics*, *7*, 295-308.

Augustin, L., et al. (2004), Eight glacial cycles from an Antarctic ice core, *Nature*, *429*(6992), 623-628.

Aydin, M., M. B. Williams, C. Tatum, and E. S. Saltzman (2008), Carbonyl sulfide in air extracted from a South Pole ice core: a 2000 year record, *Atmospheric Chemistry and Physics*, *8*(24), 7533-7542.

BADC (2007), BADC (British Atmospheric Data Center) Help File: CRYOSTAT Project Data, edited, Natural Environment Research Council's (NERC).

Bard, E., G. Raisbeck, F. Yiou, and J. Jouzel (2000), Solar irradiance during the last 1200 years based on cosmogenic nuclides, *Tellus Series B-Chemical and Physical Meteorology*, *52*(3), 985-992.

Barnola, J. M., D. Raynaud, Y. S. Korotkevich, and C. Lorius (1987), Vostok ice core provides 160,000-year record of atmospheric CO_2, *Nature*, *329*(6138), 408-414.

Barnola, J. M., P. Pimienta, D. Raynaud, and Y. S. Korotkevich (1991), CO_2-CLIMATE RELATIONSHIP AS DEDUCED FROM THE VOSTOK ICE CORE - A REEXAMINATION BASED ON NEW MEASUREMENTS AND ON A REEVALUATION OF THE AIR DATING, *Tellus Series B-Chemical and Physical Meteorology*, *43*(2), 83-90.

Barnola, J. M., M. Anklin, J. Porcheron, D. Raynaud, J. Schwander, and B. Stauffer (1995), CO_2 evolution during the last millennium as recorded by Antarctic and Greenland ice, *Tellus Series B-Chemical and Physical Meteorology*, *47*(1-2), 264-272.

Battle, M., et al. (1996), Atmospheric gas concentrations over the past century measured in air from firn at the South Pole, *Nature*, *383*(6597), 231-235.

Bauer, K., R. Conrad, and W. Seiler (1980), Photo-oxidative production of carbon monoxide by phototropic mocroorganisms, *Biochimica Et Biophysica Acta*, *589*(1), 46-55.

Bender, M., T. Sowers, and E. Brook (1997), Gases in ice cores, *Proc. Natl. Acad. Sci. U. S. A.*, *94*(16), 8343-8349.

Bender, M., T. Sowers, J. M. Barnola, and J. Chappellaz (1994), Changes in the O_2/N_2 Ratio of the Atmosphere During Recent Decades Reflected in the Composition of Air in the Firn at Vostok Station, Antarctica, *Geophysical Research Letters*, *21*(3), 189-192.

Bergamaschi, P., R. Hein, M. Heimann, and P. J. Crutzen (2000a), Inverse modeling of the global CO cycle 1. Inversion of CO mixing ratios, *Journal of Geophysical Research-Atmospheres*, *105*(D2), 1909-1927.

Bergamaschi, P., R. Hein, C. A. M. Brenninkmeijer, and P. J. Crutzen (2000b), Inverse modeling of the global CO cycle 2. Inversion of $^{13}C/^{12}C$ and $^{18}O/^{16}O$ isotope ratios, *Journal of Geophysical Research-Atmospheres*, *105*(D2), 1929-1945.

Bergamaschi, P., C. A. M. Brenninkmeijer, M. Hahn, T. Rockmann, D. H. Scharffe, P. J. Crutzen, N. F. Elansky, I. B. Belikov, N. B. A. Trivett, and D. E. J. Worthy (1998), Isotope analysis based source identification for atmospheric CH_4 and CO sampled across Russia using the Trans-Siberian railroad, *Journal of Geophysical Research-Atmospheres*, *103*(D7), 8227-8235.

Bernard, S., T. R. Rockmann, J. Kaiser, J. M. Barnola, H. Fischer, T. Blunier, and J. Chappellaz (2006), Constraints on N_2O budget changes since pre-industrial time from new firn air and ice core isotope measurements, *Atmospheric Chemistry and Physics*, *6*, 493-503.

Boden, T. A., G. Marland, and R. J. Andres (2009), Global, Regional, and National Fossil-Fuel CO_2 Emissions, *Carbon Dioxide Information Analysis Center, Oak Ridge National Laboratory, U.S. Department of Energy, Oak Ridge, Tenn., U.S.A.*, doi 10.3334/CDIAC/00001.

Bradley, R. S., and P. D. Jones (1992), Climate since A.D. 1500, Routledge, London.

Brailsford, G. (personal communication).

Brandt, E. P., Y. Y. Wang, and J. W. Grizzle (2000), Dynamic modeling of a three-way catalyst for SI engine exhaust emission control, *Ieee Transactions on Control Systems Technology*, *8*(5), 767-776.

Braunlich, M., O. Aballanin, T. Marik, P. Jockel, C. A. M. Brenninkmeijer, J. Chappellaz, J. M. Barnola, R. Mulvaney, and W. T. Sturges (2001), Changes in the global atmospheric methane budget over the last decades inferred from ^{13}C and D isotopic analysis of Antarctic firn air, *Journal of Geophysical Research-Atmospheres*, *106*(D17), 20465-20481.

Brenninkmeijer, C. A. M. (1993), Measurement of the abundance of ^{14}CO in the atmosphere and the $^{13}C/^{12}C$ and $^{18}O/^{16}O$ ratio of atmospheric CO with applications in New Zealand and Antarctica, *Journal of Geophysical Research-Atmospheres*, *98*(D6), 10595-10614.

Brenninkmeijer, C. A. M. (1993), Measurement of the abundance of ^{14}CO in the atmosphere and the $^{13}C/^{12}C$ and $^{18}O/^{16}O$ ratio of atmospheric CO with applications in

New Zealand and Antarctica, *J. Geophys. Res*, *98*(D6), 10595-10614.

Brenninkmeijer, C. A. M. (1999), Review of progress in isotope studies of atmospheric carbon monoxide, *Chemosphere-Global Change Science*, *1*, 33-52.

Brenninkmeijer, C. A. M. (personal communication).

Brenninkmeijer, C. A. M., and I. Hemmingsen (1988), Sheathed thermocouples as heater elements, *Journal of Physics E-Scientific Instruments*, *21*(5), 502-503.

Brenninkmeijer, C. A. M., and T. Rockmann (1997), Principal factors determining the $^{18}O/^{16}O$ ratio of atmospheric CO as derived from observations in the southern hemispheric troposphere and lowermost stratosphere, *Journal of Geophysical Research-Atmospheres*, *102*(D21), 25477-25485.

Brook, E. J., S. Harder, J. Severinghaus, E. J. Steig, and C. M. Sucher (2000), On the origin and timing of rapid changes in atmospheric methane during the last glacial period, *Global Biogeochemical Cycles*, *14*(2), 559-572.

Brunke, E. G., H. E. Scheel, and W. Seiler (1990), Trends of tropospheric CO, N_2O and CH_4 as observed at Cape Point, South Africa, *Atmospheric Environment Part a-General Topics*, *24*(3), 585-595.

Butler, J. H., M. Battle, M. L. Bender, S. A. Montzka, A. D. Clarke, E. S. Saltzman, C. M. Sucher, J. P. Severinghaus, and J. W. Elkins (1999), A record of atmospheric halocarbons during the twentieth century from polar firn air, *Nature*, *399*(6738), 749-755.

Cantrell, C. A., R. E. Shetter, A. H. McDaniel, J. G. Calvert, J. A. Davidson, D. C. Lowe,

S. C. Tyler, R. J. Cicerone, and J. P. Greenberg (1990), Carbon kinetic isotope effect in the oxidation of methane by the hydroxyl radical, *Journal of Geophysical Research-Atmospheres*, *95*(D13), 22455-22462.

Carcaillet, C., et al. (2002), Holocene biomass burning and global dynamics of the carbon cycle, *Chemosphere*, *49*(8), 845-863.

Chappellaz, J. (person communication).

Chappellaz, J., T. Blunier, S. Kints, A. Dallenbach, J. M. Barnola, J. Schwander, D. Raynaud, and B. Stauffer (1997), Changes in the atmospheric CH4 gradient between Greenland and Antarctica during the Holocene, *Journal of Geophysical Research-Atmospheres*, *102*(D13), 15987-15997.

Clark, I. D., L. Henderson, J. Chappellaz, D. Fisher, R. Koerner, D. E. J. Worthy, T. Kotzer, A. L. Norman, and J. M. Barnola (2007), CO_2 isotopes as tracers of firn air diffusion and age in an Arctic ice cap with summer melting, Devon Island, Canada, *Journal of Geophysical Research-Atmospheres*, *112*(D1).

Cohen, A. S., M. R. Talbot, S. M. Awramik, D. L. Dettman, and P. Abell (1997), Lake level and paleoenvironmental history of Lake Tanganyika, Africa, as inferred from late Holocene and modern stromatolites, *Geological Society of America Bulletin*, *109*(4), 444-460.

Colbeck, S. C. (1989), Air movement in snow due to windpumping, *Journal of Glaciology*, *35*(120), 209-213.

Colussi, A. J., and M. R. Hoffmann (2003), In situ photolysis of deep ice core contaminants by Cerenkov radiation of cosmic origin, *Geophysical Research Letters*, *30*(4).

Conrad, R., and W. Seiler (1980), Photooxidative production and microbial consumption of carbon monoxide in seawater, *Fems Microbiology Letters*, *9*(1), 61-64.

Coplen, T. B. (1994), Reporting of stable hydrogen, carbon, and oxygen isotopic abundances, *Pure and Applied Chemistry*, *66*(2), 273-276.

Craig, H. (1953), The geochemistry of the stable carbon isotopes, *Geochim. Cosmochim. Acta*, *3*(2-3), 53-92.

Craig, H. (1957), Isotopic standards for carbon and oxygen and correction factors for mass spectrometric analysis of carbon dioxide, *Geochim. Cosmochim. Acta*, *12*(1-2), 133-149.

Craig, H., Y. Horibe, and T. Sowers (1988a), Gravitational seperation of gases and isotopes in polar ice caps, *Science*, *242*(4886), 1675-1678.

Craig, H., C. C. Chou, J. A. Welhan, C. M. Stevens, and A. Engelkemeir (1988b), The Isotopic Composition of Methane in Polar Ice Cores, *Science*, *242*, 1535-1539.

Crutzen, P. J., and M. O. Andreae (1990), Biomass burning in the tropics: impact on atmospheric chemistry and biogeochemical cycles, *Science*, *250*(4988), 1669-1678.

Crutzen, P. J., and P. H. Zimmermann (1991), The changing photochemistry of the troposphere, *Tellus Series a-Dynamic Meteorology and Oceanography*, *43*(4), 136-151.

Daniel, J. S., and S. Solomon (1998), On the climate forcing of carbon monoxide, *Journal of Geophysical Research-Atmospheres*, *103*(D11), 13249-13260.

Deeter, M. N., et al. (2003), Operational carbon monoxide retrieval algorithm and selected results for the MOPITT instrument, *Journal of Geophysical Research-Atmospheres*, *108*(D14).

Delmas, R. A., et al. (1999), Experiment for Regional Sources and Sinks of Oxidants (EXPRESSO): An overview, *Journal of Geophysical Research-Atmospheres*, *104*(D23), 30609-30624.

Dlugokencky, E. J., R. C. Myers, P. M. Lang, K. A. Masarie, A. M. Crotwell, K. W. Thoning, B. D. Hall, J. W. Elkins, and L. P. Steele (2005), Conversion of NOAA atmospheric dry air CH4 mole fractions to a gravimetrically prepared standard scale, *Journal of Geophysical Research-Atmospheres*, *110*(D18).

Edwards, D. P., G. Petron, P. C. Novelli, L. K. Emmons, J. C. Gille, and J. R. Drummond (2006a), Southern Hemisphere carbon monoxide interannual variability observed by Terra/Measurement of Pollution in the Troposphere (MOPITT), *Journal of Geophysical Research-Atmospheres*, *111*(D16).

Edwards, D. P., et al. (2006b), Satellite-observed pollution from Southern Hemisphere biomass burning, *Journal of Geophysical Research-Atmospheres*, *111*(D14).

Ehleringer, J. R. (1993), Carbon isotope ratios and physiological processes in aridland plants, in *Stable Isotopes in Ecological Research*, edited by P. W. Rundel, J. R.

Ethleringer and K. A. Nagy, Springer, New York.

Emmons, L. (personal Communication).

Emmons, L. K., et al. (in preparation), Simulation of Stable Carbon Isotopes in MOZART-4, *in preparation*.

Emmons, L. K., et al. (2009), Description and evaluation of the Model for Ozone and Related chemical Tracers, version 4 (MOZART-4), *Geoscientific Model Development Discussions*, *2*, 1157-1213.

Emmons, L. K., et al. (2004), Validation of Measurements of Pollution in the Troposphere (MOPITT) CO retrievals with aircraft in situ profiles, *Journal of Geophysical Research-Atmospheres*, *109*(D3).

Etheridge, D. M. (personal communication).

Etheridge, D. M., L. P. Steele, R. J. Francey, and R. L. Langenfelds (1998), Atmospheric methane between 1000 AD and present: Evidence of anthropogenic emissions and climatic variability, *Journal of Geophysical Research-Atmospheres*, *103*(D13), 15979-15993.

Farquhar, G. D. (1993), Carbon isotope fractionation inplants and water-use efficiency, *Stable Isotopes in Ecological Research*(Springer, New York).

Feilberg, K. L., B. D'Anna, M. S. Johnson, and C. J. Nielsen (2005), Relative tropospheric photolysis rates of HCHO, $H^{13}CHO$, $HCH^{18}O$, and DCDO measured at the European photoreactor facility, *J. Phys. Chem. A*, *109*(37), 8314-8319.

Feilberg, K. L., S. R. Sellevag, C. J. Nielsen, D. W. T. Griffith, and M. S. Johnson (2002), CO+OH -> CO2+H: The relative reaction rate of five CO isotopologues, *Phys. Chem. Chem. Phys.*, *4*(19), 4687-4693.

Ferretti, D. F., et al. (2005), Unexpected changes to the global methane budget over the past 2000 years, *Science*, *309*(5741), 1714-1717.

Filippelli, G. M., J. C. Latimer, R. W. Murray, and J. A. Flores (2007), Productivity records from the Southern Ocean and the equatorial Pacific Ocean: Testing the glacial Shelf-Nutrient Hypothesis, *Deep-Sea Research Part Ii-Topical Studies in Oceanography*, *54*(21-22), 2443-2452.

Finkel, R. C., and K. Nishiizumi (1997), Beryllium 10 concentrations in the Greenland Ice Sheet Project 2 ice core from 3-40 ka, *Journal of Geophysical Research-Oceans*, *102*(C12), 26699-26706.

Francey, R. J., M. R. Manning, C. E. Allison, S. A. Coram, D. Etheridge, R. Langenfelds, D. C. Lowe, and P. Steele (1999a), A history of $\delta^{13}C$ in atmospheric CH4 from the Cape Grim Air Archive and Antarctic firn air, *J. Geophys Res*, *104*(D19), 23631-23643.

Francey, R. J., C. E. Allison, D. M. Etheridge, C. M. Trudinger, I. G. Enting, M. Leuenberger, R. L. Langenfelds, E. Michel, and L. P. Steele (1999b), A 1000-year high precision record of $\delta^{13}C$ in atmospheric CO_2, *Tellus Series B-Chemical and Physical Meteorology*, *51*(2), 170-193.

Friedli, H., E. Moor, H. Oeschger, U. Siegenthaler, and B. Stauffer (1984), $^{13}C/^{12}C$ Ratios

in CO_2 Extracted from Antarctic Ice, *Geophysical Research Letters*, *11*(11), 1145-1148.

Goericke, R., and B. Fry (1994), Variations of Marine Plankton $\delta^{13}C$ with Latitude, Temperature, and Dissolved CO_2 in the World Ocean, *Global Biogeochemical Cycles*, *8*(1), 85-90.

Goldammer, J. G., and C. De Ronde (2004), Wildland Fire Management Handbook for Sub-Sahara Africa, A publicaiton of Global Fire Monitoring Center (GFMC).

Goldewijk, K. K. (2001), Estimating global land use change over the past 300 years: The HYDE Database, *Global Biogeochemical Cycles*, *15*(2), 417-433.

Gonfiantini, R. (1978), Standards for stable isotope measurements in natural compounds, *Nature*, *271*(5645), 534-536.

Gros, V., et al. (2001), Detailed analysis of the isotopic composition of CO and characterization of the air masses arriving at Mount Sonnblick (Austrian Alps), *Journal of Geophysical Research-Atmospheres*, *106*(D3), 3179-3193.

Guenther, A., C. Geron, T. Pierce, B. Lamb, P. Harley, and R. Fall (2000), Natural emissions of non-methane volatile organic compounds; carbon monoxide, and oxides of nitrogen from North America, *Atmospheric Environment*, *34*(12-14), 2205-2230.

Guenther, A., et al. (1995), A global-model of natural volatile organic compounds emissions, *Journal of Geophysical Research-Atmospheres*, *100*(D5), 8873-8892.

Haan, D., and D. Raynaud (1998), Ice core record of CO variations during the last two millennia: atmospheric implications and chemical interactions within the Greenland ice,

Tellus Series B-Chemical and Physical Meteorology, *50*(3), 253-262.

Haan, D., P. Martinerie, and D. Raynaud (1996), Ice core data of atmospheric carbon monoxide over Antarctica and Greenland during the last 200 years, *Geophysical Research Letters*, *23*(17), 2235-2238.

Haan, D., Y. Zuo, V. Gros, and C. A. M. Brenninkmeijer (2001), Photochemical production of carbon monoxide in snow, *Journal of Atmospheric Chemistry*, *40*(3), 217-230.

Halfman, J. D., T. C. Johnson, and B. P. Finney (1994), New AMS dates, stratigraphic correlations and decadal climatic cycles for the past 4ka at Lake Turkana, Kenya, *Palaeogeography Palaeoclimatology Palaeoecology*, *111*(1-2), 83-98.

Hammer, C., H. Claussen, and C. Langway (1994), Electrical conductivity method (ECM) stratigraphic dating of the Bryd station ice core, Antarctica, *Annals of Glaciology*, *20*, 115-120.

Hauglustaine, D. A., G. P. Brasseur, S. Walters, P. J. Rasch, J. F. Muller, L. K. Emmons, and C. A. Carroll (1998), MOZART, a global chemical transport model for ozone and related chemical tracers 2. Model results and evaluation, *Journal of Geophysical Research-Atmospheres*, *103*(D21), 28291-28335.

Heidt, L. E., J. P. Krasnec, R. A. Lueb, W. H. Pollock, B. E. Henry, and P. J. Crutzen (1980), Latitudinal distributions of CO and CH_4 over the Pacific, *Journal of Geophysical Research-Oceans and Atmospheres*, *85*(NC12), 7329-7336.

Herron, M. M., and C. C. Langway (1980), Firn densification: an empirical model, *Journal of Glaciology*, *25*(93), 373-385.

Houghton, J. T., Y. Ding, D. J. Griggs, N. Noguer, P. J. van der Linden, X. Dai, K. Maskell, and C. A. Johnson (2001), Climate Change 2001: The Scientific Basis, *Cambridge university Press*.

Huang, Y., F. A. Street-Perrott, S. E. Metcalfe, M. Brenner, M. Moreland, and K. H. Freeman (2001), Climate change as the dominant control on glacial-interglacial variations in C_3 and C_4 plant abundance, *Science*, *293*(5535), 1647-1651.

Huff, A. K., and M. H. Thiemens (1998), $^{17}O/^{16}O$ and $^{18}O/^{16}O$ isotope measurements of atmospheric carbon monoxide and its sources, *Geophysical Research Letters*, *25*(18), 3509-3512.

Iannone, R., R. Koppmann, and J. Rudolph (2009), $^{12}C/^{13}C$ kinetic isotope effects of the gas-phase reactions of isoprene, methacrolein, and methyl vinyl ketone with OH radicals, *Atmospheric Environment*, *43*(19), 3103-3110.

Iannone, R., R. S. Anderson, J. Rudolph, L. Huang, and D. Ernst (2003), The carbon kinetic isotope effects of ozone-alkene reactions in the gas-phase and the impact of ozone reactions on the stable carbon isotope ratios of alkenes in the atmosphere, *Geophysical Research Letters*, *30*(13).

IPCC-SAR (1996), Climate Change 1995: The Science of Climate Change. Contribution of Working Group I to the Second Assessment Report of the Intergovernmental Panel on

Climate Change, *Cambridge University Press*, *Cambridge, UK*.

IPCC (2007), Climate Change 2007: The Physical Science Basis. Contribution of Working Group I to the Fourth Assessment Report of the Intergovernmental Panel on Climate Change [Solomon, S., D. Qin, M. Manning, Z. Chen, M. Marquis, K.B. Averyt, M.Tignor and H.L. Miller (eds.)], *Cambridge University Press, Cambridge*, *United Kingdom and New York, NY, USA*.

Isaksen, I. S. A. (1987), Calculation of trends in the tropospheric concentration of O_3, OH, CO, CH_4, and NO_x, *Tellus*, *39B*, 271-285.

Jauregui-Haza, U. J., E. J. Pardillo-Fontdevila, A. M. Wilhelm, and H. Delmas (2004), Solubility of hydrogen and carbon monoxide in water and some organic solvents, *Latin American Applied Research*, *34*(2), 71-74.

Jones, P. D., and M. E. Mann (2004), Climate over past millennia, *Reviews of Geophysics*, *42*(2).

Jouzel, J., et al. (1997), Validity of the temperature reconstruction from water isotopes in ice cores, *Journal of Geophysical Research-Oceans*, *102*(C12), 26471-26487.

Kato, S., H. Akimoto, T. Rockmann, M. Braunlich, and C. A. M. Brenninkmeijer (1999), Stable isotopic compositions of carbon monoxide from biomass burning experiments, *Atmospheric Environment*, *33*(27), 4357-4362.

Kato, S., Y. Kajii, H. Akimoto, M. Braunlich, T. Rockmann, and C. A. M. Brenninkmeijer (2000), Observed and modeled seasonal variation of ^{13}C, ^{18}O and ^{14}C of atmospheric CO

Happo, a remote site in Japan, and a comparison with other records, *Journal of Geophysical Research-Atmospheres*, *105*(D7), 8891-8900.

Kaye, J. A. (1987), Mechanisms and observations for isotope fractionation of molecular species in planetary atmospheres, *Reviews of Geophysics*, *25*(8), 1609-1658.

Khalil, M. A. K., and R. A. Rasmussen (1984), Carbon monoxide in the earth's atmosphere: increased trend, *Science*, *224*(4644), 54-56.

Khalil, M. A. K., and R. A. Rasmussen (1990), Atmospheric carbon monoxide: latitudinal distribution of sources, *Geophysical Research Letters*, *17*(11), 1913-1916.

Khalil, M. A. K., and R. A. Rasmussen (1994), Global decrease in atmospheric carbon monoxide concentration, *Nature*, *370*(6491), 639-641.

Kummer, J. T. (1980), Catalysis for automobile emission control, *Progress in Energy and Combustion Science*, *6*(2), 177-199.

Lamb, H. H. (1977), Climate: Past, present and future, in Climatic history and future. Vol II, Methuen, New York.

Landais, A., and E. Capron (personal communication).

Landais, A., et al. (2006), Firn-air $\delta^{15}N$ in modern polar sites and glacial-interglacial ice: a model-data mismatch during glacial periods in Antarctica?, *Quaternary Science Reviews*, *25*(1-2), 49-62.

Logan, J. A., M. J. Prather, S. C. Wofsy, and M. B. McElroy (1981), Tropospheric chemistry: a global perspective, *Journal of Geophysical Research-Oceans and*

Atmospheres, *86*(NC8), 7210-7254.

Loulergue, L., A. Schilt, R. Spahni, V. Masson-Delmotte, T. Blunier, B. Lemieux, J. M. Barnola, D. Raynaud, T. F. Stocker, and J. Chappellaz (2008), Orbital and millennial-scale features of atmospheric CH_4 over the past 800,000 years, *Nature*, *453*(7193), 383-386.

Lowe, D. C., C. A. M. Brenninkmeijer, S. C. Tyler, and E. J. Dlugkencky (1991), Determination of the Isotopic Composition of Atmospheric Methane and Its Application in the Antarctic, *Journal of Geophysical Research-Atmospheres*, *96*(D8), 15455-15467.

Lowe, D. C., M. R. Manning, G. W. Brailsford, and A. M. Bromley (1997), The 1991-1992 atmospheric methane anomaly: Southern Hemisphere ^{13}C decrease and growth rate fluctuations, *Geophysical Research Letters*, *24*(8), 857-860.

Luthi, D., et al. (2008), High-resolution carbon dioxide concentration record 650,000-800,000 years before present, *Nature*, *453*(7193), 379-382.

Maasch, K. A., P. A. Mayewski, E. J. Rohling, J. C. Stager, W. Karlen, L. D. Meeker, and E. A. Meyerson (2005), A 2000-year context for modern climate change, *Geogr. Ann. Ser. A-Phys. Geogr.*, *87A*(1), 7-15.

Mak, J. (personal communication).

Mak, J., and G. Kra (1999), The isotopic composition of carbon monoxide at Montauk Point, Long Island, *Chemosphere: Global Change Science 1*, *1*, 205-218.

Mak, J., G. Kra, T. Sandomenico, and P. Bergamaschi (2003), The seasonally varying

isotopic composition of the sources of carbon monoxide at Barbados, West Indies, *Journal of Geophysical Research-Atmospheres*, *108*(D20).

Mak, J. E. (1992), The Isotopes of Carbon Monoxide in the Free Troposphere and Their Implications to Atmospheric Chemistry, *PhD Thesis*, *The University of California, San Diego and National Center for Atmospheric Research*.

Mak, J. E., and C. A. M. Brenninkmeijer (1994), Compressed-Air Sample Technology for Isotopic Analysis of Atmospheric Carbon-Monoxide, *Journal of Atmospheric and Oceanic Technology*, *11*(2), 425-431.

Mak, J. E., and C. A. M. Brenninkmeijer (1998), Measurement of ^{13}CO and $C^{18}O$ in the free troposphere, *Journal of Geophysical Research-Atmospheres*, *103*(D15), 19347-19358.

Mak, J. E., and W. B. Yang (1998), Technique for analysis of air samples for ^{13}C and ^{18}O in carbon monoxide via continuous-flow isotope ratio mass spectrometry, *Anal. Chem.*, *70*(24), 5159-5161.

Mak, J. E., and W. Yang (1998), Technique for Analysis of Air Samples for ^{13}C and ^{18}O in Carbon Monoxide via Continuous-Flow Isotope Ratio Mass Spectrometry, *Anal. Chem.*, *70*, 5159-5161.

Mak, J. E., and C. A. M. Brenninkmeijer (1998), Measurement of ^{13}CO and $C^{18}O$ in the free troposphere, *J. Geophys. Res.*, *103*(D15), 19,347-319,358.

Mak, J. E., C. A. M. Brenninkmeijer, and J. Tamaresis (1994), Atmospheric ^{14}CO

Observations and Their Use for Estimating Carbon Monoxide Removal Rates, *Journal of Geophysical Research-Atmospheres*, *99*(D11), 22915-22922.

Mak, J. E., M. R. Manning, and D. C. Lowe (2000), Aircraft observations of $\delta^{13}C$ of atmospheric methane over the Pacific in August 1991 and 1993: Evidence of an enrichment in $^{13}CH_4$ in the Southern Hemisphere, *Journal of Geophysical Research-Atmospheres*, *105*(D1), 1329-1335.

Malhi, Y., P. Meir, and S. Brown (2002), Forests, carbon and global climate, *Philosophical Transactions of the Royal Society of London Series a-Mathematical Physical and Engineering Sciences*, *360*(1797), 1567-1591.

Mann, M. E., and P. D. Jones (2003), Global surface temperatures over the past two millennia, *Geophysical Research Letters*, *30*(15).

Manning, M. R., C. A. M. Brenninkmeijer, and W. Allan (1997), Atmospheric carbon monoxide budget of the southern hemisphere: Implications of $^{13}C/^{12}C$ measurements, *Journal of Geophysical Research-Atmospheres*, *102*(D9), 10673-10682.

Marino, B. D., and M. B. McElroy (1991), Isotopic composition of atmospheric CO_2 inferred from carbon in C_4 plant cellulose, *Nature*, *349*(6305), 127-131.

Marlon, J. R., P. J. Bartlein, C. Carcaillet, D. G. Gavin, S. P. Harrison, P. E. Higuera, F. Joos, M. J. Power, and I. C. Prentice (2008), Climate and human influences on global biomass burning over the past two millennia, *Nature Geoscience*, *1*(10), 697-702.

Martinerie, P. (2009), Personal Communication.

Martinerie, P. (personal communication).

Martinerie, P., G. P. Brasseur, and C. Granier (1995), The Chemical-Composition of Ancient Atmospheres - a Model Study Constrained by Ice Core Data, *Journal of Geophysical Research-Atmospheres*, *100*(D7), 14291-14304.

Martinerie, P., V. Y. Lipenkov, D. Raynaud, J. Chappellaz, N. I. Barkov, and C. Lorius (1994), Air Content Paleo Record in the Vostok Ice Core (Antarctica) - a Mixed Record of Climatic and Glaciological Parameters, *Journal of Geophysical Research-Atmospheres*, *99*(D5), 10565-10576.

Martinerie, P., E. Nourtier-Mazauric, J. M. Barnola, W. T. Sturges, D. R. Worton, E. Atlas, L. K. Gohar, K. P. Shine, and G. P. Brasseur (2009), Long-lived halocarbon trends and budgets from atmospheric chemistry modelling constrained with measurements in polar firn, *Atmospheric Chemistry and Physics*, *9*(12), 3911-3934.

Masson, V., et al. (2000), Holocene climate variability in Antarctica based on 11 ice-core isotopic records, *Quaternary Research*, *54*(3), 348-358.

Matthews, D. E., and J. M. Hayes (1978), Isotope ratio monitoring gas chromatography mass spectrometry, *Anal. Chem.*, *50*(11), 1465-1473.

Mayewski, P. A., et al. (2005), Solar forcing of the polar atmosphere, in *Annals of Glaciology, Vol 41, 2005*, edited by G. Hamilton, pp. 147-154, Int Glaciological Soc, Cambridge.

Mayewski, P. A., et al. (2009), STATE OF THE ANTARCTIC AND SOUTHERN

OCEAN CLIMATE SYSTEM, *Reviews of Geophysics*, *47*.

McConnell, J. R., G. W. Lamorey, and M. A. Hutterli (2002), A 250-year high-resolution record of Pb flux and crustal enrichment in central Greenland, *Geophysical Research Letters*, *29*(23).

Merritt, D. A., and J. M. Hayes (1994), Factors controlling precision and accuracy in isotope ratio monitoring mass spectrometry, *Anal. Chem.*, *66*(14), 2336-2347.

Merritt, D. A., W. A. Brand, and J. M. Hayes (1994), Isotope ratio monitoring gas chromatography mass spectrometry: methods for isotopic calibration, *Organic Geochemistry*, *21*(6-7), 573-583.

Merritt, D. A., J. M. Hayes, and D. J. D. Marias (1995), Carbon Isotopic Analysis of Atmospheric Methane by Isotope-Ratio-Monitoring Gas-Chromatography Mass-Spectrometry, *Journal of Geophysical Research-Atmospheres*, *100*(D1), 1317-1326.

Meure, C. M. (2004), The Variation of Atmospheric Carbon Dioxide, Methane and Nitrous Oxide During the Holocene from Ice Core Analysis, The University of Melbourne, Melbourne.

Meure, C. M., D. Etheridge, C. Trudinger, P. Steele, R. Langenfelds, T. van Ommen, A. Smith, and J. Elkins (2006), Law Dome CO_2, CH_4 and N_2O ice core records extended to 2000 years BP, *Geophysical Research Letters*, *33*(14).

Moberg, A., D. M. Sonechkin, K. Holmgren, N. M. Datsenko, and W. Karlen (2005),

Highly variable Northern Hemisphere temperatures reconstructed from low- and high-resolution proxy data, *Nature*, *433*(7026), 613-617.

Mulvaney, R., O. Alemany, and P. Possenti (2007), The Berkner Island (Antarctica) ice-core drilling project, *Annals of Glaciology*, *47*, 115-124.

Nakagawa, F., U. Tsunogai, T. Gamo, and N. Yoshida (2004), Stable isotopic compositions and fractionations of carbon monoxide at coastal and open ocean stations in the Pacific, *Journal of Geophysical Research-Oceans*, *109*(C6).

Neftel, A., E. Moor, H. Oeschger, and B. Stauffer (1985), Evidence from Polar Ice Cores for the Increase in Atmospheric CO_2 in the Past 2 Centuries, *Nature*, *315*(6014), 45-47.

Nisbet, E. G., and J. Chappellaz (2009), Shifting Gear, Quickly, *Science*, *324*(5926), 477-478.

Novelli, P. C., L. P. Steele, and P. P. Tans (1992), Mixing ratios of carbon monoxide in the troposphere, *Journal of Geophysical Research-Atmospheres*, *97*(D18), 20731-20750.

Novelli, P. C., K. A. Masarie, and P. M. Lang (1998a), Distributions and recent changes of carbon monoxide in the lower troposphere, *Journal of Geophysical Research-Atmospheres*, *103*(D15), 19015-19033.

Novelli, P. C., K. A. Masarie, P. P. Tans, and P. M. Lang (1994a), Recent changes in atmospheric carbon monoxide, *Science*, *263*(5153), 1587-1590.

Novelli, P. C., J. E. Collins Jr, R. C. Myers, G. W. Sachse, and H. E. Scheel (1994b), Reevaluation of the NOAA/CMDL carbon monoxide reference scale and comparisons

with CO reference gases at NASA-Langley and the Fraunhofer Institut, *J. Geophy. Res*, *99*(D6), 12833-12839.

Novelli, P. C., K. A. Masarie, P. M. Lang, B. D. Hall, R. C. Myers, and J. W. Elkins (2003), Reanalysis of tropospheric CO trends: Effects of the 1997-1998 wildfires, *Journal of Geophysical Research-Atmospheres*, *108*(D15).

Novelli, P. C., et al. (1998b), An internally consistent set of globally distributed atmospheric carbon monoxide mixing ratios developed using results from an intercomparison of measurements, *Journal of Geophysical Research-Atmospheres*, *103*(D15), 19285-19293.

Park, K. H. (personal Communication).

Park, K. H., L. Emmons, and J. E. Mak (in preparation), Implementing the oxygen isotopes of CO in MOZART, *in preparation*.

Petit, J. R., et al. (1999), Climate and atmospheric history of the past 420,000 years from the Vostok ice core, Antarctica, *Nature*, *399*(6735), 429-436.

Petrenko, V. V., J. P. Severinghaus, E. J. Brook, N. Reeh, and H. Schaefer (2006), Gas records from the West Greenland ice margin covering the Last Glacial Termination: a horizontal ice core, *Quaternary Science Reviews*, *25*(9-10), 865-875.

Petrenko, V. V., et al. (2008), A novel method for obtaining very large ancient air samples from ablating glacial ice for analyses of methane radiocarbon, *Journal of Glaciology*, *54*(185), 233-244.

Petrenko, V. V., et al. (2009), $^{14}CH_4$ Measurements in Greenland Ice: Investigating Last Glacial Termination CH_4 Sources, *Science*, *324*(5926), 506-508.

Petron, G., C. Granier, B. Khattatov, V. Yudin, J. F. Lamarque, L. Emmons, J. Gille, and D. P. Edwards (2004), Monthly CO surface sources inventory based on the 2000-2001 MOPITT satellite data, *Geophysical Research Letters*, *31*(21).

Pfister, G., G. Petron, L. K. Emmons, J. C. Gille, D. P. Edwards, J. F. Lamarque, J. L. Attie, C. Granier, and P. C. Novelli (2004), Evaluation of CO simulations and the analysis of the CO budget for Europe, *Journal of Geophysical Research-Atmospheres*, *109*(D19).

Pfister, G. G., L. K. Emmons, P. G. Hess, J. F. Lamarque, J. J. Orlando, S. Walters, A. Guenther, P. I. Palmer, and P. J. Lawrence (2008), Contribution of isoprene to chemical budgets: A model tracer study with the NCAR CTM MOZART-4, *Journal of Geophysical Research-Atmospheres*, *113*(D5).

Pinto, J. P., and M. A. K. Khalil (1991), The stability of tropospheric OH during ice ages, interglacial epochs and modern times, *Tellus Series B-Chemical and Physical Meteorology*, *43*(5), 347-352.

Pongratz, J., C. Reick, T. Raddatz, and M. Claussen (2008), A reconstruction of global agricultural areas and land cover for the last millennium, *Global Biogeochemical Cycles*, *22*(3).

Pradier, S., J. L. Attie, M. Chong, J. Escobar, V. H. Peuch, J. F. Lamarque, B. Khattatov, and D. Edwards (2006), Evaluation of 2001 springtime CO transport over West Africa

using MOPITT CO measurements assimilated in a global chemistry transport model, *Tellus Series B-Chemical and Physical Meteorology*, *58*(3), 163-176.

Prather, M. J. (1996), Time scales in atmospheric chemistry: Theory, GWPs for CH_4 and CO, and runaway growth, *Geophysical Research Letters*, *23*(19), 2597-2600.

Quay, P., J. Stutsman, D. Wilbur, A. Snover, E. Dlugokencky, and T. Brown (1999), The isotopic composition of atmospheric methane, *Global Biogeochemical Cycles*, *13*(2), 445-461.

Ramankutty, N., and J. A. Foley (1999), Estimating historical changes in global land cover: Croplands from 1700 to 1992, *Global Biogeochemical Cycles*, *13*(4), 997-1027.

Randerson, J. T., M. V. Thompson, T. J. Conway, I. Y. Fung, and C. B. Field (1997), The contribution of terrestrial sources and sinks to trends in the seasonal cycle of atmospheric carbon dioxide, *Global Biogeochemical Cycles*, *11*(4), 535-560.

Raynaud, D. (1993), Ice core records as a key to understanding the history of atmospheric trace gases, in *Biogeochemistry of global change: Radiatively active trace gases*, edited by R. Oermland, pp. 29-45, Chapman and Hill, New York.

Raynaud, D., J. Jouzel, J. M. Barnola, J. Chappellaz, R. J. Delmas, and C. Lorius (1993), The Ice Record of Greenhouse Gases, *Science*, *259*(5097), 926-934.

Reeh, N., H. Oerter, and H. H. Thomsen (2002), Comparison between Greenland ice-margin and ice-core oxygen-18 records, *Annals of Glaciology, Vol 35*, *35*, 136-144.

Reeh, N., H. Oerter, A. Letreguilly, H. Miller, and H. W. Hubberten (1991), A New,

Detailed Ice-Age O-18 Record from the Ice-Sheet Margin in Central West Greenland, *Global and Planetary Change*, *90*(4), 373-383.

Reeves, C. E., W. T. Sturges, G. A. Sturrock, K. Preston, D. E. Oram, J. Schwander, R. Mulvaney, J. M. Barnola, and J. Chappellaz (2005a), Trends of halon gases in polar firn air: implications for their emission distributions, *Atmospheric Chemistry and Physics*, *5*, 2055-2064.

Reeves, C. E., W. T. Sturges, G. A. Sturrock, K. Preston, D. E. Oram, J. Schwander, R. Mulvaney, J. M. Barnola, and J. Chappellaz (2005b), Trends of halon gases in polar firn air: implications for their emission distributions, *Atmos. Chem. Phys.*, *5*, 2055-2064.

Rhee, T. S., J. Mak, T. Rockmann, and C. A. M. Brenninkmeijer (2004), Continuous-flow isotope analysis of the deuterium/hydrogen ratio in atmospheric hydrogen, *Rapid Communications in Mass Spectrometry*, *18*(3), 299-306.

Ricci, M. P., D. A. Merritt, K. H. Freeman, and J. M. Hayes (1994), Acquisition and processing of data for isotope ratio monitoring mass spectrometry, *Organic Geochemistry*, *21*(6-7), 561-571.

Rice, A. L., and P. D. Quay (2009), Isotopic Composition of Formaldehyde in Urban Air, *Environmental Science and Technology*.

Rice, A. L., A. A. Gotoh, H. O. Ajie, and S. C. Tyler (2001), High-precision continuous-flow measurement of $\delta^{13}C$ and δD of atmospheric CH_4, *Anal. Chem.*, *73*(17), 4104-4110.

Rinsland, C. P., and J. S. Levine (1985), Free tropspheric carbon monoxide concentrations in 1950 and 1951 deduced from infrared total column amount measurements, *Nature*, *318*(6043), 250-254.

Robbins, R. C., L. A. Cavanagh, L. J. Salas, and E. Robinson (1973), ANALYSIS OF ANCIENT ATMOSPHERES, *Journal of Geophysical Research*, *78*(24), 5341-5344.

Rockmann, T., and C. A. M. Brenninkmeijer (1997), CO and CO_2 isotopic composition in Spitsbergen during the 1995 ARCTOC campaign, *Tellus Series B-Chemical and Physical Meteorology*, *49*(5), 455-465.

Rockmann, T., J. Kaiser, and C. A. M. Brenninkmeijer (2003a), The isotopic fingerprint of the pre-industrial and the anthropogenic N_2O source, *Atmospheric Chemistry and Physics*, *3*, 315-323.

Rockmann, T., J. Kaiser, C. A. M. Brenninkmeijer, and W. A. Brand (2003b), Gas chromatography/isotope-ratio mass spectrometry method for high-precision position-dependent ^{15}N and ^{18}O measurements of atmospheric nitrous oxide, *Rapid Communications in Mass Spectrometry*, *17*(16), 1897-1908.

Rockmann, T., P. Jockel, V. Gros, M. Braunlich, G. Possnert, and C. A. M. Brenninkmeijer (2002), Using ^{14}C, ^{13}C, ^{18}O and ^{17}O isotopic variations to provide insights into the high northern latitude surface CO inventory, *Atmospheric Chemistry and Physics*, *2*, 147-159.

Rockmann, T., C. A. M. Brenninkmeijer, G. Saueressig, P. Bergamaschi, J. N. Crowley, H.

Fischer, and P. J. Crutzen (1998), Mass-independent oxygen isotope fractionation in atmospheric CO as a result of the reaction CO+OH, *Science*, *281*(5376), 544-546.

Rommelaere, V., L. Arnaud, and J. M. Barnola (1997), Reconstructing recent atmospheric trace gas concentrations from polar firn and bubbly ice data by inverse methods, *Journal of Geophysical Research-Atmospheres*, *102*(D25), 30069-30083.

Rudolph, J., E. Czuba, and L. Huang (2000), The stable carbon isotope fractionation for reactions of selected hydrocarbons with OH-radicals and its relevance for atmospheric chemistry, *Journal of Geophysical Research-Atmospheres*, *105*(D24), 29329-29346.

Rudolph, J., D. C. Lowe, R. J. Martin, and T. S. Clarkson (1997), A novel method for compound specific determination of $\delta^{13}C$ in volatile organic compounds at ppt levels in ambient air, *Geophysical Research Letters*, *24*(6), 659-662.

Rudolph, J., R. S. Anderson, K. V. Czapiewski, E. Czuba, D. Ernst, T. Gillespie, L. Huang, C. Rigby, and A. E. Thompson (2003), The stable carbon isotope ratio of biogenic emissions of isoprene and the potential use of stable isotope ratio measurements to study photochemical processing of isoprene in the atmosphere, *Journal of Atmospheric Chemistry*, *44*(1), 39-55.

Sanhueza, E., Y. Dong, D. Scharffe, J. M. Lobert, and P. J. Crutzen (1998), Carbon monoxide uptake by temperate forest soils: the effects of leaves and humus layers, *Tellus Series B-Chemical and Physical Meteorology*, *50*(1), 51-58.

Sano, M., Y. Yotsui, H. Abe, and S. Sasaki (1976), New technique for detection of

metabolites labeled by isotope ^{13}C using mass fragmentography, *Biomedical Mass Spectrometry*, *3*(1), 1-3.

Santrock, J., S. A. Studley, and J. M. Hayes (1985), Isotopic analyses based on the mass spectrum of carbon dioxide, *Anal. Chem.*, *57*(7), 1444-1448.

Saueressig, G., J. N. Crowley, P. Bergamaschi, C. Bruhl, C. A. M. Brenninkmeijer, and H. Fischer (2001), ^{13}C and D kinetic isotope effects in the reactions of CH_4 with $O(^1D)$ and OH: New laboratory measurements and their implications for the isotopic composition of stratospheric methane, *Journal of Geophysical Research-Atmospheres*, *106*(D19), 23127-23138.

Savage, M., and T. W. Swetnam (1990), Early 19th century fire decline following sheep pasturing in a Vavajo Ponderosa pine forest, *Ecology*, *71*(6), 2374-2378.

Savarino, J., and M. Legrand (1998), High northern latitude forest fires and vegetation emissions over the last millennium inferred from the chemistry of a central Greenland ice core, *Journal of Geophysical Research-Atmospheres*, *103*(D7), 8267-8279.

Schaefer, H., and M. J. Whiticar (2008), Potential glacial-interglacial changes in stable carbon isotope ratios of methane sources and sink fractionation, *Global Biogeochemical Cycles*, *22*(1).

Schaefer, H., M. J. Whiticar, E. J. Brook, V. V. Petrenko, D. F. Ferretti, and J. P. Severinghaus (2006), Ice record of $\delta^{13}C$ for atmospheric CH_4 across the Younger Dryas-Preboreal transition, *Science*, *313*(5790), 1109-1112.

Schaefer, H., V. V. Petrenko, E. J. Brook, J. P. Severinghaus, N. Reeh, J. R. Melton, and L. Mitchell (2009), Ice stratigraphy at the Pakitsoq ice margin, West Greenland, derived from gas records, *Journal of Glaciology*, *55*(191), 411-421.

Schütze, M. (1949), Ein neues Oxidationsmittel für die quantitative Uberführung von Kohlenmonoxyd in Kohlendioxyd. Ein Beitrag zur Chemie des Jodpentoxids, *Ber. Dtsch. Chem. Ges*, *77b*, 484-487.

Schwander, J., and B. Stauffer (1984), Age Difference between Polar Ice and the Air Trapped in Its Bubbles, *Nature*, *311*(5981), 45-47.

Schwander, J., T. Sowers, T. Blunier, and V. Petrenko (2008), Firn Air Sampling, *Field Report NEEM 2008*.

Schwander, J., J. M. Barnola, C. Andrie, M. Leuenberger, A. Ludin, D. Raynaud, and B. Stauffer (1993), The age of the air in the firn and the ice at summit, Greenland, *Journal of Geophysical Research-Atmospheres*, *98*(D2), 2831-2838.

Seiler, W. (1974), Cycle of atmospheric CO, *Tellus*, *26*(1-2), 116-135.

Seiler, W., and C. Junge (1970), Carbon monoxide in atmosphere, *Journal of Geophysical Research*, *75*(12), 2217-&.

Severinghaus, J. P., A. Grachev, and M. Battle (2001), Thermal fractionation of air in polar firn by seasonal temperature gradients, *Geochemistry Geophysics Geosystems*, *2*, art. no.-2000GC000146.

Siegenthaler, U., E. Monnin, K. Kawamura, R. Spahni, J. Schwander, B. Stauffer, T. F.

Stocker, J. M. Barnola, and H. Fischer (2005), Supporting evidence from the EPICA Dronning Maud Land ice core for atmospheric CO_2 changes during the past millennium, *Tellus Series B-Chemical and Physical Meteorology*, *57*(1), 51-57.

Siegenthaler, U., et al. (2005), Stable Carbon Cycle-Climate Relationship During the Late Pleistocene, *Science*, *310*(25), 1313-1317.

Smiley, W. G. (1949), Note on a reagent for oxidation of carbon monoxide, *Nucl. Sci. Abstr*, *3*, 391.

Smit, H. G. J., A. Volz, D. H. Ehhalt, and H. Knappe (1982), The isotopic fractionation during the oxidation of carbon monoxide by hydroxyl radicals and its implications for the atmospheric CO-cycle., *Stable Isotopes*, *Elsevier, Amsterdam*, 147-152.

Smolinska, J. (2008), European Automobile Manufacturer's Association (ACEA), *EU ECONOMIC REPORT, February 2008*.

Sowers, T., M. Bender, and D. Raynaud (1989), Elemental and isotopic compisition of occluded O_2 and N_2 in polar ice, *Journal of Geophysical Research-Atmospheres*, *94*(D4), 5137-5150.

Sowers, T., R. B. Alley, and J. Jubenville (2003), Ice core records of atmospheric N_2O covering the last 106,000 years, *Science*, *301*(5635), 945-948.

Sowers, T., M. Bender, D. Raynaud, and Y. S. Korotkevich (1992), $\delta^{15}N$ of N_2 in air trapped in polar ice: a tracer of gas transport in the firn and a possible constraint on ice age-gas age differences, *Journal of Geophysical Research-Atmospheres*, *97*(D14),

15683-15697.

Sowers, T., A. Rodebaugh, N. Yoshida, and S. Toyoda (2002), Extending records of the isotopic composition of atmospheric N_2O back to 1800 AD from air trapped in snow at the South Pole and the Greenland Ice Sheet Project II ice core, *Global Biogeochemical Cycles*, *16*(4).

Sowers, T., S. Bernard, O. Aballain, J. Chappellaz, J. M. Barnola, and T. Marik (2005a), Records of the $\delta^{13}C$ of atmospheric CH_4 over the last 2 centuries as recorded in Antarctic snow and ice, *Global Biogeochemical Cycles*, *19*(2).

Sowers, T., S. Bernard, O. Aballain, J. Chappellaz, J. M. Barnola, and T. Marik (2005b), Record of the $\delta^{13}C$ of atmospheric CH_4 over the last 2 centuries as recorded in Antarctic snow and ice, *Global Biogeochem. Cycles*, *19*, GB2002.

Spahni, R., et al. (2005), Atmospheric methane and nitrous oxide of the late Pleistocene from Antarctic ice cores, *Science*, *310*(5752), 1317-1321.

Stevens, C. M. (1993), New isotopic perspectives on atmospheric CO sources, *Eos Transactions, AGU*, *74*(43), Fall meeting suppliment F179.

Stevens, C. M., and L. Krout (1972), Method of the determination of the carbon and of the oxygen isotopic composition of atmospheric carbon monoxide, *International Journal of Mass spectrometry*, *8*, 265-275.

Stevens, C. M., and A. Engelkemeir (1988), Stable carbon isotopic composition of methane from some natural and anthropogenic sources, *Journal of Geophysical*

Research-Atmospheres, *93*(D1), 725-733.

Stevens, C. M., and A. F. Wagner (1989), The Role of Isotope Fractionation Effects in Atmospheric Chemistry, *Zeitschrift Fur Naturforschung Section a-a Journal of Physical Sciences*, *44*(5), 376-384.

Stevens, C. M., D. Walling, A. Venters, L. E. Ross, Engelkem.A, and L. Krout (1972), Isotopic Composition of Atmospheric Carbon-Monoxide, *Earth and Planetary Science Letters*, *16*(2), 147-&.

Stevens, C. M., L. Kaplan, R. Gorse, S. Durkee, M. Compton, S. Cohen, and K. Bielling (1980), The kinetic isotope effect for carbon and oxygen in the reaction CO + OH, *International Journal of Chemical Kinetics*, *12*(12), 935-948.

Sturges, W. T., H. P. McIntyre, S. A. Penkett, J. Chappellaz, J.-M. Barnola, R. Mulvaney, E. Atlas, and V. Stroud (2001), Methyl bromide, other brominated methanes, and methyl iodide in polar firn air, *J. Geophys Res*, *106*(D2), 1595-1606.

Swetnam, T. W. (1993), Fire history and climate change in giant sequoia groves, *Science*, *262*(5135), 885-889.

Tarr, M. A., W. L. Miller, and R. G. Zepp (1995), DIRECT CARBON-MONOXIDE PHOTOPRODUCTION FROM PLANT MATTER, *Journal of Geophysical Research-Atmospheres*, *100*(D6), 11403-11413.

Thompson, A. M. (1992), The oxidizing capacity of the earth's atmosphere: probable past and future changes, *Science*, *256*(5060), 1157-1165.

Thompson, A. M., and R. J. Cicerone (1986), Possible perturbations to atmospheric CO, CH_4, and OH, *Journal of Geophysical Research-Atmospheres*, *91*(D10), 853-864.

Thompson, L. G., E. Mosleythompson, J. F. Bolzan, and B. R. Koci (1985), A 1500-year record of tropical precipitation in ice cores from the Quelccaya ice cap, Peru, *Science*, *229*(4717), 971-973.

Thompson, L. G., E. Mosleythompson, W. Dansgaard, and P. M. Grootes (1986), The Little Ice age as recorded in the stratigraphy of the tropical Quelccaya ice cap, *Science*, *234*(4774), 361-364.

Trudinger, C. M., D. M. Etheridge, P. J. Rayner, I. G. Enting, G. A. Sturrock, and R. L. Langenfelds (2002), Reconstructing atmospheric histories from measurements of air composition in firn, *Journal of Geophysical Research-Atmospheres*, *107*(D24).

Trudinger, C. M., I. G. Enting, D. M. Etheridge, R. J. Francey, V. A. Levchenko, L. P. Steele, D. Raynaud, and L. Arnaud (1997), Modeling air movement and bubble trapping in firn, *Journal of Geophysical Research-Atmospheres*, *102*(D6), 6747-6763.

Tschumi, J., and B. Stauffer (2000), Reconstructing past atmospheric CO_2 concentration based on ice-core analyses: open questions due to in situ production of CO_2 in the ice, *Journal of Glaciology*, *46*(152), 45-53.

Tsunogai, U., F. Nakagawa, D. D. Komatsu, and T. Gamo (2002), Stable Carbon and Oxygen Isotopic Analysis of Atmospheric Carbon Monoxide Using Continuous -Flow Isotope Ratio MS by Isotope Ratio Monitoring of CO, *Analytical Chemistry*, *74*,

5659-5700.

Tsunogai, U., F. Nakagawa, D. D. Komatsu, and T. Gamo (2002), Stable carbon and oxygen isotopic analysis of atmospheric carbon monoxide using continuous-flow isotope ratio MS by isotope ratio monitoring of CO, *Anal. Chem.*, *74*(22), 5695-5700.

Tsunogai, U., F. Nakagawa, T. Gamo, and J. Ishibashi (2005), Stable isotopic compositions of methane and carbon monoxide in the Suiyo hydrothermal plume, Izu-Bonin arc: Tracers for microbial consumption/production, *Earth and Planetary Science Letters*, *237*(3-4), 326-340.

Tsunogai, U., Y. Hachisu, D. D. Komatsu, F. Nakagawa, T. Gamo, and K. Akiyama (2003), An updated estimation of the stable carbon and oxygen isotopic compositions of automobile CO emissions, *Atmospheric Environment*, *37*(35), 4901-4910.

Verschuren, D., K. R. Laird, and B. F. Cumming (2000), Rainfall and drought in equatorial east Africa during the past 1,100 years, *Nature*, *403*(6768), 410-414.

Wang, Y. H., and D. J. Jacob (1998), Anthropogenic forcing on tropospheric ozone and OH since preindustrial times, *Journal of Geophysical Research-Atmospheres*, *103*(D23), 31123-31135.

Wang, Z. H., and J. Mak (2009), A new CF-IRMS system for the quantification of the stable isotopes of carbon monoxide from ice cores and small air samples, *Atmospheric Measurement Techniques Discussions*, *2*, 1-17.

Weinstock, B. (1969), Carbon monoxide: residence time in atmosphere, *Science*,

166(3902), 224-225.

Weinstock, B., and H. Niki (1972), Carbon monoxide balance in nature, *Science*, *176*(4032), 290-292.

Williams, M. B., M. Aydin, C. Tatum, and E. S. Saltzman (2007), A 2000 year atmospheric history of methyl chloride from a South Pole ice core: Evidence for climate-controlled variability, *Geophysical Research Letters*, *34*(7).

Young, L. C., and B. A. Finlayson (1976), Mathematical models of monolith catallytic converter 2: application to automobile exhaust, *Aiche J.*, *22*(2), 343-353.

Appendix A: South Pole Ice Core Measurements

Depth(m)	Gas Age (AD)	[CO] (ppbv)	$\delta^{13}C$ (‰, VPDB)	$\delta^{18}O$ (‰, VSMOW)	[CO]_blank (ppbv)	Ice Weight (g)	Process Date
130	1876	50.7	-27.37	2.01	18	905	6/10/2009
132	1854	51.2	-27.39	0.94	20	858	6/11/2009
135	1821	57.0	-29.43	-2.99	22	872	11/21/2008
139	1777	48.2	-28.50	-0.11	18	921	5/19/2009
141	1755	43.8	-29.39	-1.92	18	923	5/15/2009
144	1722	41.2	-28.92	-2.54	18	946	5/21/2009
147	1688	38.7	-30.00	-3.09	18	877	12/8/2008
150	1655	37.4	-30.10	-3.24	18	966	5/14/2009
152	1633	37.7	-30.31	-3.74	18	866	6/16/2009
153	1622	36.5	-30.20	-3.62	18	900	6/9/2009
157	1578	36.6	-29.75	-2.22	18	918	11/25/2008
160	1545	36.2	-29.33	-1.70	18	922	5/20/2009
162	1523	46.1	-29.46	-2.56	18	891	5/22/2009
165	1490	42.4	-29.07	-1.69	18	922	11/20/2008
165	1490	45.9	-29.55	-2.16	18	957	12/3/2008
168	1457	41.1	-28.36	-2.10	18	882	6/14/2009
170	1435	46.5	-28.60	-0.94	20	937	6/17/2009
173	1402	48.0	-28.08	0.82	18	927	6/13/2009
177	1358	57.0	-28.00	0.23	22	939	11/24/2008
177	1358	49.9	-27.92	1.01	18	752	6/15/2009

Appendix B: D47 Ice Core Measurements

Depth(m)	Gas Age (AD)	[CO] (ppbv)	$\delta^{13}C$ (‰, VPDB)	$\delta^{18}O$ (‰, VSMOW)	[CO]_blank (ppbv)	Ice Weight (g)	Process Date
76	1897	53	-27.40	1.05	12	1044	7/13/2007
76¶	1897	54.8	-27.44	0.61	12	1098	6/18/2007
79	1887	56.3	-27.15	0.97	13	1110	7/17/2007
80	1884	57.3	-27.81	1.27	11	1020	7/13/2007
80	1884	51.8	-27.90	1.72	12	1080	7/18/2007
81¶	1881	56	-27.27	1.62	12	1118	6/20/2007
81#	1881	53.8	-27.54	2.09	20	732	4/10/2009
86	1865	52.1	-26.69	-0.24	13	1148	7/17/2007
86	1865	54.8	-27.11	1.17	13	1084	7/18/2007
86#	1865	51.4	-27.57	0.44	20	568	4/11/2009
89	1855	52	-27.49	0.13	10	688	7/23/2007
95	1835	55.1	-27.90	0.55	20	989	4/9/2009
95#	1835	49.9	-27.87	0.79	7	492	7/17/2007
98	1826	47.4	-28.75	-0.43	10	804	7/19/2007
98	1826	55.3	-28.62	-0.70	13	1128	7/19/2007
100	1819	47.5	-29.27	-0.61	10	756	7/16/2007
100	1819	46.5	-28.30	0.01	10	982	7/16/2007
109#	1790	45	-28.97	-1.31	10	1052	6/15/2007
109¶	1790	43.5	-28.82	-0.95	17	809	4/7/2009
111#	1783	46	-28.91	-1.55	17	806	4/8/2009

Note: ¶: The first batch of D47 ice core samples prepared in LGGE, and the process date shown is ice extraction date, CO analysis date is 6/30/2007; #: the third batch of D47 ice core samples analyzed with the new on-line analysis; others are the second batch of D47 ice core samples prepared in LGGE, and the process date shown is ice extraction date, CO analysis date is 8/7/2007-8/8/2007.